1. Hydrostatic equilibrium and virial theorem

Textbook: §10.1, 2.4

Assumed known: §2.1–2.3

Equation of motion in spherical symmetry

$$\rho \frac{\mathrm{d}^2 r}{\mathrm{d}t^2} = -\frac{GM_r \rho}{r^2} - \frac{\mathrm{d}P}{\mathrm{d}r} \tag{1.1}$$

Hydrostatic equilibrium

$$\frac{\mathrm{d}P}{\mathrm{d}r} = -\frac{GM_r \rho}{r^2} \tag{1.2}$$

Mass conservation

$$\frac{\mathrm{d}M_r}{\mathrm{d}r} = 4\pi r^2 \rho \tag{1.3}$$

Virial Theorem

$$E_{\mathrm{pot}} = -2E_{\mathrm{kin}} \qquad \text{or} \qquad E_{\mathrm{tot}} = \frac{1}{2} E_{\mathrm{pot}} \tag{1.4}$$

Derivation for gaseous spheres: multiply equation of hydrostatic equilibrium by r on both sides, integrate over sphere, and relate pressure to kinetic energy (easiest to verify for ideal gas).

For next time

- Read derivation of virial theorem for set of particles (§2.4).
- Remind yourself of interstellar dust and gas, and extinction (§12.1).
- Remind yourself about thermodynamics, in particular adiabatic processes (bottom of p. 317 to p. 321).

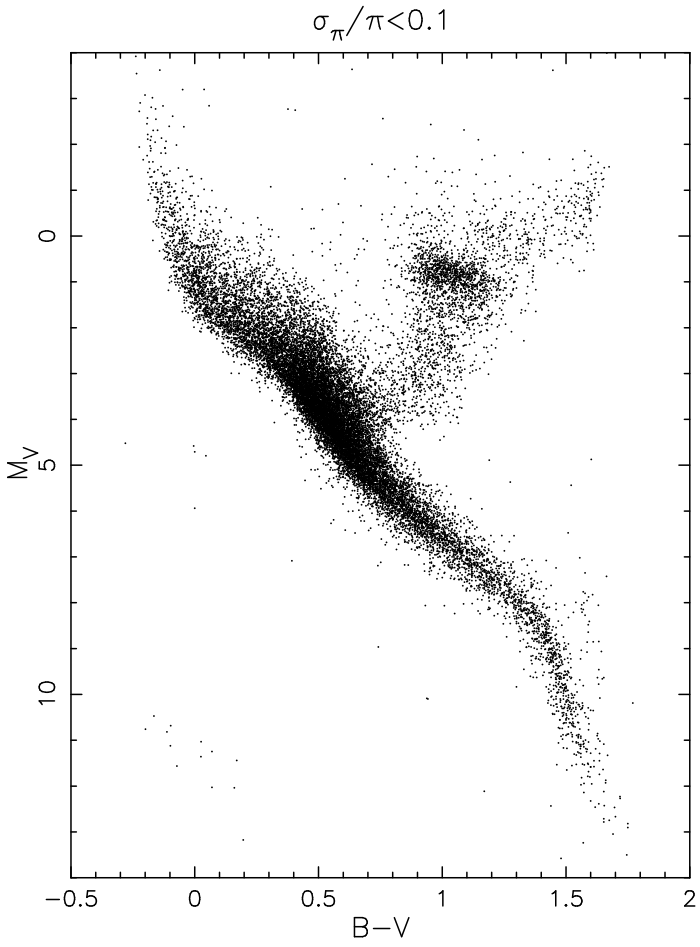

Fig. 1.1. The HRD of nearby stars, with colours and distances measured by the Hipparcos satellite. Taken from Verbunt (2000, first-year lecture notes, Utrecht University).

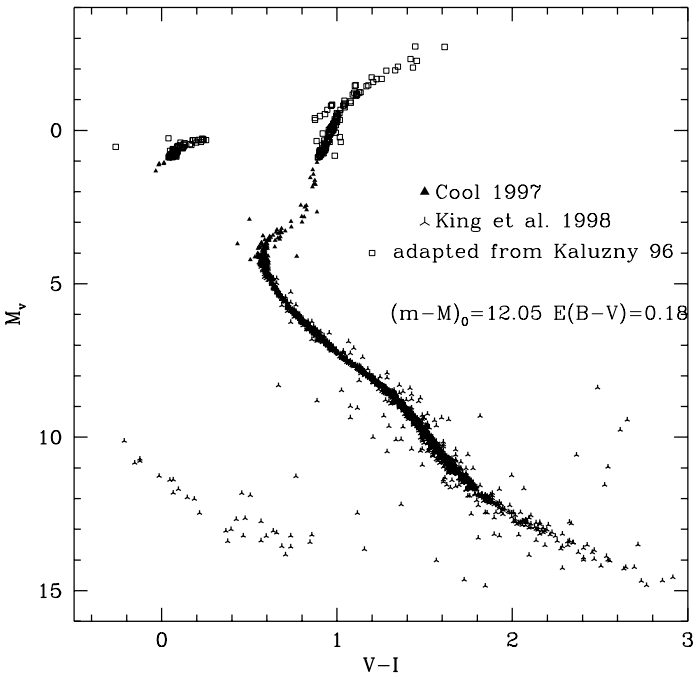

Fig. 1.2. Observed HRD of the stars in NGC 6397. Taken from D'Antona (1999, in "The Galactic Halo: from Globular Clusters to Field Stars", 35th Liege Int. Astroph. Colloquium).

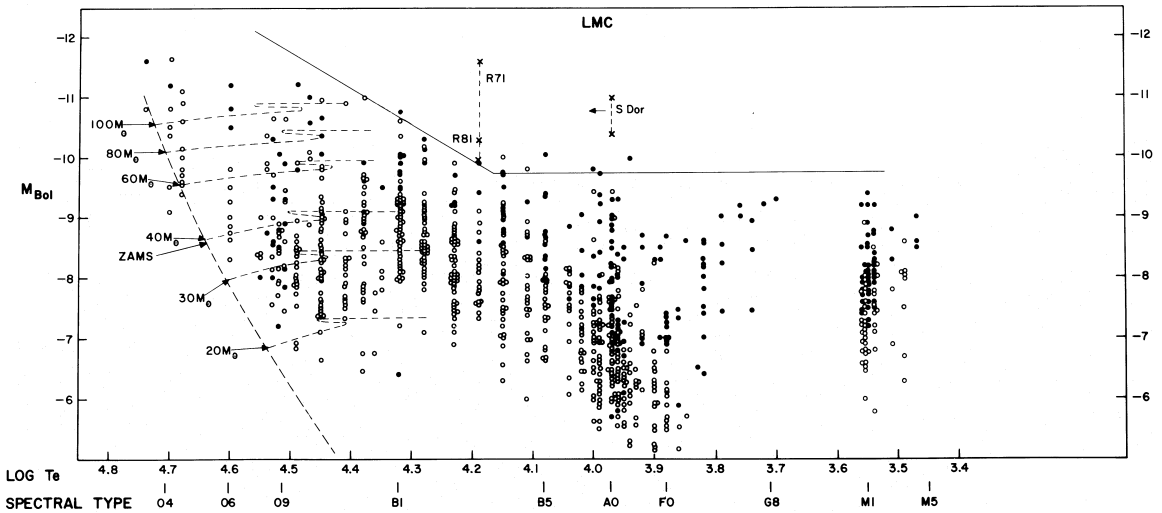

Fig. 1.3. HRD of the brightest stars in the LMC, with observed spectral types and magnitudes transformed to temperatures and luminosities. Overdrawn is the empirical upper limit to the luminosity, as well as a theoretical main sequence. Taken from Humphreys & Davidson (1979, ApJ 232, 409).

2. Star formation

Textbook: §12.2

Jeans Mass and Radius

$$M_{\rm J} = \left(\frac{3}{4\pi}\right)^{1/2}\left(\frac{5k}{G\mu m_{\rm H}}\right)^{3/2}\frac{T^{3/2}}{\rho^{1/2}} = 29\,M_\odot\,\mu^{-2}\left(\frac{T}{10\,{\rm K}}\right)^{3/2}\left(\frac{n}{10^4\,{\rm cm}^{-3}}\right)^{-1/2}, \tag{2.1}$$

$$R_{\rm J} = \left(\frac{3}{4\pi}\frac{5k}{G\mu m_{\rm H}}\right)^{1/2}\frac{T^{1/2}}{\rho^{1/2}} = 0.30\,{\rm pc}\,\mu^{-1}\left(\frac{T}{10\,{\rm K}}\right)^{1/2}\left(\frac{n}{10^4\,{\rm cm}^{-3}}\right)^{-1/2}. \tag{2.2}$$

Dynamical or free-fall timescale

$$t_{\rm ff} \simeq \sqrt{\frac{R^3}{GM}} \qquad \left(\text{exact: } \sqrt{\frac{3\pi}{32G\rho}};\ \text{often also: } \sim\sqrt{\frac{1}{G\rho}}\right). \tag{2.3}$$

Pulsation time scale

$$t_{\rm puls} \simeq \frac{R}{c_{\rm s}} \simeq \sqrt{\frac{1}{\gamma G\rho}} \qquad \left(\text{usually simply: } \sim\sqrt{\frac{1}{G\rho}}\right). \tag{2.4}$$

Contraction or Kelvin-Helmholtz timescale

$$t_{\rm KH} = \frac{-E_{\rm pot}}{L} \simeq \frac{GM^2}{RL} \tag{2.5}$$

For next time

- Think about initial mass-radius relation;
- Remind yourself about pressure integral (§10.2, in particular eq. 10.9), as well as mean molecular weight; and
- Remind yourself of relativistic energy and momentum (§4.4)

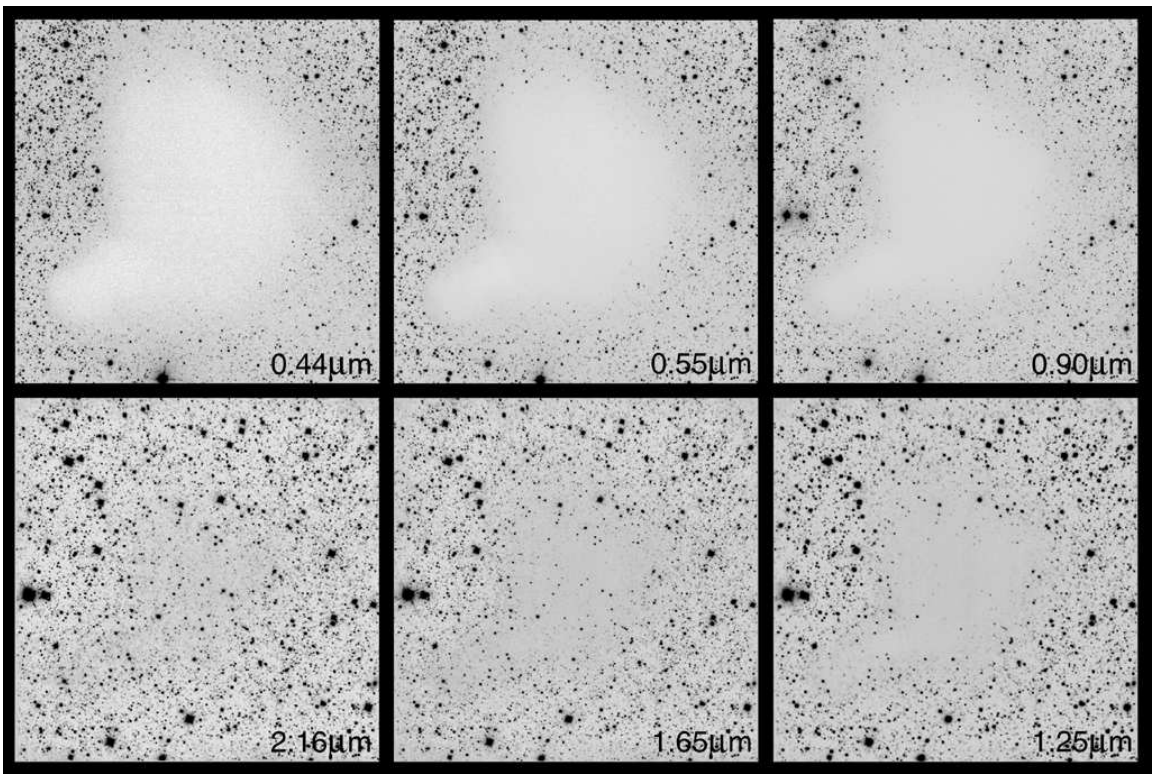

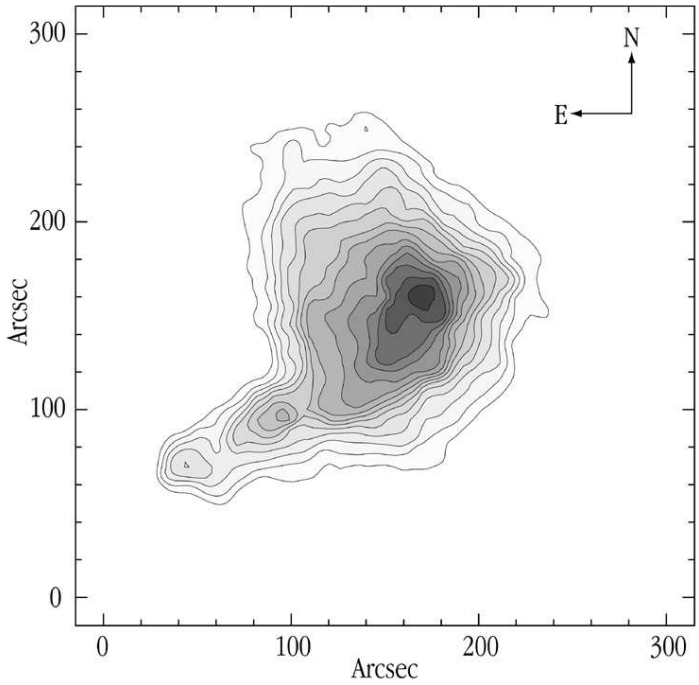

Fig. 2.1. (top) Images towards the dark globule Barnard 68 in B, V, I, J, H, and K (clockwise from upper left to lower left). The images are 4′.9 on the side; North is up, East to the left.

Fig. 2.2. (left) Inferred extinction through Barnard 68. Contours of V-band optical depth are shown, starting at 4 and increasing in steps of 2. Both pictures are taken from ESO press release 29/99.

3. Equation of state

Textbook: §10.2, 16.3

General expressions for number density, pressure, and energy

Given a momentum distribution $n(p)\mathrm{d}p$, then the particle density n, kinetic energy density U, and pressure P are given by

$$n = \int_0^\infty n(p)\mathrm{d}p, \tag{3.1}$$

$$U = \int_0^\infty n(p)\epsilon_p \,\mathrm{d}p, \tag{3.2}$$

$$P = \frac{1}{3}\int_0^\infty n(p)v_p p \,\mathrm{d}p. \tag{3.3}$$

For non-relativistic particles, $v_p = p/m$ and $\epsilon_p = p^2/2m$, while for (extremely) relativistic particles, $v_p \simeq c$, and $\epsilon_p = pc$. Hence,

$$P_{\mathrm{NR}} = \frac{1}{3}\int_0^\infty 2\epsilon_p n(p)\mathrm{d}p \qquad \Rightarrow \qquad P = \frac{2}{3}U, \tag{3.4}$$

$$P_{\mathrm{ER}} = \frac{1}{3}\int_0^\infty \epsilon_p n(p)\mathrm{d}p \qquad \Rightarrow \qquad P = \frac{1}{3}U. \tag{3.5}$$

General momentum distribution

$$n(p)\mathrm{d}p = n(\epsilon)\frac{g}{h^3}4\pi p^2\mathrm{d}p \qquad \text{(where g is the statistical weight).} \tag{3.6}$$

Here, $n(\epsilon)$ depends on the nature of the particles:

$$n(\epsilon) = \begin{cases} \dfrac{1}{\mathrm{e}^{(\epsilon-\mu)/kT}+0} & \text{classical; Maxwell-Boltzmann statistics,} \\ \dfrac{1}{\mathrm{e}^{(\epsilon-\mu)/kT}+1} & \text{fermions; Fermi-Dirac statistics,} \\ \dfrac{1}{\mathrm{e}^{(\epsilon-\mu)/kT}-1} & \text{bosons; Bose-Einstein statistics.} \end{cases} \tag{3.7}$$

Here, μ is the chemical potential; one can view the latter as a normalisation term that ensures $\int_0^\infty n(p)\mathrm{d}p = n$.

Classical: Maxwellian

After solving for μ, one recovers the Maxwellian momentum distribution:

$$n(p)\mathrm{d}p = n\frac{4\pi p^2\mathrm{d}p}{(2\pi mkT)^{3/2}}\mathrm{e}^{-p^2/2mkT} \tag{3.8}$$

Bosons: application to photons

For photons, the normalisation is not by total number of particles, but by energy; one finds $\mu = 0$. The statistical weight is $g = 2$ (two senses of polarisation). With $\epsilon = h\nu$ and $p = h\nu/c$, one finds for

$n(\nu)\mathrm{d}\nu$ and $U(\nu)\mathrm{d}\nu = h\nu n(\nu)\mathrm{d}\nu$,

$$n(\nu)\mathrm{d}\nu = \frac{4\pi\nu^2\mathrm{d}\nu}{c^3}\frac{2}{\mathrm{e}^{h\nu/kT}-1}; \tag{3.9}$$

$$U(\nu)\mathrm{d}\nu = \frac{8\pi h\nu^3}{c^3}\frac{\mathrm{d}\nu}{\mathrm{e}^{h\nu/kT}-1}. \tag{3.10}$$

Fermions: application to electrons

$$n(p)\mathrm{d}p = \frac{g}{h^3}\frac{4\pi p^2\mathrm{d}p}{\mathrm{e}^{(\epsilon-\mu)/kT}+1}. \tag{3.11}$$

Complete degeneracy

$$n(\epsilon) = \left\{\begin{array}{l} 1 \text{ for } \epsilon < \epsilon_\mathrm{F} \\ 0 \text{ for } \epsilon > \epsilon_\mathrm{F} \end{array}\right\} \quad \Leftrightarrow \quad n(p) = \left\{\begin{array}{ll} \frac{g}{h^3}4\pi p^2\mathrm{d}p & \text{for } p < p_\mathrm{F} \\ 0 & \text{for } p > p_\mathrm{F} \end{array}\right. . \tag{3.12}$$

Expressing p_F as a function of the number density n,

$$p_\mathrm{F} = h\left(\frac{3n}{4\pi g}\right)^{1/3}. \tag{3.13}$$

NRCD: non-relativistic complete degeneracy

For non-relativistic particles, one has $\epsilon_p = p^2/2m$, and thus $P = \frac{2}{3}U$. Hence,

$$P = \frac{2}{3}\int_0^{p_\mathrm{F}} n(p)\epsilon_p\,\mathrm{d}p = \frac{1}{20}\left(\frac{3}{\pi}\right)^{2/3}\frac{h^2}{m}\,n^{5/3}. \tag{3.14}$$

For electrons: $P_\mathrm{e} = K_1(\rho/\mu_\mathrm{e}m_\mathrm{H})^{5/3}$ with $K_1/m_\mathrm{H}^{5/3} = 9.91\times10^{12}$ (cgs). (3.15)

ERCD: extremely relativistic complete degeneracy

For relativistic particles, $\epsilon_p = pc$, and thus $P = \frac{1}{3}U$ (Eq. 3.5). Hence,

$$P = \frac{1}{3}\int_0^{p_\mathrm{F}} n(p)\epsilon_p\,\mathrm{d}p = \frac{1}{8}\left(\frac{3}{\pi}\right)^{1/3} hc\,n^{4/3}. \tag{3.16}$$

For electrons: $P_\mathrm{e} = K_2(\rho/\mu_\mathrm{e}m_\mathrm{H})^{4/3}$ with $K_2/m_\mathrm{H}^{4/3} = 1.231\times10^{15}$ (cgs). (3.17)

For next time

– Is degeneracy importantant for daily materials?

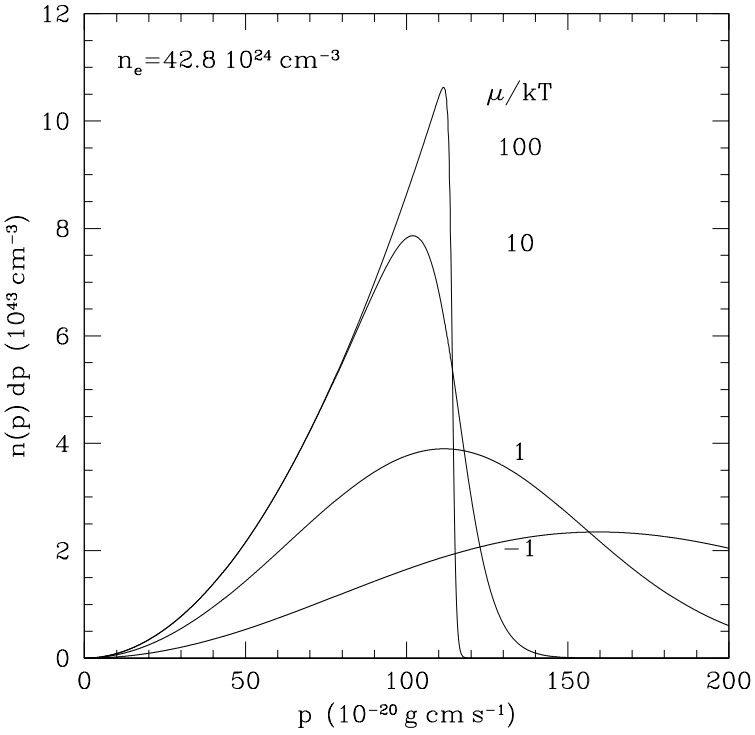

Fig. 3.1. The distribution of the number of particles $n(p)$ as a function of momentum p for a number of values of μ/kT.

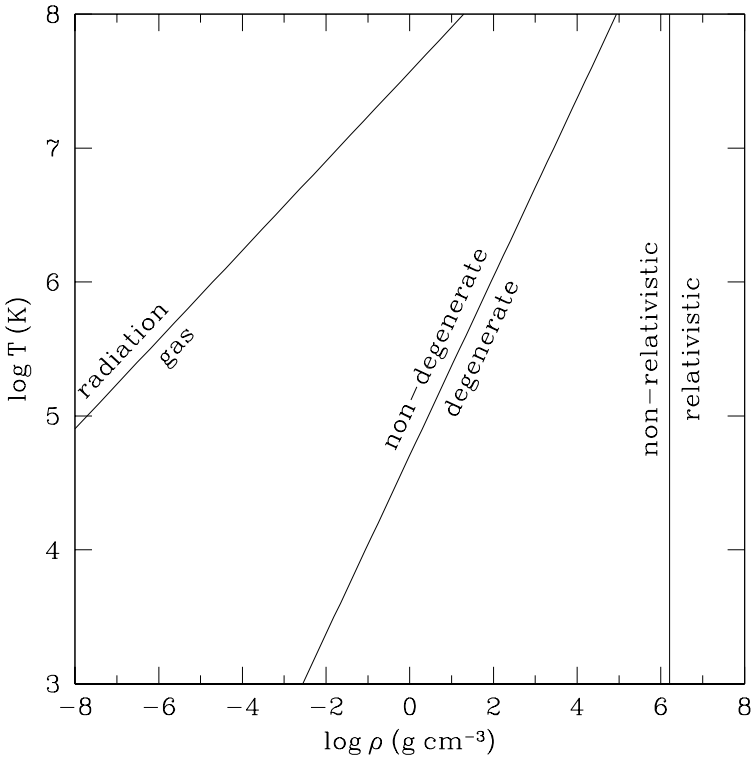

Fig. 3.2. The T, ρ diagram for $X = 0.7$ and $Z = 0.02$, with the areas indicated where matter behaves as an ideal gas ($P \propto nT$), non-relativistic degenerate gas ($P \propto n_{\rm e}^{5/3}$), relativistic degenerate gas ($P \propto n_{\rm e}^{4/3}$), or radiation-dominated gas. Note that these are not "sharp" boundaries. Also, at high enough T relativistic effects will become significant at all densities, not just for degenerate matter.

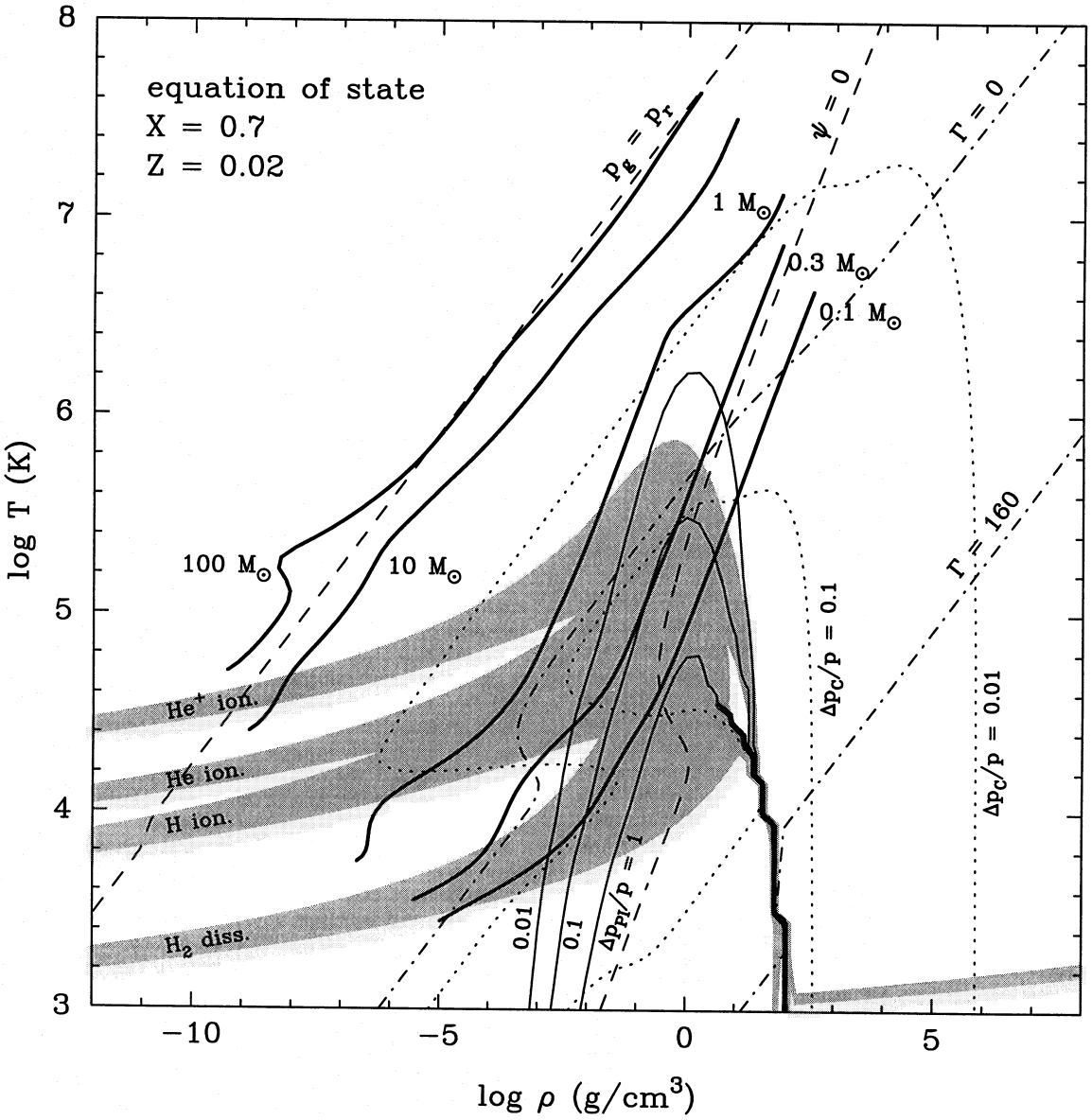

Fig. 3.3. T, ρ diagram for $X = 0.7$ and $Z = 0.02$ from Pols et al. (1995, MNRAS 274, 964). Dashed lines indicates where radiation pressure equals the gas pressure ($P_g = P_r$), and where degeneracy becomes important ($\psi = 0$); note that the latter is defined differently. The shaded regions indicate regions where various ions become ionised. None of the other lines were discussed in the text. Dash-dotted lines indicate constant plasma-interaction parameter Γ; dotted lines constant contribution from Coulomb interactions; thin solid lines constant contribution from pressure ionisation. The thick solid lines indicate the run of temperature as a function of temperature as found in zero-age main sequence (ZAMS) stellar models for several masses.

4. Simple stellar models

Textbook: – p. 334–340, applications in §16.4

Polytropic models

$$\left.\begin{array}{l} M_r = -\dfrac{r^2}{\rho G}\dfrac{\mathrm{d}P}{\mathrm{d}r} \Rightarrow \dfrac{\mathrm{d}M_r}{\mathrm{d}r} = -\dfrac{1}{G}\dfrac{\mathrm{d}}{\mathrm{d}r}\left(\dfrac{r^2}{\rho}\dfrac{\mathrm{d}P}{\mathrm{d}r}\right) \\ \dfrac{\mathrm{d}M_r}{\mathrm{d}r} = 4\pi r^2\rho \\ P = K\rho^\gamma \end{array}\right\} \quad \Rightarrow \quad \frac{1}{\rho r^2}\frac{\mathrm{d}}{\mathrm{d}r}\left(r^2\rho^{\gamma-2}\frac{d\rho}{\mathrm{d}r}\right) = -\frac{4\pi G}{K\gamma}. \tag{4.1}$$

Making the equation dimensionless, we derive the *Lane-Emden equation* of index n,

$$\left.\begin{array}{l} \rho = \rho_\mathrm{c}\theta^n \quad \text{with} \quad n = \dfrac{1}{\gamma-1} \quad \left(\text{i.e.,}\gamma = 1+\dfrac{1}{n}\right) \\ r = \alpha\xi \quad \text{with} \quad \alpha = \left(\dfrac{n+1}{4\pi G}K\rho_\mathrm{c}^{(1/n)-1}\right)^{1/2} \end{array}\right\} \quad \Rightarrow \quad \frac{1}{\xi^2}\frac{\mathrm{d}}{\mathrm{d}\xi}\left(\xi^2\frac{\mathrm{d}\theta}{\mathrm{d}\xi}\right) = -\theta^n. \tag{4.2}$$

The boundary conditions are $\theta_\mathrm{c} = 1$ and $(\mathrm{d}\theta/\mathrm{d}\xi)_\mathrm{c} = 0$.

Solutions of the Lane-Emden equations

In general, the Lane-Emden equation does not have an analytic solution, but needs to be solved numerically. The exceptions are $n = 0$, 1, and 5, for which,

$$\begin{array}{lllll} n=0 \quad (\gamma=\infty): & \theta = 1-\dfrac{\xi^2}{6} & \Rightarrow & \rho = \rho_\mathrm{c}, \\ n=1 \quad (\gamma=2): & \theta = \dfrac{\sin\xi}{\xi} & \Rightarrow & \rho = \rho_\mathrm{c}\dfrac{\sin\alpha r}{\alpha r}, \\ n=5 \quad (\gamma=1.20): & \theta = \left(1+\dfrac{\xi^2}{3}\right)^{-1/2} & \Rightarrow & \rho = \rho_\mathrm{c}\left(1+\dfrac{(\alpha r)^2}{3}\right)^{-5/2}. \end{array} \tag{4.3}$$

The stellar radius

Since one has $r = \alpha\xi$, the stellar radius is given by

$$R = \alpha\xi_1 = \left[\frac{(n+1)K}{4\pi G}\right]^{1/2}\rho_\mathrm{c}^{(1-n)/2n}\xi_1, \tag{4.4}$$

where ξ_1 is the value of ξ for which $\theta(\xi)$ reaches its first zero. In Table 4.1, values of ξ_1 are listed for various n.

The total mass

Integration of $\rho(r)$ gives the total mass of the star,

$$M = 4\pi\alpha^3\rho_\mathrm{c}\int_0^{\xi_1}\xi^2\theta^n\mathrm{d}\xi = 4\pi\alpha^3\rho_\mathrm{c}\int_0^{\xi_1}\mathrm{d}\left(-\xi^2\frac{d\theta}{d\xi}\right) = 4\pi\left[\frac{(n+1)K}{4\pi G}\right]^{3/2}\rho_\mathrm{c}^{(3-n)/2n}\left(-\xi^2\frac{\mathrm{d}\theta}{\mathrm{d}\xi}\right)_{\xi_1} \tag{4.5}$$

Table 4.1. Constants for the Lane-Emden functions

n	γ	ξ_1	$-\xi^2 \frac{\mathrm{d}\theta_n}{\mathrm{d}\xi}\Big\vert_{\xi_1}$	$\frac{\rho_\mathrm{c}}{\overline{\rho}}$	$K\frac{R^{(n-3)/n}}{GM^{(n-1)/n}}$	$\frac{P_\mathrm{c}}{GM^2/R^4}$
0.0	∞	2.4494	4.8988	1.0000	...	0.119366
0.5	3	3.7528	3.7871	1.8361	2.270	0.26227
1.0	2	3.14159	3.14159	3.28987	0.63662	0.392699
1.5	5/3	3.65375	2.71406	5.99071	0.42422	0.770140
2.0	3/2	4.35287	2.41105	11.40254	0.36475	1.63818
2.5	7/5	5.35528	2.18720	23.40646	0.35150	3.90906
3.0	4/3	6.89685	2.01824	54.1825	0.36394	11.05066
3.5	9/7	9.53581	1.89056	152.884	0.40104	40.9098
4.0	5/4	14.97155	1.79723	622.408	0.47720	247.558
4.5	11/9	31.83646	1.73780	6189.47	0.65798	4922.125
5.0	6/5	∞	1.73205	∞	∞	∞

Taken from Chandrasekar, 1967, Introduction to the study of stellar structure (Dover: New York), p. 96

where we used the Lane-Emden equation to substitute for θ^n. Values of $(-\xi^2 \mathrm{d}\theta/\mathrm{d}\xi)_{\xi_1}$ are again listed in Table 4.1. By combining the relations for the radius and the mass, one also derives a relation between the radius, mass, and K, which, for given K, gives the mass-radius relation. The appropriate numbers are listed in the table.

The central density and pressure

We can express the central density ρ_c in terms of the mean density $\overline{\rho} = M/\frac{4}{3}\pi R^3$ using the relations for the mass and radius. Solving K from the expressions for the mass and radius, one can also find the ratio of the central pressure to GM^2/R^4. Values of $\rho_\mathrm{c}/\overline{\rho}$ and $P_\mathrm{c}/(GM^2/R^4)$ are listed in Table 4.1.

The potential energy

Given the polytropic relation, one can also calculate the total potential energy. We just list the result here:

$$E_\mathrm{pot} = -\frac{3}{5-n}\frac{GM^2}{R}. \tag{4.6}$$

For next time

– Remind yourself of mean-free path and of basic radiation processes (example 9.2.1, pp 239–247).

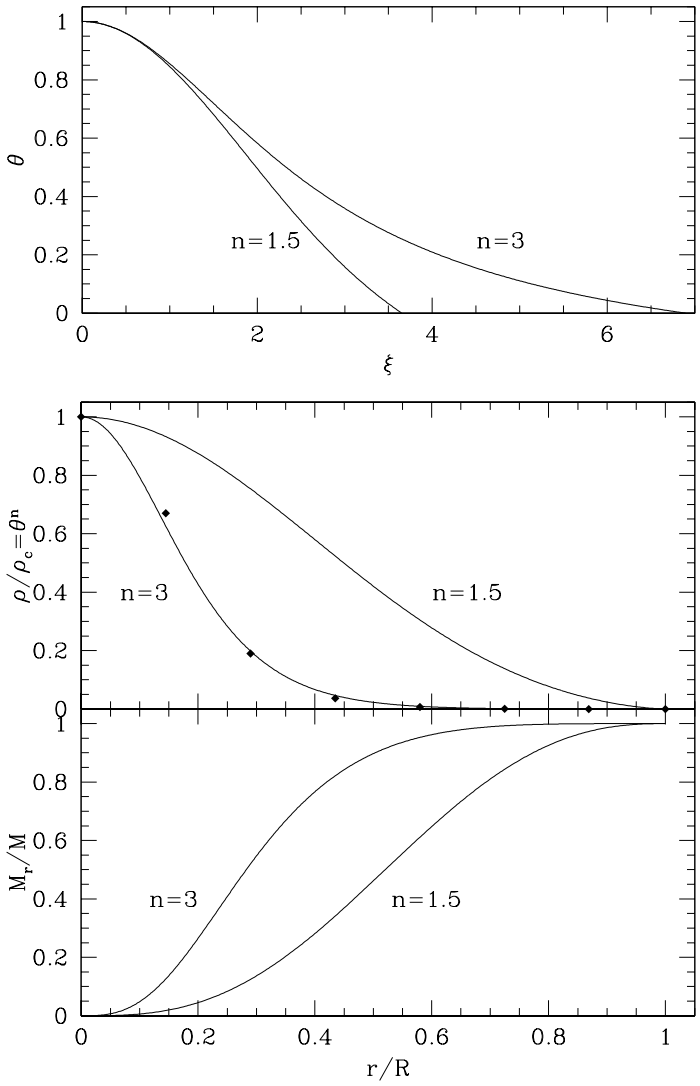

Fig. 4.1. *(top)* Run of $\theta(\xi)$ as a function of ξ for $n = 1.5$ and $n = 3$ (i.e., $\gamma = \frac{5}{3}$ and $\gamma = \frac{4}{3}$). Note that $\xi \propto r$ and $\theta^n \propto \rho$. For non-degenerate stars, $T \propto \theta$. *(middle)* Corresponding run of $\rho(r)/\rho_c$ as a function of r/R. The black dots indicate the values appropriate for the Sun; see Table 4.2. *(bottom)* Run of M_r/M as a function of r/R. Note how much more centrally condensed the $n = 3$ polytrope is compared to the $n = 1.5$ one.

Table 4.2. The run of density of a polytropic model with $n = 3$ and $\gamma = \frac{4}{3}$

ξ	0	1	2	3	4	5	6	6.9011
θ	1	0.855	0.583	0.359	0.209	0.111	0.044	0
r/R_*	0	0.145	0.290	0.435	0.580	0.725	0.869	1
ρ/ρ_c	1	0.625	0.198	0.0463	0.00913	0.00137	0.0000858	0
$(\rho/\rho_c)_\odot$	1	0.67	0.19	0.037	0.0065	0.0011	0.00015	0

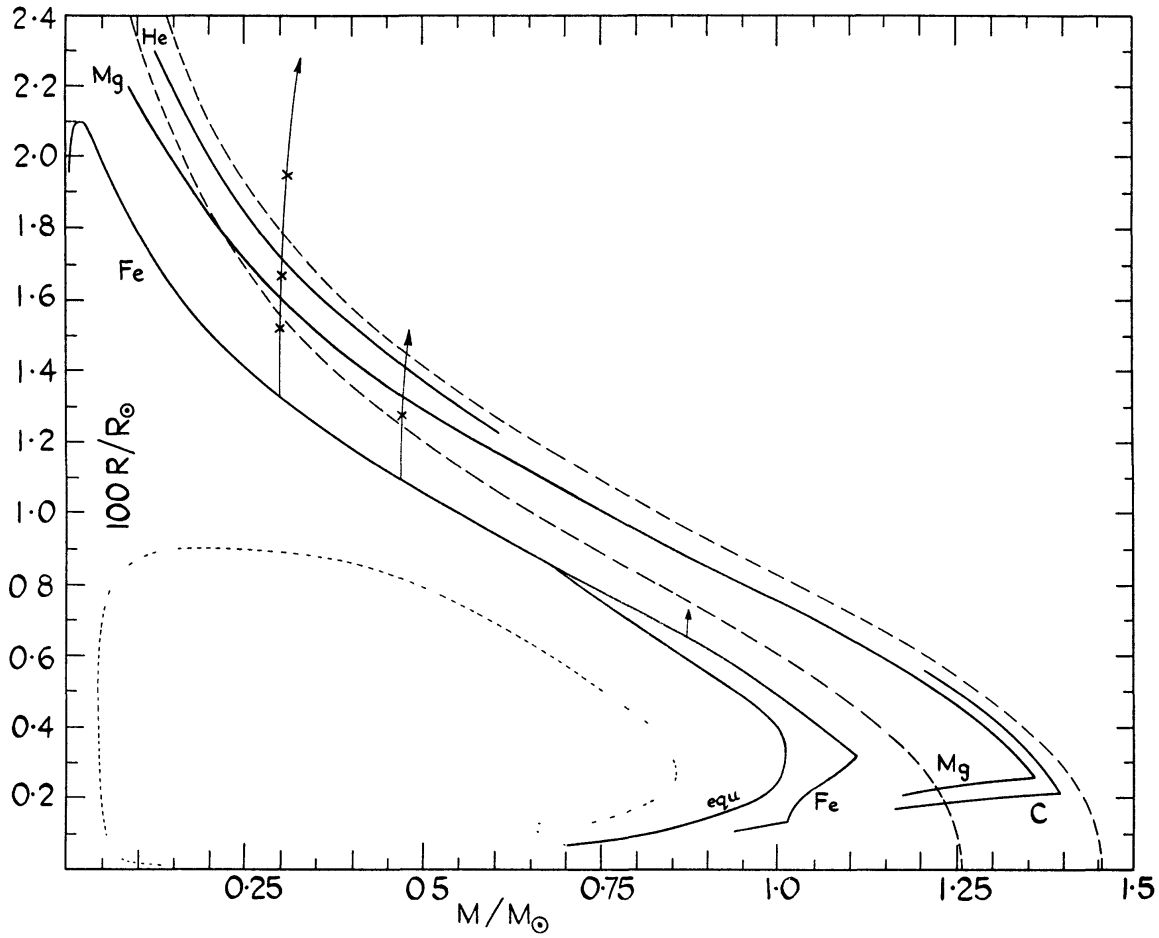

Fig. 4.2. Mass-radius relation for white dwarfs of various compositions. The dashed curves indicate Chandrasekhar models for $\mu_e = 2$ (upper) and 2.15 (lower), in which simple estimates like those discussed in class are used, except that the mildly relativistic regime is treated correctly. The models deviate from these idealized curves because the elements are not become completely ionized, and at very high densities, inverse beta decay becomes important (the curve labelled 'equ' takes into account the resulting changes in elemental abundances). For both reasons, there are variations in μ_e. The arrows indicate the effects of adding a hydrogen atmosphere. The dotted curve is a mass-radius relation for neutron stars. Taken from Hamada & Salpeter (1961, ApJ 134, 683).

5. Diffusive energy transport, Ionisation/excitation, Opacity

Textbook: §9.2, 8.1, and parts of 9.3, 10.4

Radiative and conductive energy transport

Radiative flux

$$F_{\rm rad} = -\frac{1}{3}\frac{c}{\kappa\rho}\frac{{\rm d}U_{\rm rad}}{{\rm d}r} = -\frac{4ac}{3}\frac{T^3}{\kappa\rho}\frac{{\rm d}T}{{\rm d}r}. \tag{5.1}$$

Eddington equation

$$\frac{{\rm d}T}{{\rm d}r} = -\frac{3}{4ac}\frac{\kappa\rho}{T^3}\frac{L_r}{4\pi r^2}, \tag{5.2}$$

where $L_r = 4\pi r^2 F_{\rm rad}$.

Rosseland mean

$$\frac{1}{\overline{\kappa}} = \frac{1}{\kappa_{\rm R}} \equiv \frac{\pi}{acT^3}\int_0^\infty \frac{1}{\kappa_\nu}\frac{{\rm d}B_\nu}{{\rm d}T}\,{\rm d}\nu\,, \qquad \text{where} \quad B_\nu \equiv \frac{c}{4\pi}U(\nu) = \frac{2h\nu^3}{c^2}\,\frac{1}{e^{h\nu/kT}-1} \tag{5.3}$$

Since $\int ({\rm d}B_\nu/{\rm d}T){\rm d}\nu = acT^3/\pi$, the Rosseland mean is the harmonic mean of κ_ν weighted by ${\rm d}B_\nu/{\rm d}T$.

Conduction

Usually, conduction is irrelevant. The exception is degenerate cores, where it dominates, making the cores isothermal. One can combine conduction with radiative transport by defining

$$F = F_{\rm rad} + F_{\rm cond} = -(k_{\rm rad} + k_{\rm cond})\nabla T. \tag{5.4}$$

If we define a conductive opacity $\kappa_{\rm cond}$ via

$$k_{\rm cond} \equiv \frac{4ac}{3}\frac{T^3}{\kappa_{\rm cond}}, \tag{5.5}$$

and by redefining $1/\overline{\kappa} = 1/\kappa_{\rm R} + 1/\kappa_{\rm cond}$, we can include conduction also in this way in the radiative transport equation.

Excitation and Ionisation

In general, the different states of ions and atoms will be populated according to the *Boltzmann equation,*

$$\frac{N_b}{N_a} = \frac{g_b}{g_a}{\rm e}^{-(\chi_b-\chi_a)/kT}. \tag{5.6}$$

Here, $g_{a,b}$ are the statistical weights (e.g., $g = 2n^2$ for level n in Hydrogen), and $\chi_{a,b}$ are the excitation potentials.

Comparing the ground state of one ionisation stage with the ground state of the next one, one has to take into account that the electron can have a range of kinetic energies and associated states. One finds

$$\frac{{\rm d}n_{i+1,0}(p)}{n_{i,0}} = \frac{g_{i+1,0}{\rm d}g_{\rm e}(p)}{g_{i,0}}{\rm e}^{-(\chi_i+p_{\rm e}/2m_{\rm e})/kT} \tag{5.7}$$

where $\mathrm{d}n_{i+1,0}(p)$ is the number density of atoms in the ground state of ionisation stage $i+1$ with an electron with momentum p, $n_{i,0}$ the number density of atoms in the ground state of ionisation stage i, and $g_\mathrm{e}(p)$ the statistical weight of the electron at momentum p. The latter is given by

$$\mathrm{d}g_\mathrm{e}(p) = \frac{2}{h^3}\frac{1}{n_\mathrm{e}} 4\pi p^2 \,\mathrm{d}p. \tag{5.8}$$

Integrating over all possible electron momenta and summing over all possible excitation states n (using the "partition function" $\mathcal{Z} = \sum_n g_n \exp(-\chi_n/kT)$), one finds the *Saha equation*,

$$\frac{n_{i+1}}{n_i} n_\mathrm{e} = \frac{\mathcal{Z}_{i+1}}{\mathcal{Z}_i} 2 \frac{(2\pi m_\mathrm{e} kT)^{3/2}}{h^3} \mathrm{e}^{-\chi_i/kT}. \tag{5.9}$$

Opacity

In general, the opacity is a complicated function of density, temperature and abundances. Three main processes dominate the continuum opacity at temperatures typically encountered in stars.

Electron scattering

$$\sigma_\mathrm{T} = \frac{8\pi}{3}\left(\frac{e^2}{m_\mathrm{e}c^2}\right)^2 = 6.65\ 10^{-29}\,\mathrm{m}^2 \quad \Rightarrow \quad \kappa_\mathrm{es} = \sigma_\mathrm{T}\frac{1+X}{2m_\mathrm{H}} = 0.0200(1+X)\,\mathrm{m}^2\,\mathrm{kg}^{-1}. \tag{5.10}$$

Free-free absorption

The free-free cross section for a certain ion i is given by

$$\sigma^\mathrm{ff}_{\nu,i} = \left(\frac{2m_\mathrm{e}}{\pi kT}\right)^{1/2} n_\mathrm{e} \frac{4\pi}{3\sqrt{3}} \frac{Z_i^2 e^6}{hcm_\mathrm{e}^2\nu^3} g^\mathrm{ff}_\nu. \tag{5.11}$$

For a general mixture of ions, one has to add over all constituents and their corresponding Z_i^2:

$$\overline{n_\mathrm{ion}Z^2} = \sum \frac{\rho X_i}{m_\mathrm{H} A_i} Z_i^2 = \frac{\rho}{m_\mathrm{H}}\left[X + Y + \sum_{i\geq 3}\frac{X_i}{A_i}Z_i^2\right], \tag{5.12}$$

where hydrogen and helium are assumed to be completely ionised.

In the integration over frequency required to calculate the Rosseland mean, one finds that the dependence on ν leads to the introduction of a T^{-3} term. The result is the so-called *Kramers free-free opacity*,

$$\kappa_\mathrm{ff} = 3.8\ 10^{21}\,\mathrm{m}^2\,\mathrm{kg}^{-1}\ \rho T^{-7/2} g_\mathrm{ff}(1+X)\,(X+Y+B), \tag{5.13}$$

where B is the sum in Eq. 5.12 and the Gaunt factor g_ff is a suitably averaged value of g^ff_ν.

Bound-free absorption

The semi-classical Kramers cross section for an ion with charge Z_i with an electron in state n is given by

$$\sigma^\mathrm{bf}_{\nu,i,n} = \frac{64\pi^4}{3\sqrt{3}} \frac{m_\mathrm{e} e^{10}}{ch^6} \frac{Z_i^4}{n^5\nu^3} g^\mathrm{bf}_{\nu,i,n} = 2.82\,10^{25}\,\mathrm{cm}^2\ \frac{Z_i^4}{n^5\nu^3} g^\mathrm{bf}_{\nu,i,n}. \tag{5.14}$$

Most of the ions will be in an ionisation state $i+1$ which cannot be ionised by a typical photon with $h\nu \simeq kT \ll \chi_{i+1}$; the relevant ions for the opacity are the somewhat rarer ions in ionisation state i. Combining the Boltzmann and Saha equations, and writing $n_{i,n}$ explicitly in terms of $n_{i+1,1}$,

$$n_{i,n} = n_{i+1,1} n_\mathrm{e} \frac{n^2}{2} \left(\frac{h^2}{2\pi m_\mathrm{e} kT} \right)^{3/2} \mathrm{e}^{\chi_{i,n}/kT}, \tag{5.15}$$

where the hydrogenic approximation ($g_n = 2n^2$) was made.

For the Rosseland mean, one needs to add all states of all ions. For stellar interiors, hydrogen and helium will be completely ionised, so the mean opacity will be proportional to the metallicity Z. One finds the *Kramers bound-free opacity*,

$$\kappa_\mathrm{bf} = 4.3\ 10^{24}\,\mathrm{cm}^2\,\mathrm{g}^{-1}\ \frac{g_\mathrm{bf}}{t} Z(1+X)\rho T^{-7/2}, \tag{5.16}$$

where g is a mean Gaunt factor and t the "guillotine" factor that accounts for the number of different ions being available.

Negative hydrogen ion

Hydrogen atom has a bound state for a second electron in the field of the proton, though it has a very low ionisation potential, $\chi_{\mathrm{H}^-} = 0.75\,\mathrm{eV}$. The number density of negative hydrogen ions will be proportional to the electron density, which, in all but the most metal-poor stars, will be set by ionisation of the metals (which have much lower ionisation potentials that hydrogen and helium). Thus, the H^- opacity will scale as $\kappa_{\mathrm{H}^-} \propto \rho X Z$ at low temperatures; H^- is of course easily ionized at higher temperatures, and at it very low temperatures even metals will not be ionized, so there will be no electrons to form H^- by combining with H.

For next time

– Read ahead about convection (10.4)

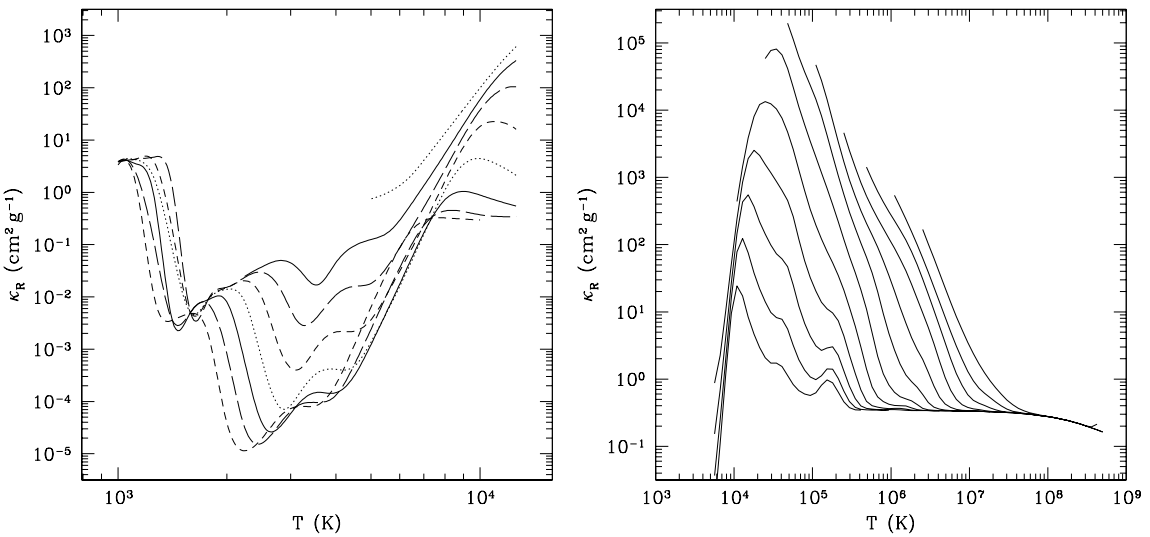

Fig. 5.1. Opacities as a function of temperature. *(left)* Low-temperature regime, from Alexander & Ferguson (1994, ApJ 437, 879). Opacities are shown for densities from 10^{-13} to $10^{-6}\,\mathrm{g\,cm^{-3}}$ in factors of ten, with lower densities corresponding to lower opacities. The sequence in line types is short-dashed, long-dashed, solid, dotted. The bump on the left is due to dust, that in the middle mostly to water, and that on the right to H^-. *(right)* High-temperature regime, for densities from 10^{-9} to $10^{2}\,\mathrm{g\,cm^{-3}}$, from the OPAL group (Iglesias & Rogers, 1996, ApJ 464, 943). The bump at the right is due to bound-free and free-free absorption, and the lower level at the left to electron scattering. Note the difference in scale between the two panels.

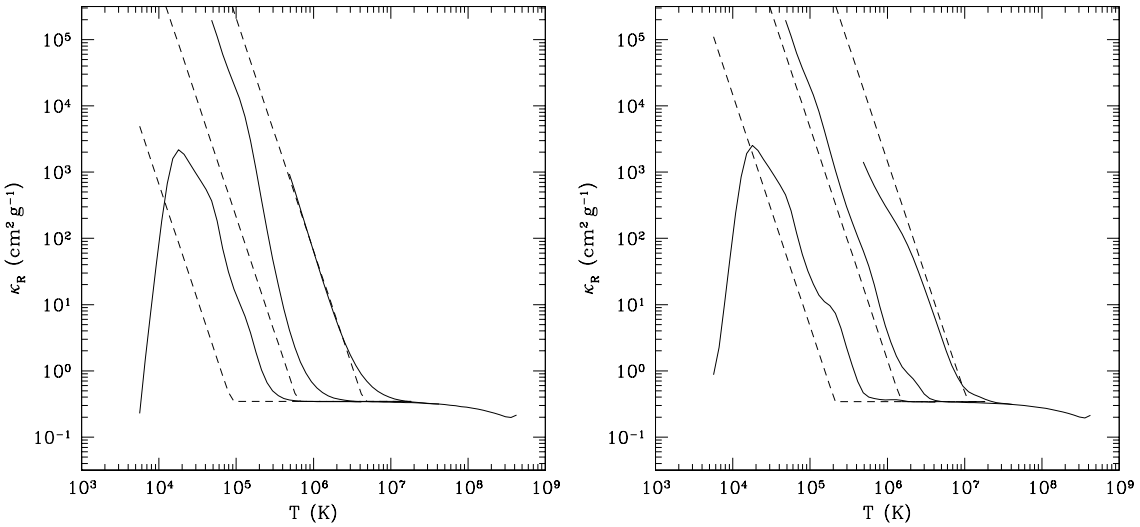

Fig. 5.2. Opacities as a function of temperature as estimated with the Kramers formulae (short-dashed lines) compared to those calculated by the OPAL group, for densities 10^{-6}, 10^{-3}, and $1\,\mathrm{g\,cm^{-3}}$. *(left)* $Z = 0$: OPAL vs. the Kramers free-free opacity; *(right)* $Z = 0.02$: OPAL vs. the Kramers bound-free opacity.

6. Convection, Mixing Length Theory

Textbook: §10.4

General stability criterion

$$-\frac{1}{\gamma}\frac{1}{P}\frac{\mathrm{d}P}{\mathrm{d}r} > -\frac{1}{\rho}\frac{\mathrm{d}\rho}{\mathrm{d}r}. \tag{6.1}$$

Schwarzschild instability criterion

$$\left.\frac{\mathrm{d}\ln T}{\mathrm{d}\ln P}\right|_{\mathrm{ad}} < \left.\frac{\mathrm{d}\ln T}{\mathrm{d}\ln P}\right|_{\mathrm{rad}} \quad \Leftrightarrow \quad \nabla_{\mathrm{ad}} < \nabla_{\mathrm{rad}}. \tag{6.2}$$

Ledoux instability criterion

$$\frac{\gamma-1}{\gamma} < \frac{\mathrm{d}\ln T}{\mathrm{d}\ln P} - \frac{(\partial\ln\rho/\partial\ln\mu)}{(-\partial\ln\rho/\partial\ln T)}\frac{\mathrm{d}\ln\mu}{\mathrm{d}\ln P}, \quad \Leftrightarrow \quad \nabla_{\mathrm{ad}} < \nabla_{\mathrm{rad}} - \frac{(\partial\ln\rho/\partial\ln\mu)}{(-\partial\ln\rho/\partial\ln T)}\nabla_\mu, \tag{6.3}$$

where we have defined $\nabla_\mu = \mathrm{d}\ln\mu/\mathrm{d}\ln P$ to be the changes in μ due to changes in composition X_i only, and where for a fully-ionised ideal gas, the term with the partial derivatives equals unity.

Efficiency of convection

A general expression for the convective flux is

$$F_{\mathrm{conv}} = \rho\overline{v}_{\mathrm{conv}}\Delta q = \rho\overline{v}_{\mathrm{conv}}c_P\Delta T = \rho\overline{v}_{\mathrm{conv}}c_P T\frac{\ell_{\mathrm{mix}}}{2H_P}\left(\nabla-\nabla_{\mathrm{ad}}\right), \tag{6.4}$$

where ℓ_{mix} is the *mixing length*, usually parametrized as a fraction of the scale height, i.e., $\ell_{\mathrm{mix}} \equiv \alpha_{\mathrm{mix}}H_P$, with α_{mix} the *mixing length parameter*.

To estimate v_{conv}, we use a method different from that used in the textbook: balance buoyancy ($Vg\Delta\rho = \rho Vg\Delta T/T$) and friction ($-A\rho v^2$); evaluate velocity at $l_{\mathrm{mix}}/2$; define $V/A = \beta\ell_{\mathrm{mix}}$, where β is a shape factor; and find

$$v_{\mathrm{conv}}^2 = \frac{\beta g}{H_P}\frac{\ell_{\mathrm{mix}}^2}{2}\left(\nabla-\nabla_{\mathrm{ad}}\right). \tag{6.5}$$

This leads to a convective flux given by

$$F_{\mathrm{conv}} = \rho c_P T\alpha_{\mathrm{mix}}^2\sqrt{\frac{\beta g H_P}{8}}\left(\nabla-\nabla_{\mathrm{ad}}\right)^{3/2}. \tag{6.6}$$

7. Completely convective stars and the Hayashi line

Textbook: –

Generalities

For completely convective stars, the temperature gradient needs to be only very slightly superadiabatic for substantial luminosities to be transported. The implication is that whatever luminosity the star manages to radiate away, will be brought to the surface without any problem by a corresponding energy flux in the convective regions. Thus, the actual luminosity of the star is determined in the only radiative region in the star, the photosphere.

A completely convective star

To find a solution for the whole star, we need to match a photosphere to the interior solution, where the latter is given by a polytrope $P = K\rho^{5/3}$. Matching the two solutions will set K, and for fixed K one knows how the radius depends on mass. For the run of pressure in the atmosphere, we have

$$\frac{\mathrm{d}P}{\mathrm{d}r} = -\frac{GM}{R^2}\rho \quad \text{or} \quad \frac{\mathrm{d}P}{\mathrm{d}h} = -g\rho,$$

where h is the height above some reference level. For the photosphere, $\tau = \kappa\rho h = \frac{2}{3}$, or

$$h = \frac{2}{3\kappa\rho} \quad \Rightarrow \quad P_{\rm phot} = \frac{2g}{3\kappa}. \tag{7.1}$$

Now, assume that the opacity is given by a law of the form

$$\kappa = \kappa_0 P^a T^b, \tag{7.2}$$

where in general a will be a positive number of order unity, while for cool temperatures b will be a relatively large positive number. Given this general opacity law, one has

$$P_{\rm phot}^{1+a} = \frac{2}{3\kappa_0 T_{\rm eff}^b} g \quad \Rightarrow \quad P_{\rm phot} = \left(\frac{2}{3\kappa_0 G}\frac{M}{R^2 T_{\rm eff}^b}\right)^{1/(1+a)}. \tag{7.3}$$

For the interior, we write the polytropic relation in terms of pressure and temperature, and combine it with the mass-radius relation for polytropes of $n = 1.5$ (Table 4.1),

$$\left.\begin{array}{l} P = K\rho^{5/3} \\ P = \dfrac{\rho}{\mu m_{\rm H}} kT \\ K = C_{1.5} G M^{1/3} R \quad \text{with} \quad C_{1.5} = 0.42422 \end{array}\right\} \quad \Rightarrow \quad P = K\left(\frac{P\mu m_{\rm H}}{kT}\right)^{5/3} \quad \Rightarrow \quad P_{\rm int} = \frac{M^{-1/2}}{(RC_{1.5}G)^{-3/2}}\left(\frac{kT}{\mu m_{\rm H}}\right)^{5/2}. \tag{7.4}$$

Equating $P_{\rm int}$ with $P_{\rm phot}$, raising to the $2(1+a)$ power, and sorting, one finds

$$\left(\frac{2}{3\kappa_0}\right)^2 G^{1+3a} M^{3+a} R^{-1+3a} = C_{1.5}^{-3-3a}\left(\frac{k}{\mu m_{\rm H}}\right)^{5+5a} T^{5+5a+2b}. \tag{7.5}$$

Solving for $T_{\rm eff}$,

$$T_{\rm eff} = \mathcal{C}_R M^{\frac{3+a}{5+5a+2b}} R^{\frac{-1+3a}{5+5a+2b}} \quad \text{with} \quad \mathcal{C}_R = \left[\left(\frac{2}{3\kappa_0}\right)^2 G^{1+3a} C_{1.5}^{3+3a}\left(\frac{k}{\mu m_{\rm H}}\right)^{-5-5a}\right]^{\frac{1}{5+5a+2b}}. \tag{7.6}$$

For a of order unity and large positive b one thus sees that $T_{\rm eff}$ depends only very weakly on the mass and radius. With $L = 4\pi R^2 \sigma T_{\rm eff}^4$, we can determine the dependencies on M and L, and thus where the star would be in the HRD. One finds

$$\left(\frac{2}{3\kappa_0}\right)^2 G^{1+3a} M^{3+a} \left(\frac{L}{4\pi\sigma}\right)^{(3a-1)/2} = C_{1.5}^{-3-3a} \left(\frac{k}{\mu m_{\rm H}}\right)^{5+5a} T^{3+11a+2b}, \tag{7.7}$$

$$T_{\rm eff} = \mathcal{C}_L M^{\frac{6+2a}{6+22a+4b}} L^{\frac{3a-1}{6+22a+4b}} \quad \text{with} \quad \mathcal{C}_L = \left[\left(\frac{2}{3\kappa_0}\right)^2 G^{1+3a} C_{1.5}^{3+3a} \left(\frac{k}{\mu m_{\rm H}}\right)^{-5-5a}\right]^{\frac{2}{6+22a+4b}}. \tag{7.8}$$

Again, for a of order unity and large b, $T_{\rm eff}$ depends extremely weakly on the luminosity, and thus one expects nearly vertical lines in the HRD. Given the slight positive dependence on M, one expects the lines to move slightly towards higher temperatures for larger masses.

Complications

The scaling that one finds from the above relations is reasonable. If one were to calculate numerical values, however, the answers would be very puzzling. The reason is that the assumption of a polytrope breaks down near the surface. Going towards the surface, it first fails in the ionisation zone, where recombination is an additional source of heat. Due to the recombination, the temperature of an adiabatically expanding blob does not decrease as it would otherwise, and therefore, above the ionisation zone the temperatures will be higher than would be the case if recombination were ignored. The effect can be seen Fig. 7.1.

Just below the photosphere, the convective energy transport becomes much less efficient, i.e., the superadiabatic gradient becomes substantial, while in the assumption of a $n = 1.5$ polytrope it is assumed to be negligible. With less efficient energy transport, the temperature will decrease more rapidly than adiabatic. Thus, the substantially superadiabatic region near the photosphere counteracts the effects of the ionisation zone. Net, the ionisation zone is more important.

7.1. Contraction along the Hayashi track

The star needs to contract in order to provide the energy it radiates away. Since it is completely convective, the entropy remains constant through the star, but decreases (increasing the entropy of the universe in order not to violate the second law). Since $\mathrm{d}q = T\mathrm{d}s$, the energy generated per gram is proportional to the local temperature. Therefore, the increase in luminosity in a shell $\mathrm{d}M_r$ is $\mathrm{d}L_r \propto T\mathrm{d}M_r$. With this, and with $P \propto T^{5/2}$, we can estimate whether the radiative gradient decreases towards the surface or towards the centre of the star. We assume again an opacity law of the form $\kappa \propto P^a T^b$, with $a = 1$, $b = -4.5$ for a Kramers-type law. We find

$$\begin{aligned}\frac{\mathrm{d}\ln\nabla_{\rm rad}}{\mathrm{d}\ln r} &= \frac{\mathrm{d}\ln L_r}{\mathrm{d}\ln r} - \frac{\mathrm{d}\ln M_r}{\mathrm{d}\ln r} + \frac{\mathrm{d}\ln\kappa}{\mathrm{d}\ln r} + \frac{\mathrm{d}\ln P}{\mathrm{d}\ln r} - 4\frac{\mathrm{d}\ln T}{\mathrm{d}\ln r} \\ &= \frac{\mathrm{d}\ln L_r}{\mathrm{d}\ln r} - \frac{\mathrm{d}\ln M_r}{\mathrm{d}\ln r} + [b - 4 + 2.5(a+1)]\frac{\mathrm{d}\ln T}{\mathrm{d}\ln r}.\end{aligned} \tag{7.9}$$

Generally, one has $M_r = \int \rho r^2 \mathrm{d}r$ and $L_r \propto \int T\rho r^2 \mathrm{d}r$. With the polytropic relations, therefore, $M_r \propto \int \theta^n \xi^2 \mathrm{d}\xi$ and $L_r \propto \int \theta^{n+1}\xi^2\mathrm{d}\xi$. Thus, one can use the solution $\theta(\xi)$ for a polytropic star to calculate $\mathrm{d}\ln(M_r, L_r, T)/\mathrm{d}\ln r$. The result for $n = 1.5$ is shown in Fig. 7.2. Also drawn is $\mathrm{d}\ln\nabla_{\rm rad}/\mathrm{d}\ln r$, assuming $a = 1$ and $b = -4.5$. One sees that it is always larger than zero, i.e., the radiative gradient decreases inwards. This is true for any reasonable opacity law. In consequence, the interior is always the first part of the star to become radiative.

We can also estimate how the radiative gradient scales scales with the stellar parameters in the core. There, the temperature hardly varies, and one has $L_r \propto (L/M)T_{\rm c}M_r$. Furthermore, for

any two stars with the same structure, $T_c \propto M/R$ and $P_c \propto M^2/R^4$, with the same constants of proportionality. Taking again $\kappa \propto P^a T^b$, one finds for the radiative gradient in the core,

$$\nabla_{\rm rad,c} \propto \frac{L_r \kappa P}{M_r T^4} \propto \frac{L}{M} T^{1+b-4} P^{a+1} \propto L M^{-2+b+2a} R^{-1-b-4a} \propto L M^{-4.5} R^{-0.5} \tag{7.10}$$

where in the last proportionality we used $a = 1$, $b = -4.5$ (Kramers). From Eqs. 7.6, 7.8, one sees that for given mass, $L \propto R^\alpha$, with $\alpha = (6 + 22a + 4b)/(5 + 5a + 2b)$, where a and b are now the coefficients in the atmospheric opacity law. Generally, $a \simeq 1$ and b large, hence, $\alpha \simeq 2$. Thus, the radiative gradient decreases as one descends the Hayashi track. At constant luminosity, one has $R \propto M^\beta$, with $\beta = (6 + 2a)/(7 - a + 2b) \lesssim 1$. Hence, the radiative gradient is smaller for larger masses, and more massive stars will become radiative in their core sooner.

For next time

- Think about why a star cannot be to the right of Hayashi limit.
- Read ahead on stellar energy sources (§10.3)

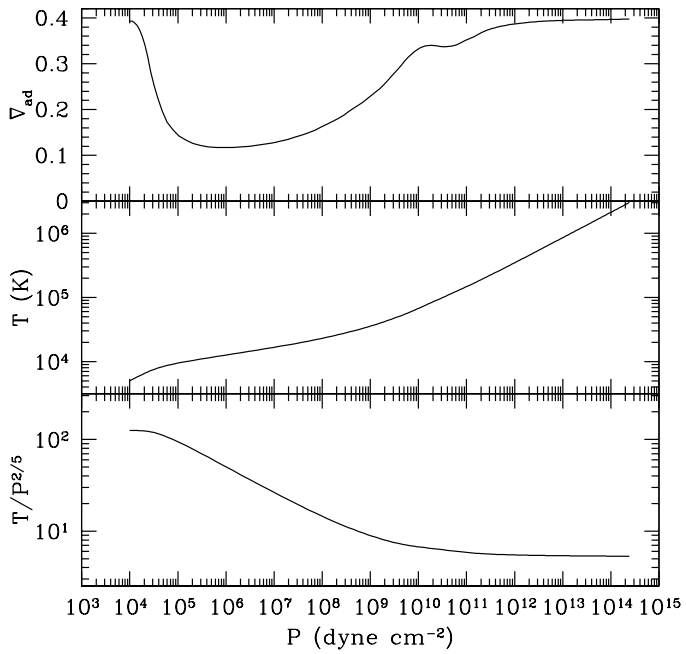

Fig. 7.1. Adiabatic gradient *(top)*, temperature *(middle)* and $T/P^{2/5}$ *(bottom)* as a function of pressure, calculated using the OPAL equation of state for a solar mixture. The effect of the hydrogen and helium ionisation zones is clearly seen in the depressions in $\nabla_{\rm ad}$ and the changes in slope in the other panels. As a result, a completely convective star will have a higher surface temperature than would be expected if the ionisation zone were ignored. The effect is partly undone by the superadiabatic gradient becoming substantial just below the photosphere.

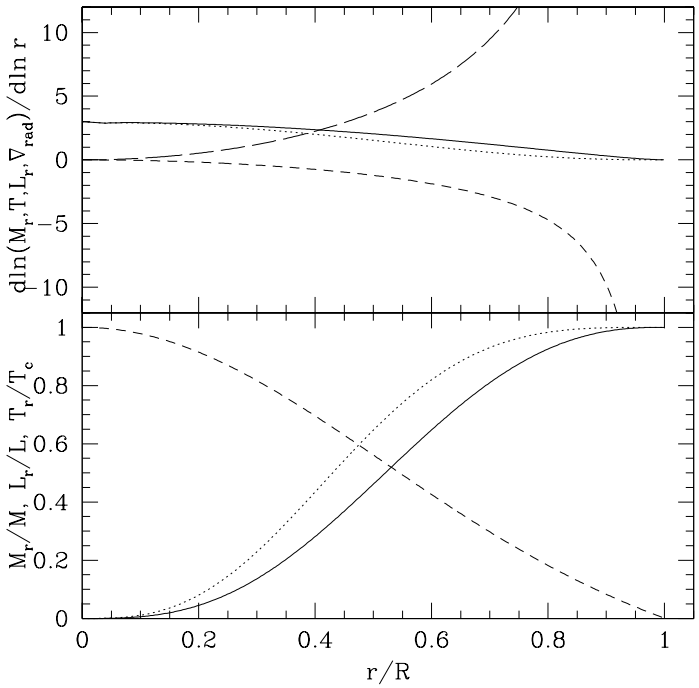

Fig. 7.2. *(Bottom)* Run of mass (solid line), luminosity (dotted line), and temperature (dashed line) as a function of radius for a contracting polytrope with $n = 1.5$ (i.e., the local energy generation per unit mass is proportional to temperature). *(Top)* Logarithmic derivatives of mass (solid line), luminosity (dotted line), temperature (short-dashed line), and radiative gradient (long-dashed line) as a function of radius. A Kramers-type opacity law was assumed.

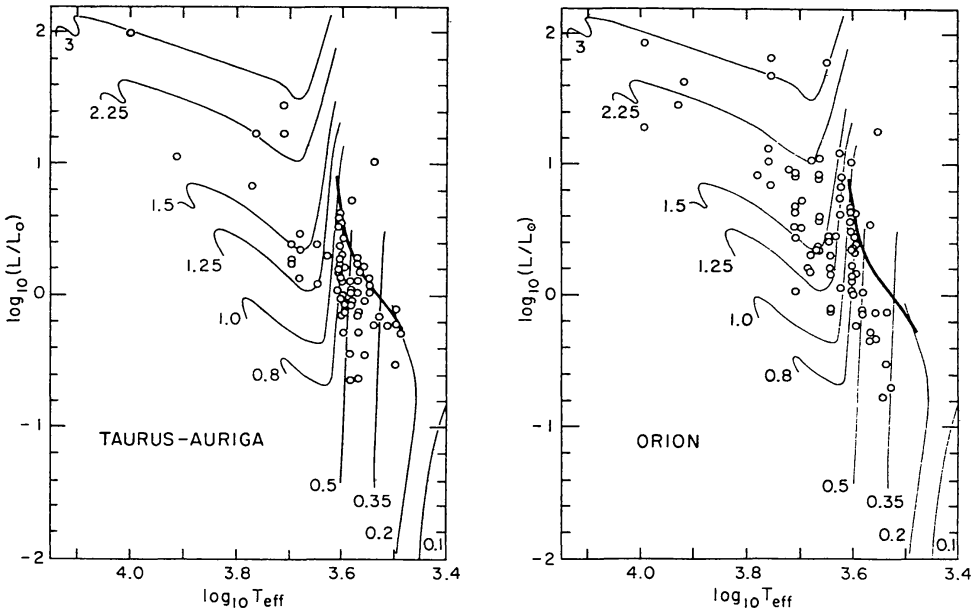

Fig. 7.3. Theoretical tracks for the pre-main sequence contraction phase for several different masses (as indicated). Overdrawn are observed temperatures and luminosities for pre-main sequence stars in two star-forming regions with rather different properties. In both, stars first appear along a very similar "birth line" (indicated with the thick line).

8. Energy balance: Contraction/expansion and nuclear processes

Textbook: §10.3

Energy Balance

$$\frac{\mathrm{d}L_r}{\mathrm{d}r} = 4\pi r^2 \rho\, \epsilon \quad \Leftrightarrow \quad \frac{\mathrm{d}L_r}{\mathrm{d}M_r} = \epsilon, \tag{8.1}$$

where ϵ is the energy generated per unit mass. In general,

$$\epsilon = \epsilon_{\rm grav} + \epsilon_{\rm nuc} - \epsilon_\nu, \tag{8.2}$$

where $\epsilon_{\rm grav}$ is the energy liberated or lost by contraction or expansion, $\epsilon_{\rm nuc}$ is the energy produced (or lost) in nuclear processes, and ϵ_ν is that part of the latter that escapes the star immediately in the form of neutrinos.

Contraction or expansion

The energy gained or lost in mass movements inside the star can be derived from the first law of thermodynamics, and written in various equivalent forms as

$$\epsilon_{\rm grav} = -\frac{\mathrm{d}Q}{\mathrm{d}t} = -T\frac{\mathrm{d}S}{\mathrm{d}t} = -\frac{\mathrm{d}u}{\mathrm{d}t} - P\frac{\mathrm{d}\mathcal{V}}{\mathrm{d}t}, \tag{8.3}$$

where $\mathcal{V} \equiv 1/\rho$ and u is the energy density per unit mass.

Nuclear processes

The main source of energy in stars is nuclear fusion, which we will now treat in more detail than in CO, § 10.3 (Kippenhahn & Weigert, chapter 18, was used extensively below).

Basic considerations

The energy gained or lost in nuclear processes is related to the mass defect Δm:

$$E = \Delta m\, c^2 = \left(\sum_i m_{{\rm init},i} - \sum_j m_{{\rm final},j} \right) c^2. \tag{8.4}$$

The mass defect reflects the different binding energies per nucleon in different nuclei,

$$\frac{E_{\rm bind}}{A} = \frac{1}{A}\left(Z m_{\rm p} + (A-Z) m_{\rm n} - m_{\rm nucleus}\right) c^2 \ . \tag{8.5}$$

The binding energy per nucleon increases steeply from hydrogen, then flattens out and starts to decrease, having reached a maximum at ^{56}Fe; see Fig. 8.1. Defining hydrogen to have zero binding energy, helium has 7.07 MeV per nucleon, carbon 7.68 MeV, and iron 8.73 MeV.

For fusion, nuclei must be brought close enough together that the short-range strong nuclear force can dominate over the weaker, but long-range repulsive Coulomb force. The range of the strong nuclear force is set by the Compton wavelength of its carrier, the pi meson, $\hbar/m_\pi c = 1.41\,$fm. The repulsive Coulomb potential at a distance of $\sim 1\,$fm ($10^{-13}\,$cm) is $E_{\rm Coul} = Z_1 Z_2 e^2/r \simeq 1.44\,{\rm MeV}\,\left(\frac{1\,{\rm fm}}{r}\right) Z_1 Z_2$, where Z_1 and Z_2 are the atomic numbers of the colliding nuclei. This should be compared with typical kinetic energy of a particle, of order $kT = 0.86\,T_7\,$keV, where T_7 is the

temperature in units of 10^7 K. Thus, classically, in the centre of the Sun (where $T_7 \approx 1.5$), particles trying to interact should be turned around by the Coulomb force at $\sim 10^3$ fm; as a result, no reactions would be expected.

From quantum mechanics, however, a particle has a certain finite probability of "tunneling" through the Coulomb barrier (see CO, p. 147–148, which is perhaps more insightful than the motivation on p. 335-338). The reaction cross section per nucleus is usually written as,

$$\sigma(E) = \frac{S(E)}{E} \mathrm{e}^{-b/\sqrt{E}} \quad \text{with} \quad b = \frac{1}{h} 2\pi^2 \sqrt{2m'} Z_1 Z_2 e^2 \quad \text{and} \quad m' = \frac{m_1 m_2}{m_1 + m_2}. \tag{8.6}$$

Here, the term $1/E$ reflect the effective area for the interaction (for which one can take $\pi\lambda^2 \propto 1/p^2 \propto 1/E$), and the exponential term the penetration probability; effects from the nuclear force are absorbed into a function $S(E)$ which is, under most conditions, a relatively slowly varying function of the interaction energy E (but see "resonances" below).

The fusion product is at first a compound nucleus in an excited state with positive total energy. Often, this compound nucleus will decay into the same particles that formed it – i.e., the incoming particle is just scattered by the collision. The cases in which the decay products are different define the net reaction rate, the details of which are hidden in $S(E)$. The rates $S(E)$ can be calculated (with great difficulty!), or one can extrapolate from measurements (which are typically done at far larger energies than those relevant to stellar conditions).

In general, the compound nucleus has several discrete bound states at negative energies in the nuclear potential well, the stable ground state of the nucleus and some excited states that can decay into lower-energy states by emission of photons (γ-rays). These states are similar to the bound states of electrons in an atom, but comprising nucleons instead of electrons. However, the compound nucleus may also have quasi-stable excited states of positive energy (below the top of the Coulomb barrier), which can decay by emission of particles (by quantum tunnelling *outwards* through the Coulomb barrier) as well as by emission of a photon. Incoming particles with "resonant" energy corresponding to such a quasi-stable state can form a compound nucleus much more easily, leading to a greatly enhanced reaction rate.

Given the cross section $\sigma(E)$, the reaction rate between particles of types a and b (at a given energy E) is given by

$$r_{a,b}(E)\,\mathrm{d}E = n_a n_b v \sigma(E) f(E)\,\mathrm{d}E\,, \tag{8.7}$$

where n_a and n_b are the number densities of a and b, v is the relative velocity between a and b (corresponding to energy E), $f(E)$ is the energy probability distribution, and $\sigma(E)$ is the cross section defined above. The factor v accounts for the fact that for larger velocities v, more particles pass each other per unit time. Note that if particles a and b are identical, we need to multiply the above by $\frac{1}{2}$ in order to avoid counting double. Including that in the integrated reaction rate, we find a rate

$$r_{a,b} = \frac{1}{1+\delta_{a,b}} n_a n_b \langle \sigma v \rangle\,, \qquad \text{where} \quad \langle \sigma v \rangle \equiv \int_0^\infty v(E)\sigma(E)f(E)\,\mathrm{d}E \tag{8.8}$$

is the average reaction rate per pair of particles, i.e., $\langle \sigma v \rangle$ is an effective cross-section.

If the velocity probability distributions are Maxwellian for both particles (i.e., particles have momenta as in Eq. 3.8, divided by n), the distribution of the *relative velocity* of the particles is also Maxwellian, but with $m = m' = m_a m_b/(m_a + m_b)$ [verify this]. We can rewrite the Maxwell distribution in Eq. 3.8 as a function of energy using $p = \sqrt{2mE}$ and $\mathrm{d}p = \frac{1}{2}\sqrt{2m/E}\,\mathrm{d}E$,

$$f(E)\,\mathrm{d}E = \frac{2\pi\sqrt{E}}{(\pi kT)^{3/2}} \mathrm{e}^{-E/kT}\,\mathrm{d}E\,. \tag{8.9}$$

Hence, for the effective cross section (using $v(E) = p/m = \sqrt{2E/m}$),

$$\langle \sigma v \rangle = \left(\frac{8}{m'\pi}\right)^{1/2} \left(\frac{1}{kT}\right)^{3/2} \int_0^\infty S(E) \mathrm{e}^{-E/kT} \mathrm{e}^{-b/\sqrt{E}} \, \mathrm{d}E \; . \tag{8.10}$$

The integrand will be small everywhere but near where the two exponentials cross, which is called the "Gamow peak"; see Fig. 8.2. Assuming $S(E)$ is a slowly varying function, the maximum of the integrand will be where the term $h(E) \equiv -E/kT - b/\sqrt{E}$ in the exponential reaches a maximum; this position E_0 is thus obtained via:

$$\begin{aligned} \frac{\mathrm{d}h(E)}{\mathrm{d}E} &= \frac{\mathrm{d}}{\mathrm{d}E}(-E/kT - b/\sqrt{E}) = 0 \quad \Rightarrow \\ E_0 &= \left(\frac{bkT}{2}\right)^{2/3} = 5.665\,\mathrm{keV}\,(Z_1 Z_2)^{2/3} \left(\frac{m'}{m_\mathrm{u}}\right)^{1/3} T_7^{2/3} \; , \end{aligned} \tag{8.11}$$

where m_u is the atomic unit mass. Using a Taylor expansion of $h(E)$ around its maximum,

$$h(E) = h_0 + h_0'(E - E_0) + \frac{1}{2} h_0''(E - E_0)^2 + \ldots \simeq -\tau - \frac{1}{4}\tau \left(\frac{E}{E_0} - 1\right)^2 + \ldots \; , \tag{8.12}$$

where we have used the fact that the first derivative h_0' must be zero (since we are expanding around the maximum), and where we have defined

$$\tau = \frac{3E_0}{kT} = 19.721\,(Z_1 Z_2)^{2/3} \left(\frac{m'}{m_\mathrm{u}}\right)^{1/3} T_7^{-1/3} \; . \tag{8.13}$$

Using this in the integral, the exponential is approximately a Gaussian, as one can see by substituting $\xi = (E/E_0 - 1)\sqrt{\tau}/2$,

$$\int_0^\infty \mathrm{e}^{h(E)} \, \mathrm{d}E = \int_0^\infty \mathrm{e}^{-\tau - \frac{1}{4}\tau (E/E_0 - 1)^2} \, \mathrm{d}E = \frac{2}{3} kT \tau^{1/2} \mathrm{e}^{-\tau} \int_{-\sqrt{\tau}/2}^\infty \mathrm{e}^{-\xi^2} \, \mathrm{d}\xi \; . \tag{8.14}$$

Since τ is relatively large and the main contribution to the integral comes from the range close to E_0 (i.e., $\xi = 0$), the error introduced by extending the integration to $-\infty$ is small, i.e., the integral is approximately $\sqrt{\pi}$. For the Gaussian, the fractional full width at half maximum $\Delta E/E_0$ is

$$\frac{\Delta E}{E_0} = 4 \left(\frac{\ln 2}{\tau}\right)^{1/2} = 0.750\,(Z_1 Z_2)^{-1/3} \left(\frac{m'}{m_\mathrm{u}}\right)^{-1/6} T_7^{1/6} \; . \tag{8.15}$$

Doing the integration using the Gaussian and inserting the result in Eq. 8.10 (after taking out the slowly varying $S(E)$), one obtains

$$\langle \sigma v \rangle = \frac{4}{3} \left(\frac{2}{m'}\right)^{1/2} \left(\frac{1}{kT}\right)^{1/2} S_0 \tau^{1/2} \mathrm{e}^{-\tau} \; , \tag{8.16}$$

where $S_0 = S(E_0)$. Since $T \propto \tau^{-3}$ (Eq. 8.13), one thus has that $\langle \sigma v \rangle \propto \tau^2 \mathrm{e}^{-\tau}$. It is the exponential, however, that really determines the reaction speeds. The dependences on Z_1, Z_2, and m' ensure that more massive, more highly charged ions hardly react at all as long as the fusion processes of the lighter elements still are taking place.

It is often useful to know the temperature dependence of the reaction rate, given by

$$\nu \equiv \frac{\partial \ln \langle \sigma \nu \rangle}{\partial \ln T} = \frac{1}{3}(\tau - 2) = 6.574\,(Z_1 Z_2)^{2/3} \left(\frac{m'}{m_\mathrm{u}}\right)^{1/3} T_7^{-1/3} - \frac{2}{3} \tag{8.17}$$

(note that, for a given reaction, ν usually becomes smaller with increasing temperature). For the fusion of two protons in the centre of the Sun, $Z_1 = Z_2 = 1$, $m' = \frac{1}{2}$, $T_7 \simeq 1.5$, hence $\nu \simeq 4$, which is a relatively mild temperature dependence. For other fusion processes, we will find exponents of $\nu \sim 20$ and above, making these processes among the most strongly varying functions in physics.

Corrections to the above rate formulae

A few corrections are usually made in more detailed derivations. The first is a small correction factor $g_{a,b}$ to account for any temperature dependence of S_0 and for the inaccuracy of approximating the Gamow peak by a Gaussian. The second is more physical, and is a correction $f_{a,b}$ for the effect of electron screening — due to the presence of electrons, the effective potential that two ions see is slightly reduced ("screened"); as a result, the reaction will be faster. This correction is more important at higher densities, and at *very* high densities burning starts to depend more sensitively on the density than on the temperature. (For this case, one speaks of *pycnonuclear reactions*.) Also, separate terms may be added to account for resonances.

Timescales

For a reaction of particles a and b, the number densities decrease with time. We define a timescale for each type of particle

$$\tau_a \equiv -\frac{n_a}{\mathrm{d}n_a/\mathrm{d}t} = \frac{n_a}{(1+\delta_{a,b})r_{a,b}} = \frac{1}{n_b \langle \sigma v \rangle_{a,b}} \,. \tag{8.18}$$

With this definition, $n_a \propto \mathrm{e}^{-t/\tau_a}$. Note that when two particles of the same type react (i.e., when $b = a$), the rate as defined in Eq. 8.7 above is a factor two smaller, but two particles of type a are destroyed per reaction, so the final expression for the timescale does not contain the factor $1 + \delta_{a,b}$. [Show that when there are multiple reactions, the timescale is given by $\tau_a^{-1} = \sum_b (1/\tau_{a,b})$.]

Hydrogen burning

In principle, many nuclear reactions can occur at the same time. As we saw above, however, the weighting of the exponential with $(Z_1 Z_2)^{2/3}$ strongly inhibits processes involving more massive, more highly charged particles. In combination with the initial abundances of stars, with the largest fraction of the mass being hydrogen, generally only a small number of fusion processes turn out to be relevant in a given evolutionary stage.

P-P chain

In less massive stars ($M \lesssim 1.2\ M_\odot$), the fusion of hydrogen to helium on the main sequence is mostly by the *proton-proton chain* (p-p chain). The possible variants of the p-p chain are:

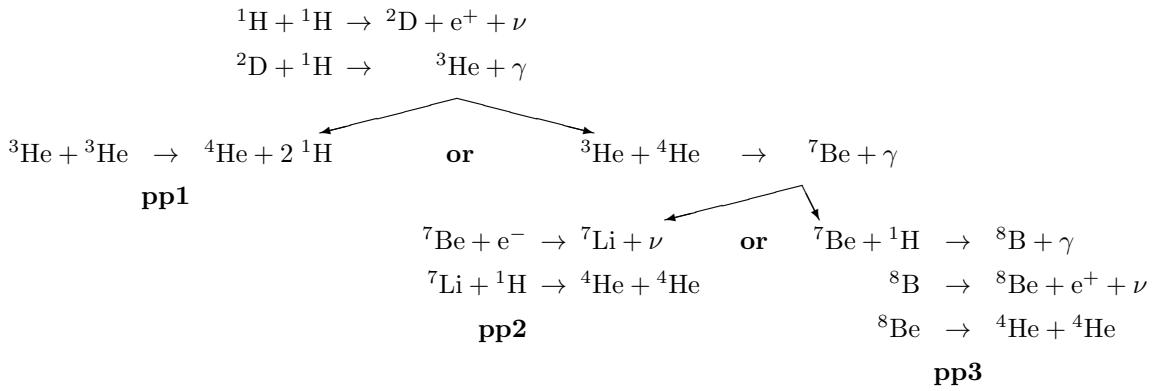

In these chains, the positrons made will meet an electron and annihilate, adding 1.022 MeV of photon energy. Note that while the total energy released (per ^{4}He produced) for the three chains

is equal, the fraction of that energy put in *neutrinos* is not the same. The net energy put into the local medium per ^{4}He nucleus produced is 26.20 MeV for pp1, 25.67 for pp2, and 19.20 for pp3.

The relative frequency of the branches depends on the temperature, density, and chemical composition. Since the reduced mass is slightly larger for the ^{3}He+^{4}He reaction than it is for the ^{3}He+^{3}He reaction, it will have a slightly larger temperature sensitivity. With increasing temperature, pp2 and pp3 will therefore start to dominate over pp1 if ^{4}He is present in appreciable amounts. Similarly, with increasing temperature, the importance of proton capture on ^{7}Be will start to dominate over the electron capture.

For low temperatures, say $T_7 \lesssim 0.8$, one has to calculate all the reactions independently and keep track of relative abundances. For higher temperatures, the intermediate reactions will be in equilibrium, and the energy generation can be taken to be proportional to the first step, which is the slowest. This is because it involves the weak nuclear force in the decay of a proton to a neutron during the short time the two protons are together. Indeed, in by far most cases, the compound two-proton nucleus that is formed at first, will simply break apart into two protons again. As a result, the effective cross-section is very small, $\sim 10^{-47}\,\mathrm{cm}^2$. For the energy, one finds

$$\epsilon_{\rm pp} = 2.54\,10^6\ \mathrm{erg\,s^{-1}\,g^{-1}}\ \psi f_{1,1}\, g_{1,1}\, X_1^2\, \rho\, T_6^{-2/3}\, \mathrm{e}^{-33.81/T_6^{1/3}}, \tag{8.19}$$

with an uncertainty of about 5%. Here, $g_{1,1} \simeq 1 + 0.00382 T_6$, $f_{1,1} \simeq 1$ for electron screening, and ψ corrects for the relative contributions of the different chains. At $T_7 \lesssim 1$, $\psi \simeq 1$, but at $T_7 = 2$, it varies between 1.4 for $Y = 0.3$ to nearly 2 for $Y = 0.9$. At still higher temperatures, when pp3 starts to dominate, it goes to 1.5 almost independent of Y. The temperature dependence of the reaction, as calculated from Eq. 8.17, is relatively mild: $\nu \simeq 4$ (i.e., $\epsilon_{\rm pp} \propto T^4$, much less steep than we will find below for other reactions).

CNO cycle

At sufficiently high temperatures, hydrogen can be burned to helium via the CNO cycle, in which carbon, nitrogen, and oxygen act more or less as catalysts (these have to be present, of course). The reactions are split in a main cycle (CN cycle) and a secondary cycle (ON cycle), as follows:

M1. $^{12}\mathrm{C} + {}^1\mathrm{H} \rightarrow {}^{13}\mathrm{N} + \gamma$

M2. $^{13}\mathrm{N} \rightarrow {}^{13}\mathrm{C} + \mathrm{e}^+ + \nu$

M3. $^{13}\mathrm{C} + {}^1\mathrm{H} \rightarrow {}^{14}\mathrm{N} + \gamma$

M4. $^{14}\mathrm{N} + {}^1\mathrm{H} \rightarrow {}^{15}\mathrm{O} + \gamma$

M5. $^{15}\mathrm{O} \rightarrow {}^{15}\mathrm{N} + \mathrm{e}^+ + \nu$

M6. $^{15}\mathrm{N} + {}^1\mathrm{H} \rightarrow \begin{cases} {}^{12}\mathrm{C} + {}^4\mathrm{He} & \text{and back to line M1 (main CN cycle).} \\ {}^{16}\mathrm{O} + \gamma & \text{(secondary ON cycle):} \end{cases}$

S1. $^{16}\mathrm{O} + {}^1\mathrm{H} \rightarrow {}^{17}\mathrm{F} + \gamma$

S2. $^{17}\mathrm{F} \rightarrow {}^{17}\mathrm{O} + \mathrm{e}^+ + \nu$

S3. $^{17}\mathrm{O} + {}^1\mathrm{H} \rightarrow \begin{cases} {}^{14}\mathrm{N} + {}^4\mathrm{He} & \text{and back to line M4.} \\ {}^{18}\mathrm{F} + \gamma \end{cases}$

S4. $^{18}\mathrm{F} \rightarrow {}^{18}\mathrm{O} + \mathrm{e}^+ + \nu$

S5. $^{18}\mathrm{O} + {}^1\mathrm{H} \rightarrow {}^{15}\mathrm{N} + {}^4\mathrm{He}$ and back to line M6.

The branch to the ON cycle (at line M6) is roughly 10^{-3} to 10^{-4} times less likely than the main branch back to the beginning of the CN cycle. The ON cycle is important, however, since it results

in oxygen being converted to nitrogen (which takes part in the CN cycle) — the branching *inside* the ON cycle (at line S3) does not strongly favor one branch over the other, but both branches lead to the CN cycle. The beta-decay times are of order $10^2 \ldots 10^3$ seconds, *much* shorter than typical nuclear reaction timescales.

Again, for high enough temperatures the reaction cycle will reach equilibrium, and the reaction rate will be set by the slowest link in the CN cycle, which is the proton-capture on ^{14}N. Because of this bottleneck in the CN cycle, and due to the small branching ratio into the ON cycle, most of the CNO originally present will be turned into ^{14}N. The energy gain of the whole cycle, after taking out neutrino losses, is 24.97 MeV, and one finds

$$\epsilon_{\rm CNO} = 7.48\,10^{27}\,{\rm erg\,s^{-1}\,g^{-1}}\; g_{14,1}\, f_{14,1}\, X_{\rm CNO}\, X_1\, \rho\, T_6^{-2/3}\, {\rm e}^{-152.31/T_6^{1/3}-(T_6/800.)^2} \tag{8.20}$$

(with an uncertainty of ±10%), where $g_{14,1} \simeq 1 - 0.002T_6$, $f_{14,1} \sim 1$ for electron screening, and $X_{\rm CNO} = X_{\rm C} + X_{\rm N} + X_{\rm O}$. At somewhat lower temperatures, the CN cycle can reach equilibrium, but the burning of ^{16}O proceeds slowly; Eq. 8.20 is still quite a good approximation, but with $X_{\rm CNO} = X_{\rm C} + X_{\rm N} + |\Delta X_{\rm O\to N}(t)|$, where $|\Delta X_{\rm O\to N}(t)|$ is the amount of ^{16}O that has been burned to nitrogen as of time t (note that the intermediate ^{17}O stage may also slow down the conversion of ^{16}O to nitrogen, since the reaction rates of ^{16}O and ^{17}O may be comparable).

Inside stars that burn predominantly via the CNO cycle, the nitrogen abundance will be far larger than it normally is, while carbon and oxygen will be correspondingly underabundant. Indeed, such abundance patterns are observed in massive stars which have lost a lot of mass, so that processed material reaches the surface. Examples of these are the ON stars and Wolf-Rayet stars of type WN. (In carbon-rich Wolf-Rayet stars, one even sees the products of helium fusion.) Also, in lower-mass red giants, some CNO-processed material is mixed to the surface.

For the CNO cycle, the temperature sensitivity is high, $\nu = 23 \ldots 13$ for $T_6 = 10 \ldots 50$. As a result, the p-p chain dominates at low temperatures, and the CNO cycle at high temperatures, as is illustrated in Fig. 8.3. Furthermore, because of the steep temperature dependence, the energy production will be highly concentrated towards the centre. Therefore, L_r/r^2 will be large, and thus $\nabla_{\rm rad}$ will be large as well. This is why massive stars have convective cores.

Helium burning

When all the hydrogen has been fused into helium, it is difficult to continue, because until one reaches carbon, the elements following helium have lower binding energy per nucleon (see Fig. 8.1). As a result, the fusion of two helium nuclei leads to a ^{8}Be nucleus whose ground state is nearly 100 keV lower in energy; therefore, it decays back into two alpha particles in a few 10^{-16} s. Nevertheless, this is still about 10^5 times longer than the encounter time — in fact, a ^{8}Be abundance of about 10^{-9} builds up in stellar matter. Occasionally, it will happen that another alpha particle comes by so that a carbon nucleus can be formed. This whole process is called the *triple-alpha reaction* because it almost is a three-body interaction. Writing out the reactions,

$$^4{\rm He} + {}^4{\rm He} \;\rightleftharpoons\; {}^8{\rm Be}$$
$$^8{\rm Be} + {}^4{\rm He} \;\rightarrow\; {}^{12}{\rm C} + \gamma$$

The total energy released per carbon nucleus formed is 7.274 MeV. For these reactions, it is much less straightforward to derive an energy generation rate, because "*resonances*" (as described above) are important for both the above steps. Roughly, the energy generation rate is

$$\epsilon_{3\alpha} = 4.99\,10^{11}\,{\rm erg\,s^{-1}\,g^{-1}}\; f_{3\alpha}\, Y^3\, \rho^2\, T_8^{-3}\left(1 + 0.00354 T_8^{-0.65}\right) {\rm e}^{-43.92/T_8} \tag{8.21}$$

(with an uncertainty of ±14%), where $f_{3\alpha} = f_{4,4} f_{8,4}$ is the combined electron screening factor. For this reaction, the temperature sensitivity is very high, $\nu = 40 \ldots 19$ for $T_8 = 1 \ldots 2$.

Other fusion processes can occur simultaneously (energy gain in MeV is shown to the right):

$$
\begin{aligned}
&{}^{12}\mathrm{C} + {}^{4}\mathrm{He} \;\rightarrow\; {}^{16}\mathrm{O} + \gamma && && 7.162 \\
&{}^{16}\mathrm{O} + {}^{4}\mathrm{He} \;\rightarrow\; {}^{20}\mathrm{Ne} + \gamma && && 4.730 \\
&{}^{14}\mathrm{N} + {}^{4}\mathrm{He} \;\rightarrow\; {}^{18}\mathrm{F} + \gamma\,, && {}^{18}\mathrm{F} \;\rightarrow\; {}^{18}\mathrm{O} + \mathrm{e}^{+} + \nu && 5.635 \;\text{(total, excluding neutrino energy)} \\
&{}^{18}\mathrm{O} + {}^{4}\mathrm{He} \;\rightarrow\; {}^{22}\mathrm{Ne} + \gamma && && 9.667
\end{aligned}
$$

The second of these is slow, and for the last two ^{14}N is not very abundant (and thus its product ^{18}O is not very abundant either). The first reaction is therefore the most important one. It is rather complicated (and has an uncertainty of $\pm 40\%$); approximately,

$$
\begin{aligned}
\epsilon_{12,\alpha} \;\simeq\; 9.58\,10^{26}\,\mathrm{erg\,s^{-1}\,g^{-1}}\; f_{12,4}\, X_{12}\, Y \rho\, T_8^{-2} \Big[& \left(1 + 0.254 T_8 + 0.00104 T_8^2 - 0.000226 T_8^3\right) \mathrm{e}^{-(T_8/46.)^2} \\
& + \left(0.985 + 0.9091 T_8 - 0.1349 T_8^2 + 0.00729 T_8^3\right) \mathrm{e}^{-(T_8/13.)^2} \Big] \, \mathrm{e}^{-71.361/T_8^{1/3}} \,. \qquad (8.22)
\end{aligned}
$$

Carbon burning and onward

After helium has been exhausted, the next processes to start are those of carbon burning, at temperatures of order $T_9 = 0.5 \ldots 1$. The situation is very complicated, since the excited ^{24}Mg nucleus that is produced is unstable and can decay in a number of different ways:

$$
\begin{aligned}
{}^{12}\mathrm{C} + {}^{12}\mathrm{C} \;&\rightarrow\; {}^{24}\mathrm{Mg} + \gamma && 13.931 \\
&\rightarrow\; {}^{23}\mathrm{Mg} + \mathrm{n} && -2.605 \\
&\rightarrow\; {}^{23}\mathrm{Na} + \mathrm{p} && 2.238 \\
&\rightarrow\; {}^{20}\mathrm{Ne} + \alpha && 4.616 \\
&\rightarrow\; {}^{16}\mathrm{O} + 2\alpha && -0.114
\end{aligned}
$$

The last column lists the energy gain in MeV. Here, the most probable reactions are those leaving ^{23}Na and ^{20}Ne. The next complication that arises, is that the proton and alpha particle produced in these two reactions immediately fuse with other particles (since for them, the temperatures are extremely high). As a result of these complications, the energy rate is rather uncertain. For some approximate values, see Kippenhahn & Weigert, p. 167.

For temperatures above 10^9 K, the photon energies become so large that they can lead to the break-up of not-so-tightly bound nuclei. Reaction rates analogous to the Saha equation for ionization can be written to determine equilibrium conditions. Generally, however, equilibrium will not be reached as time is most definitely running out if a star reaches these stages. A reaction which is important subsequent to Carbon burning is ${}^{20}\mathrm{Ne} + \gamma \rightarrow {}^{16}\mathrm{O} + \alpha$ (the *reverse* of the helium burning reaction). The alpha particles resulting from this photo-disintegration are captured faster by Neon (via ${}^{20}\mathrm{Ne} + \alpha \rightarrow {}^{24}\mathrm{Mg} + \gamma$) than by the Oxygen nuclei, and hence the net reaction is $2\,{}^{20}\mathrm{Ne} + \gamma \rightarrow {}^{16}\mathrm{O} + {}^{24}\mathrm{Mg} + \gamma$, with an energy gain of 4.583 MeV. This is called Neon burning.

The next phase is oxygen burning, for which temperatures in excess of 10^9 K are required. As for carbon burning, the reaction can proceed via a number of channels:

$$
\begin{aligned}
{}^{16}\mathrm{O} + {}^{16}\mathrm{O} \;&\rightarrow\; {}^{32}\mathrm{S} + \gamma && 16.541 \\
&\rightarrow\; {}^{31}\mathrm{S} + \mathrm{n} && 1.453 \\
&\rightarrow\; {}^{31}\mathrm{P} + \mathrm{p} && 7.677 \\
&\rightarrow\; {}^{28}\mathrm{Si} + \alpha && 9.593 \\
&\rightarrow\; {}^{24}\mathrm{Mg} + 2\alpha && -0.393
\end{aligned}
$$

For these reactions, the most frequent product is ^{31}P; next most frequent is ^{28}Si. Again, the small particles immediately lead to a multitude of other reactions. Among the end products will be a large amount of ^{28}Si.

At the end of Oxygen burning, photo-disintegration becomes more and more important. In particular, photo-disintegration of ^{28}Si leads to the ejection of protons, neutrons and alpha particles, which fuse with other ^{28}Si particles to form bigger nuclei that in turn are subjected to photo-disintegration. Still, gradually larger nuclei are built up, up to ^{56}Fe. Since iron is so strongly bound, it may survive as the dominant species. The whole process is called silicon burning.

For next time

- Think about what happens when the core has turned into Iron.
- Read ahead about stellar models: textbook §10.5 and Appendix H.

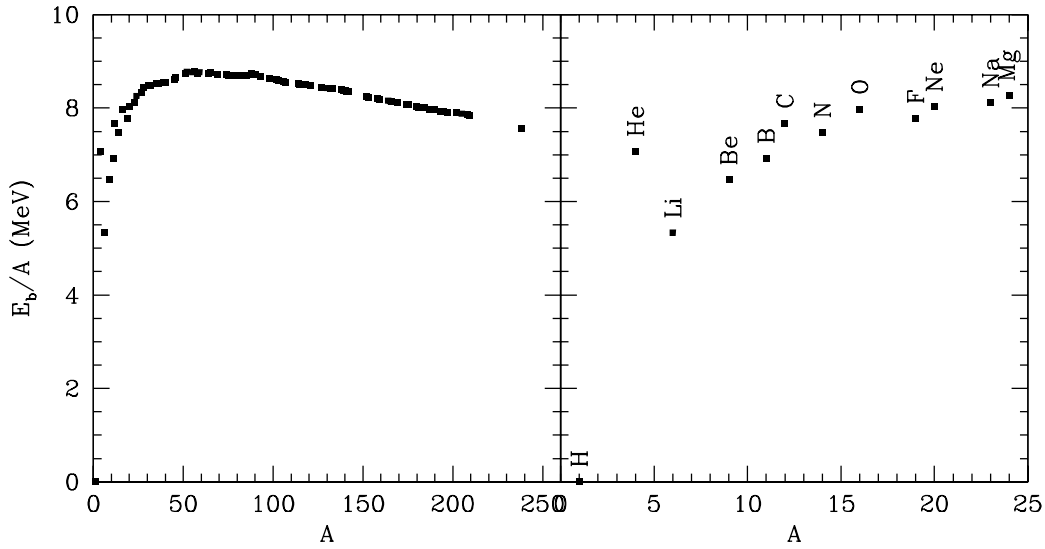

Fig. 8.1. Binding energy per nucleon for the different elements. In the right-hand panel an enlargement of the plot is shown and the elements are labeled. From Verbunt (2000, first-year lecture notes, Utrecht University).

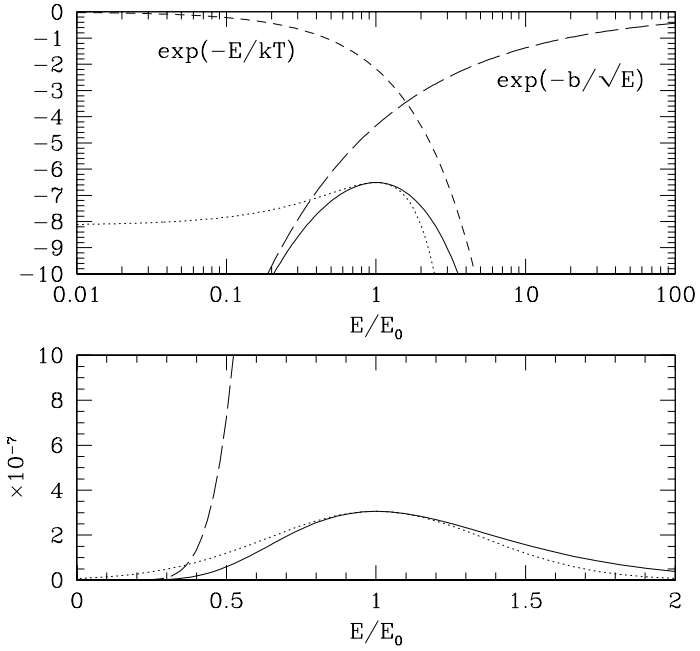

Fig. 8.2. Gamow peak resulting from the competing exponential terms: (1) from the Maxwellian (short-dashed line: $\propto \exp(-E/kT)$, with $kT = 0.2\,E_0$ here), and (2) from the penetration probability (long-dashed line: $\propto \exp(-b/\sqrt{E})$, with $b = 10\sqrt{E_0}$ here). The solid line indicates the product, and the dotted line the approximating Gaussian discussed in the text. *Upper panel:* logarithmic scale; *lower panel:* linear scale.

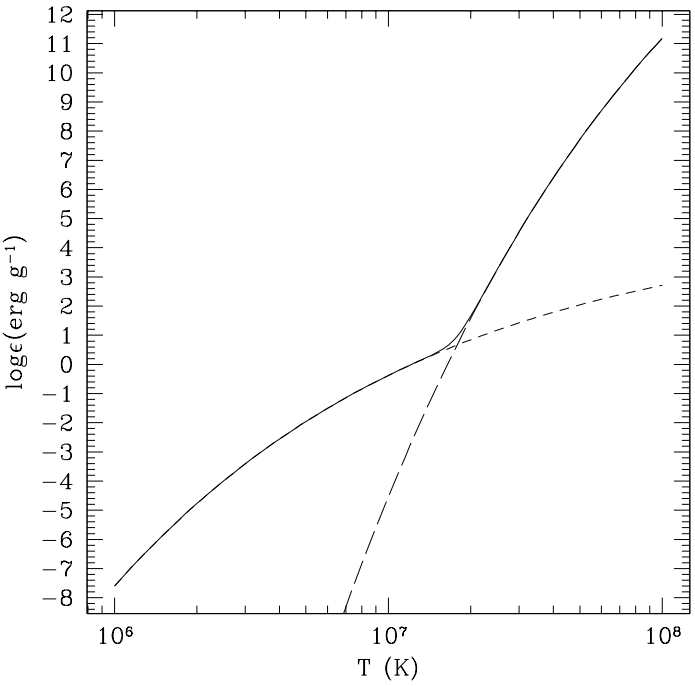

Fig. 8.3. Energy generation rates for matter with $\rho = 10\,\mathrm{g\,cm^{-3}}$, $X_1 = 0.7$, $X_{\mathrm{CNO}} = 0.01$, and a range of temperatures. The contributions from the p-p chain (short-dashed) and CNO cycle (long-dashed) are also indicated separately.

9. Stellar Models

Textbook: §10.5, App. H

The problem

To calculate a star's structure, we need to solve the equations of hydrostatic equilibrium, mass continuity, energy balance, and energy transport. It makes most sense to write these in terms of fractional mass M_r rather than fractional radius r (since composition profiles are determined by the position in terms of M_r, which, unlike r, does not change when the star expands or contracts). The mass continuity equation (Eq. 1.3) can be used to put the equations into the following form:

$$\text{[mass continuity (Eq. 1.3)]:} \quad \frac{\mathrm{d}r}{\mathrm{d}M_r} = \frac{1}{4\pi r^2 \rho} \,, \tag{9.1}$$

$$\text{[hydrostatic equilibrium (Eq. 1.2)]:} \quad \frac{\mathrm{d}P}{\mathrm{d}M_r} = -\frac{GM_r}{4\pi r^4} \,, \tag{9.2}$$

$$\text{[energy balance (Eq. 8.1)]:} \quad \frac{\mathrm{d}L_r}{\mathrm{d}M_r} = \epsilon_{\rm nuc} - \epsilon_\nu + \epsilon_{\rm grav} \,, \tag{9.3}$$

$$\text{[generalized Eddington equation]:} \quad \frac{\mathrm{d}T}{\mathrm{d}M_r} = -\frac{GM_rT}{4\pi r^4 P}\nabla_* \,. \tag{9.4}$$

In Eq. 9.4, depending on whether the layer is radiative or convective, one has

$$\nabla_* = \begin{cases} \nabla_{\rm rad} = \dfrac{3}{16\pi acG}\dfrac{\kappa L_r P}{M_r T^4} & \text{(radiative layers)} \,, \\ \nabla_{\rm ad} + \nabla_{\rm sa} & \text{(convective layers)} \,. \end{cases} \tag{9.5}$$

Here, $\nabla_{\rm sa}$ is the super-adiabatic part of the gradient (i.e., $\nabla_{\rm sa} \equiv \nabla_{\rm conv} - \nabla_{\rm ad}$); $\nabla_{\rm sa}$ can be neglected in the interior (where $\nabla_{\rm conv} \simeq \nabla_{\rm ad}$) but not near the surface (where $\nabla_{\rm conv} > \nabla_{\rm ad}$). The condition for convection can either be the Ledoux or the Schwarzschild criterion.

Evolution consists of thermal adjustments (via $\epsilon_{\rm grav}$) and changes in the abundances, due to the fusion reactions that proceed with rates $r_{a,b}$ (Eq. 8.8 — note that $\langle\sigma v\rangle$ is a function of T):

$$\frac{\mathrm{d}X_i}{\mathrm{d}t} = \frac{m_i}{\rho}\left(\sum_{j,k} r_{j,k(\to i)} - \sum_{k'}(1+\delta_{i,k'})\, r_{i,k'}\right), \qquad i = 1, \ldots, I \,, \tag{9.6}$$

where i labels all isotopes being considered, $r_{j,k(\to i)}$ are reactions that produce isotope i (from j and k), and $r_{i,k'}$ are reactions that destroy i (and also k'). One of the relations can be replaced by the normalization condition, $\sum_i X_i = 1$ (or this condition can be used to check that you have coded the nuclear reactions correctly!). Furthermore, the abundances should be mixed in convective (and semi-convective) zones, taking account of possible overshooting.

In the above equations, we assume that the equation of state, the opacity, and the nuclear reactions are known functions of composition, temperature, and either density or pressure – these are equivalent, as the usual expression of the equation of state $P = P(\rho, T, X_i)$ can be inverted and expressed as $\rho = \rho(P, T, X_i)$ instead. In other words, as functions of (ρ, T, X_i) or (P, T, X_i), we have:

Equation of state:	$\{\ P(\rho,T,X_i)$ or $\rho(P,T,X_i)\ \},\ \nabla_{\rm ad},\ s,\ C_V,\ C_P,\ \left(\frac{\partial \ln P}{\partial \ln T}\right)_\rho \,,\ \left(\frac{\partial \ln P}{\partial \ln \rho}\right)_T$
Opacity (incl. conduction):	κ
Nuclear reaction rates:	$r_{j,k},\ \epsilon_{\rm nuc},\ \epsilon_\nu$

[Note that equation-of-state quantities s, C_V, C_P, $\left(\frac{\partial \ln P}{\partial \ln T}\right)_\rho$, and $\left(\frac{\partial \ln P}{\partial \ln \rho}\right)_T$ enter into $\epsilon_{\rm grav}$ and the formulae that can be used to obtain $\nabla_{\rm conv}$ in regions where $\nabla_{\rm sa}$ is not negligible.] With the above given, there are as many differential equations as unknowns.

While the equations can be expressed equally well in terms of (ρ, T, X_i), for simplicity, we will assume hereafter that the above are expressed as functions of (P, T, X_i). The unknowns are then $(P, r, L_r, T, X_1, \ldots, X_I)$, whose dependence as a function of M_r and t is to be determined. For this purpose, we need boundary conditions at $M_r = 0$ and $M_r = M$ and initial values for the composition X_i and gravitational energy (e.g., an entropy profile).

Boundary conditions

The inner boundary condition is simple: $r = 0$, $L_r = 0$ for $M_r = 0$. Unfortunately, we cannot put any a priori constraints on $P_{\rm c}$ and $T_{\rm c}$, so that integrating from the centre outwards we have families of two-parameter solutions $r(P_{\rm c}, T_{\rm c})$ and $L_r(P_{\rm c}, T_{\rm c})$. For small M_r, we can write these functions as expansions in M_r,

$$r(P_{\rm c}, T_{\rm c}) \;=\; \left(\frac{3}{4\pi\rho_{\rm c}}\right)^{1/3} M_r^{1/3} \;, \tag{9.7}$$

$$L_r(P_{\rm c}, T_{\rm c}) \;=\; (\epsilon_{\rm nuc,c} - \epsilon_{\nu,{\rm c}} + \epsilon_{\rm grav,c})\, M_r \;, \tag{9.8}$$

where $\rho_{\rm c}$ and the various $\epsilon_{\rm c}$ are known functions of $(P_{\rm c}, T_{\rm c})$. These expansions are often more useful than the $M_r = 0$ conditions, since Eqs. 9.1, 9.2, and 9.4 become indeterminate at $M_r = 0$.

At the surface, we will have conditions for P and T, but R and L are unknown a priori, leading to a situation similar to that in the centre: for given M, R, and L, one can calculate $\log g$ and $T_{\rm eff}$, which determine the run of pressure and temperature in the atmosphere. Thus, integrating from the surface downwards we have families of two-parameter solutions $P(R, L)$ and $T(R, L)$. Unfortunately, the surface condition is not simple. One could use $P = 0$, $T = 0$ for $M_r = M$, but for convective envelopes this leads to gross errors. Somewhat more elegant is to use the photosphere, where $T_{\rm eff} = (L/4\pi R^2\sigma)^{1/4}$ and $P_{\rm phot} = 2g/3\kappa$. The condition for the pressure is derived from requiring $\tau = \frac{2}{3}$ at the photosphere, as was done in the discussion of the Hayashi line (Eq. 7.1); for κ, a suitably chosen average of the opacity above the photosphere has to be used in order to get an accurate value for $P_{\rm phot}$ (see Fig. 9.1).

The main problem with these simple boundary conditions is that near the surface the assumptions underlying the energy transport equation break down: the photon mean-free path becomes substantial. In these regions, much more detailed radiative transfer calculations are required. One can use a simple "grey atmosphere" approximation (in which one assumes that the opacity κ_ν is equal to the Rosseland value, independent of wavelength) to perform an approximate integral over the atmosphere. An alternate solution to this problem is to leave it to those interested in detailed stellar atmospheres, and use a grid of their results. For given (R, L), one calculates $T_{\rm eff}$ and $\log g$, and uses this to to interpolate in the (R, L, M) grid of model atmosphere results to find P_*, T_* at the bottom of the atmosphere.

Computational methods

There are several ways one could attempt to calculate stellar models and evolution numerically. First consider the case where $X_i(M_r)$ and $\epsilon_{\rm grav}(M_r)$ are known, i.e., where we have to solve just the structure of the star.

In principle, one could simply start integrating from both sides for trial values of $(P_{\rm c}, T_{\rm c})$ and (R, L), and try to match the two solutions at some intermediate fitting point, by varying the trial values. This is called the *shooting method*. In general, given a good scheme, the solution converges quickly (the program `statstar` in CO, App. H, is a simple example; see NUMERICAL RECIPES, § 17.2 for more details). It is not very efficient, however, if one wants to calculate the evolution,

in which the star evolves through a series of spatial models which are very similar. For this case, it is better to use a method which uses the spatial model from a previous step as an initial guess and makes small adjustments in order to find the new equilibrium. Most commonly used for this purpose is the *Henyey method*, which is especially well-suited for solving differential equations with boundary conditions on both sides.

The method works as follows. Take a grid of points $M_r^{(j)}$, with $j = 1, \ldots, N$. Then, discretise the differential equations, bring both sides to the left-hand side, and call these $A_i^{(j)}$. Then, a solution will be given by

$$A_i^{(j)} \;=\; \frac{y_i^{(j+1)} - y_i^{(j)}}{M_r^{(j+1)} - M_r^{(j)}} \;-\; f_i(M_r^{(j+\frac{1}{2})}, y_1^{(j+\frac{1}{2})}, y_2^{(j+\frac{1}{2})}, y_3^{(j+\frac{1}{2})}, y_4^{(j+\frac{1}{2})}) = 0 \,, \qquad i = 1, \ldots, 4 \,, \quad j = 1, \ldots, N-1 \tag{9.9}$$

where $y_1, \ldots, y_4$ are the four variables of interest (e.g., $y_1 = r$, $y_2 = P$, $y_3 = L_r$, $y_4 = T$), the index i numbers the four equations, and $f_1, \ldots, f_4$ are the right–hand side functions in the differential equations. The superscript $j + \frac{1}{2}$ is meant to indicate that a suitable average of the values at grid points j and $j + 1$ is taken (e.g., just a straight mean).

At the inner and outer boundaries, we have

$$\begin{aligned}
B_1^{(\mathrm{in})} &= r^{(1)} - r(P_\mathrm{c}, T_\mathrm{c}) = y_1^{(1)} - f_1^{(\mathrm{in})}(y_2^{(1)}, y_4^{(1)}) = 0 \,, \\
B_3^{(\mathrm{in})} &= L_r^{(1)} - L_r(P_\mathrm{c}, T_\mathrm{c}) = y_3^{(1)} - f_3^{(\mathrm{in})}(y_2^{(1)}, y_4^{(1)}) = 0 \,, \\
B_2^{(\mathrm{out})} &= P^{(N)} - P(R, L) = y_2^{(N)} - f_2^{(\mathrm{out})}(y_1^{(N)}, y_3^{(N)}) = 0 \,, \\
B_4^{(\mathrm{out})} &= T^{(N)} - T(R, L) = y_4^{(N)} - f_4^{(\mathrm{out})}(y_2^{(N)}, y_4^{(N)}) = 0 \,,
\end{aligned} \tag{9.10}$$

where we assumed one could determine $(P_\mathrm{c}, T_\mathrm{c})$ from the values at the first grid point and (R, L) from those at the last. Note that for the simple case for which $M_r^{(1)} = 0$, the functions $r(P, T)$ and $L_r(P, T)$ are identical to zero. If one choses to work in logarithmic units for $\{\rho, P, r, T\}$, however, the first point cannot be at $M_r = 0$, and therefore the inner boundary conditions are written in their more general form above. Thus, with the above definitions of A, B, a solution for the problem requires $A_i^{(j)} = 0$, $B_i = 0$.

Considering the whole grid, we have $4N$ unknowns $y_i^{(j)}$ and $4(N-1) + 2 + 2 = 4N$ equations. Now suppose that we have a first approximation $y_i^{(j)}(1)$ to the solution. For this initial guess, the constraints will not be met, i.e., $A_i^{(j)}(1) \neq 0$, $B_i(1) \neq 0$, and we need to find corrections $\delta y_i^{(j)}$ such that a second approximation $y_i^{(j)}(2) = y_i^{(j)}(1) + \delta y_i^{(j)}$ does give a solution, i.e., we are looking for changes $\delta y_i^{(j)}$ that imply changes $\delta A_i^{(j)}$, δB_i, such that $A_i^{(j)}(1) + \delta A_i^{(j)} = 0$, $B_i(1) + \delta B_i = 0$, or

$$\begin{aligned}
\delta B_i^{(\mathrm{in})} &= -B_i^{(\mathrm{in})}(1) \,, \qquad i = 1, 3 \\
\delta A_i^{(j)} &= -A_i^{(j)}(1) \,, \qquad i = 1, \ldots, 4 \,, \quad j = 1, \ldots, N-1 \\
\delta B_i^{(\mathrm{out})} &= -B_i^{(\mathrm{out})}(1) \,, \qquad i = 2, 4 \,.
\end{aligned} \tag{9.11}$$

For small enough corrections, we can expand the A and B linearly in $\delta y_i^{(j)}$, and write

$$\begin{aligned}
\sum_{k=1}^{4} \frac{\partial B_i^{(\mathrm{in})}}{\partial y_k^{(1)}} \delta y_k^{(1)} &= -B_i^{(\mathrm{in})} \,, \qquad i = 1, 3 \\
\sum_{k=1}^{4} \frac{\partial A_i^{(j)}}{\partial y_k^{(j)}} \delta y_k^{(j)} + \sum_{k=1}^{4} \frac{\partial A_i^{(j)}}{\partial y_k^{(j+1)}} \delta y_k^{(j+1)} &= -A_i^{(j)} \,, \qquad i = 1, \ldots, 4 \,, \quad j = 1, \ldots, N-1 \\
\sum_{k=1}^{4} \frac{\partial B_i^{(\mathrm{out})}}{\partial y_k^{(N)}} \delta y_k^{(N)} &= -B_i^{(\mathrm{out})} \,, \qquad i = 2, 4
\end{aligned} \tag{9.12}$$

[we have dropped the (1) numbering the 1st approximation]. This system has $2 + 4(N-1) + 2 = 4N$ equations which need to be solved for the $4N$ unknown corrections $\delta y_i^{(j)}$. In matrix form,

$$\mathcal{H} \begin{pmatrix} \delta y_1^{(1)} \\ \vdots \\ \delta y_i^{(j)} \\ \vdots \\ \delta y_4^{(N)} \end{pmatrix} = - \begin{pmatrix} B_1^{(\mathrm{in})} \\ \vdots \\ A_i^{(j)} \\ \vdots \\ B_4^{(\mathrm{out})} \end{pmatrix} , \tag{9.13}$$

where $\mathcal{H}$ is called the *Henyey matrix*. Generally, this matrix equation can be solved ($\det \mathcal{H} \neq 0$), but since we used a first-order expansion, the next approximation $y + \delta y$ will still not fulfill the conditions accurately. Thus, one iterates, until a certain pre-set convergence criterion is met.

Note that Henyey matrix has a relatively simple form, as can be seen by writing out which elements are actually used for the case $N = 3$,

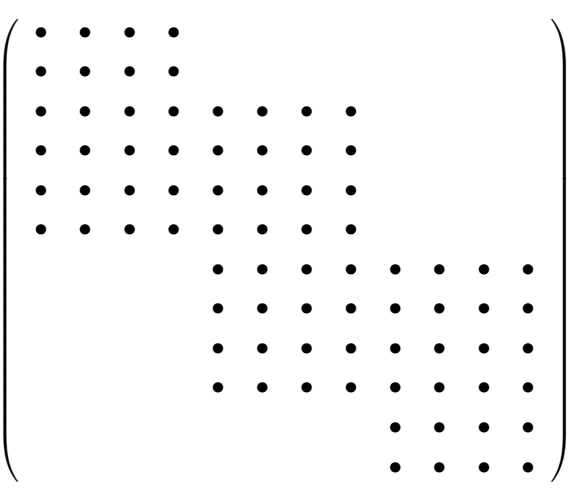

$$= - \begin{pmatrix} B_1^{(\mathrm{in})} \\ B_3^{(\mathrm{in})} \\ A_1^{(1)} \\ A_2^{(1)} \\ A_3^{(1)} \\ A_4^{(1)} \\ A_1^{(2)} \\ A_2^{(2)} \\ A_3^{(2)} \\ A_4^{(2)} \\ B_2^{(\mathrm{out})} \\ B_4^{(\mathrm{out})} \end{pmatrix} .$$

Here, the bullets indicate the elements that are used; all others are zero. Because of the simple structure, the solution can be found in a relative straightforward manner. See Numerical Recipes, § 17.3, for details, and for a method that is fast and minimizes storage.

Evolution

So far, we have ignored the chemical evolution and assumed that $\epsilon_{\rm grav}$ was a known function. The latter function can be estimated easily once we have made an initial model and want to compute a model one time step later, by approximating

$$\epsilon_{\rm grav}^{(j+\frac{1}{2})} = -T^{(j+\frac{1}{2})} \frac{\mathrm{d}}{\mathrm{d}t} s^{(j+\frac{1}{2})} = -\frac{T^{(j+\frac{1}{2})}}{\Delta t} \left(s^{(j+\frac{1}{2})} - s_{\rm prev}^{(j+\frac{1}{2})} \right), \tag{9.14}$$

Here, we expressed $\epsilon_{\rm grav}$ in terms of the entropy change, but the other expressions in Eq. 8.3 can be used in the same way. The point to note is that $s_{\rm prev}$, which is the entropy that the element had in the previous model, is known. Since the current entropy is a known function $s(P, T, X_i)$ (from the equation of state), also $\mathrm{d}s/\mathrm{d}t$ is a known function of (P, T, X_i). Thus, $\epsilon_{\rm grav}$ is a known function of (P, T, X_i) and can be used without problems in deriving the stellar structure. [A complication arises in convective regions, especially ones that are advancing into regions of different chemical composition. Mixing at constant pressure has no energy cost, but since it is an irreversible process, it results in an increase of entropy (which of course does *not* contribute towards $\epsilon_{\rm grav}$). On the other hand, when one is mixing the products of nuclear burning (i.e., *heavy* nuclei) outwards against gravity while mixing unburned stellar material (i.e., *light* nuclei) downwards, there is an energy cost involved in doing this (which is incurred throughout the region where material mixed upwards has a higher mean molecular weight than material mixed downwards). These effects may need to be accounted for correctly during stages when the star is evolving on a short timescale, which involves some modification of Eq. 8.3 for $\epsilon_{\rm grav}$.]

A scheme like the above for including a variable that changes in time is usually called an *implicit scheme*, since the time derivative is calculated implicitly, using parameters from the new model one is trying to determine. Schemes which rely only on previous model(s) are called *explicit*; these are often easier to code but in order to keep good accuracy small timesteps need to be taken.

For the abundances, an explicit scheme is simpler. In such a scheme, one determine the time derivatives $(\mathrm{d}X_i/\mathrm{d}t)_{\rm prev}$ from the previous models according to Eq. 9.6 and then for the next model uses

$$X_i = X_{i,\rm prev} + \Delta t \left(\frac{\mathrm{d}X_i}{\mathrm{d}t} \right)_{\rm prev}. \tag{9.15}$$

Note that it is also possible to calculate the chemical evolution using an implicit scheme. For a more detailed but quite readable discussion, see Eggleton (1971, MNRAS 151, 351). In the same reference, another choice of independent grid variable is discussed, which allows one to regrid the model automatically so that fine grid spacing is used where required.

For next time

– Read ahead about the main sequence: textbook §10.6, 13.1.

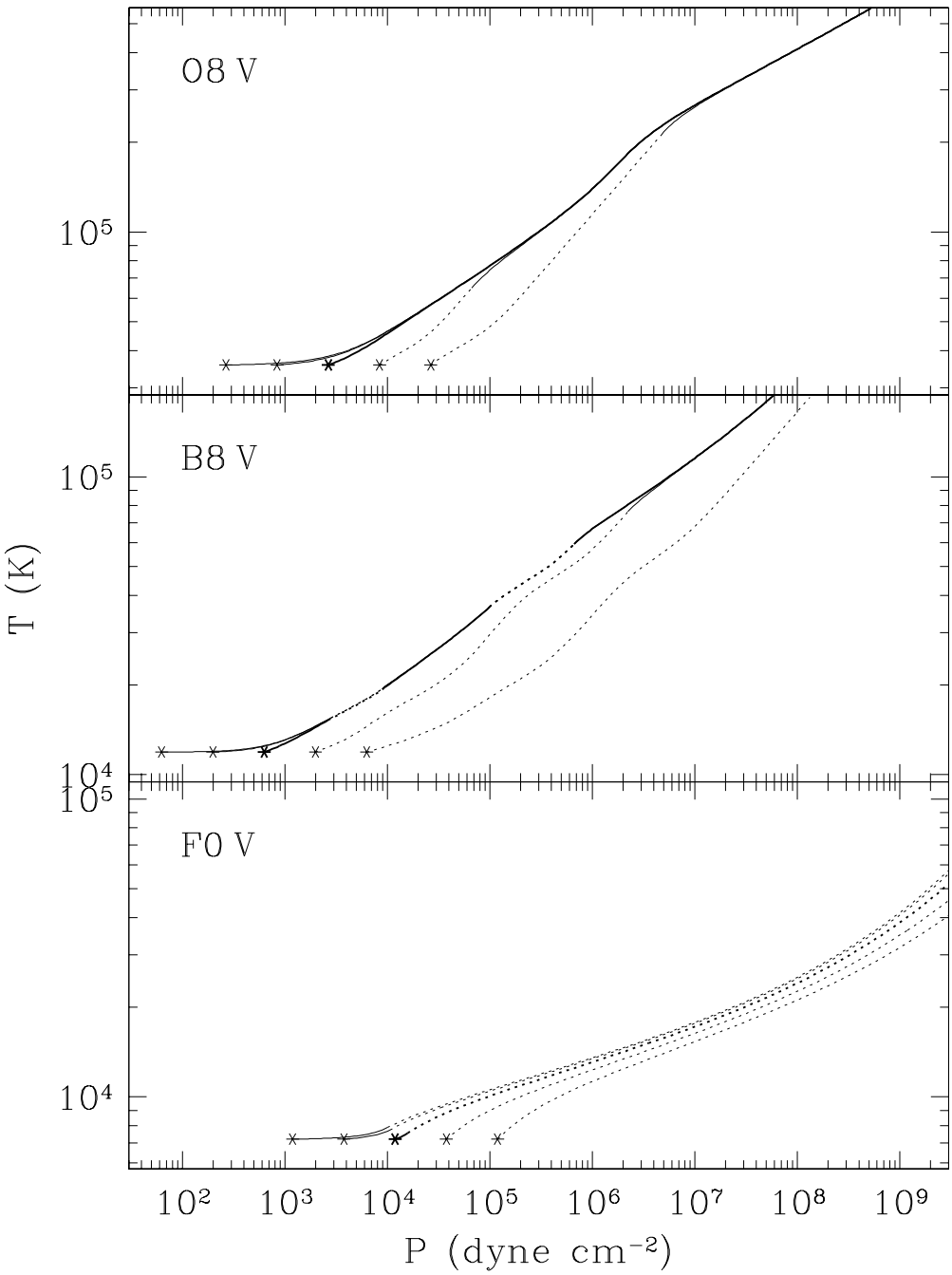

Fig. 9.1. Effect on the stellar envelope of choosing an incorrect value of $P_{\rm phot}$ in main sequence stars of solar metallicity, for a massive star with a fully radiative envelope (O8 V: $T_{\rm eff} \approx 37{,}000$ K, $M \approx 15\ M_\odot$), an intermediate mass star with very small convective zones in ionization regions (B8 V: $T_{\rm eff} \approx 12{,}000$ K, $M \approx 2.5\ M_\odot$), and a relatively low-mass star with a convective envelope of non-negligible extent (F0 V: $T_{\rm eff} \approx 7{,}200$ K, $M \approx 1.2\ M_\odot$). Star symbols ("$*$") indicate choices for $P_{\rm phot}$ at the relevant $T_{\rm eff}$, and lines indicate run of T with P inside the photosphere (solid lines indicate radiative regions, dashed lines indicate convective regions). **Heavy** symbols and lines indicate the **correct** models.

10. Main Sequence and Brown Dwarfs

Textbook: §10.6, 13.1 (p. 446–451)

Zero-age main sequence

The zero-age main sequence (ZAMS) is defined as the beginning of the long, stable period of core hydrogen burning during the star's lifetime. Stars burn up their (primordial) deuterium via $^2\mathrm{D}+\mathrm{p} \rightarrow {}^3\mathrm{He}+\gamma$ before this point, while they are still contracting towards the main sequence (see Fig. 10.1). Also, the *initial* carbon abundance in stars is much larger than the CN-cycle equilibrium value. For stars of solar metallicity of mass $\gtrsim 1\ M_\odot$, the reactions that convert $^{12}\mathrm{C}$ to $^{14}\mathrm{N}$ (part of the CN-cycle) can supply the star's total luminosity for a brief period at the start of hydrogen-burning. This stage is so short that it is often ignored — e.g., it is not shown in the evolutionary tracks of Fig. 10.2 below. In the pre–main-sequence evolutionary tracks of Fig. 7.3, this $^{12}\mathrm{C} \rightarrow {}^{14}\mathrm{N}$ stage causes the last, small upwards-and-downwards wiggle at the end (at left).

Brown Dwarfs

Stars of masses $\lesssim 0.08\ M_\odot$ do not ignite hydrogen burning in their cores (except possibly for the brief deuterium-burning stage): see the dashed lines in Fig. 10.1. Such stars are known as *brown dwarfs*. A reasonable number of them have been studied, and new spectral classes (e.g., L and T) have been defined to distinguish them via features in their infrared spectra.

Zero-age main sequence luminosity

For a crude estimate of the luminosity[1], we use the energy transport equation in terms of mass (Eq. 9.4), and apply it at $T \simeq \frac{1}{2}T_\mathrm{c}$, where we assume $L_r \simeq L$ [why?], $r \simeq \frac{1}{4}R$, (see Fig. 4.1 for $n = 3$ and also CO, Fig. 11.4), and take some appropriately averaged opacity $\overline{\kappa}$. Furthermore, we approximate $\mathrm{d}T/\mathrm{d}M_r \simeq T_\mathrm{c}/M$. Thus,

$$\frac{T_\mathrm{c}}{M} \simeq \frac{3}{64\pi^2 ac}\frac{\overline{\kappa}L}{(\frac{1}{4}R)^4(\frac{1}{2}T_\mathrm{c})^3} \simeq \frac{96}{\pi^2 ac}\frac{\overline{\kappa}L}{R^4T_\mathrm{c}^3} \quad \Rightarrow \quad L \simeq \frac{\pi^2 ac}{96}\frac{R^4T_\mathrm{c}^4}{\overline{\kappa}M}. \tag{10.1}$$

Expressing the central temperature in terms of the central pressure and density using the ideal gas law, and using the expressions for P_c and ρ_c appropriate for a polytrope with $n = 3$,

$$T_\mathrm{c} = \frac{\mu m_\mathrm{H}}{k}\frac{P_\mathrm{c,gas}}{\rho_\mathrm{c}} = 1.95\,10^7\ \mathrm{K}\ \mu\beta\left(\frac{M}{M_\odot}\right)\left(\frac{R}{R_\odot}\right)^{-1}, \tag{10.2}$$

where β was defined as the ratio of the gas pressure and the total pressure. Inserting this in Eq. 10.1,

$$\frac{L}{L_\odot} \simeq 10\ \frac{\mu^4\beta^4}{\overline{\kappa}}\left(\frac{M}{M_\odot}\right)^3. \tag{10.3}$$

Hot zero-age main-sequence stars

For a hot star, electron scattering dominates in the interior. Thus, $\overline{\kappa} \simeq 0.2(1+X)\,\mathrm{cm}^2\,\mathrm{g}^{-1}$ (Eq. 5.10). For a star with solar abundaces which has just arrived on the main sequence, $\mu \simeq 0.613$, and $L \simeq 4\,L_\odot\,(M/M_\odot)^3$. For intermediate-mass stars, this estimate agrees reasonably well with detailed models (see Fig. 10.2). The slope, however ($L \propto M^3$) is slightly too shallow between 2 and $8\,M_\odot$, where the detailed models give $L \propto M^{3.7}$; above $8\,M_\odot$ it is too steep. These effects are due to the presence of a central convection zone and the contribution of radiation pressure. The convection zone increases in size with increasing mass (see Fig. 10.3 and Table 10.1).

[1] See KW, chapter 20, for somewhat less crude approximations.

Table 10.1. Fractional sizes of the convective core in main-sequence stars

	ZAMS				TAMS			
M_* ($M_\odot$)	$\log L$ ($L_\odot$)	$\log T_{\rm eff}$ (K)	$M_{\rm cc}$ ($M_\odot$)	$M_{\rm cc}/M$	t (yr)	M_* ($M_\odot$)	$M_{\rm cc}$ ($M_\odot$)	$M_{\rm cc}/M$
120	6.254	4.739	102.4	0.853	$2.9\ 10^6$	80.9	63.6	0.786
60	5.731	4.693	46.3	0.772	$3.7\ 10^6$	43.0	27.5	0.640
20	4.643	4.552	10.8	0.540	$8.8\ 10^6$	19.1	6.5	0.339
5	2.720	4.244	1.52	0.304	$9.9\ 10^7$	5	0.39	0.078
2	1.177	3.952	0.46	0.229	$1.7\ 10^9$	2	0.13	0.065
1	−0.207	3.732	0	0	$9.7\ 10^9$	1	0	0

Cool zero-age main-sequence stars

For stars with $M \lesssim 1\,M_\odot$, the opacity is dominated by bound-free processes. Inserting the estimate Eq. 5.16 in Eq. 10.3, and using $\rho \simeq \frac{1}{8}\rho_{\rm c} \simeq 7\,\overline{\rho}$ (for an $n = 3$ polytrope) as well as Eq. 10.2,

$$\frac{L}{L_\odot} \simeq 0.07\,\frac{\mu^{7.5}}{Z(1+X)}\left(\frac{M}{M_\odot}\right)^{5.5}\left(\frac{R}{R_\odot}\right)^{-0.5}. \tag{10.4}$$

Thus, given that R depends approximately linearly on M, we find a very steep mass-luminosity relation, much steeper than that observed or inferred from models. Furthermore, the luminosity of the Sun is underestimated ($L \simeq 0.05\,L_\odot$ for $\mu = 0.613$, $Z = 0.02$, $X = 0.708$). The reason this does not work as well as for the massive stars, is that with decreasing mass, more and more of the outer region becomes convective; see Fig. 10.3. Only $\sim 2\%$ of the Sun's mass is convective (although this is nearly the outer $\sim 30\%$ of the Sun's radius), so a $n = 3$ polytrope is not completely unreasonable, but stars of $M \lesssim 0.2\,M_\odot$ are completely convective (so a $n = 1.5$ polytrope would be more appropriate). Furthermore, for very low masses, degeneracy becomes important.

Evolution on the main sequence

For both hot and cool stars, the luminosity scales with a high power of the mean molecular weight. As hydrogen is burnt, μ increases, and therefore the luminosity will increase as well, as can be seen in Fig. 10.2. Numbers for parameters at the beginning and end of the main sequence for massive stars are given in Table 10.1.

For next time

- Make sure you understand *why* the slopes from the simple estimates are somewhat different from those from detailed models.
- Read about the end of the main sequence: remainder of §13.1.

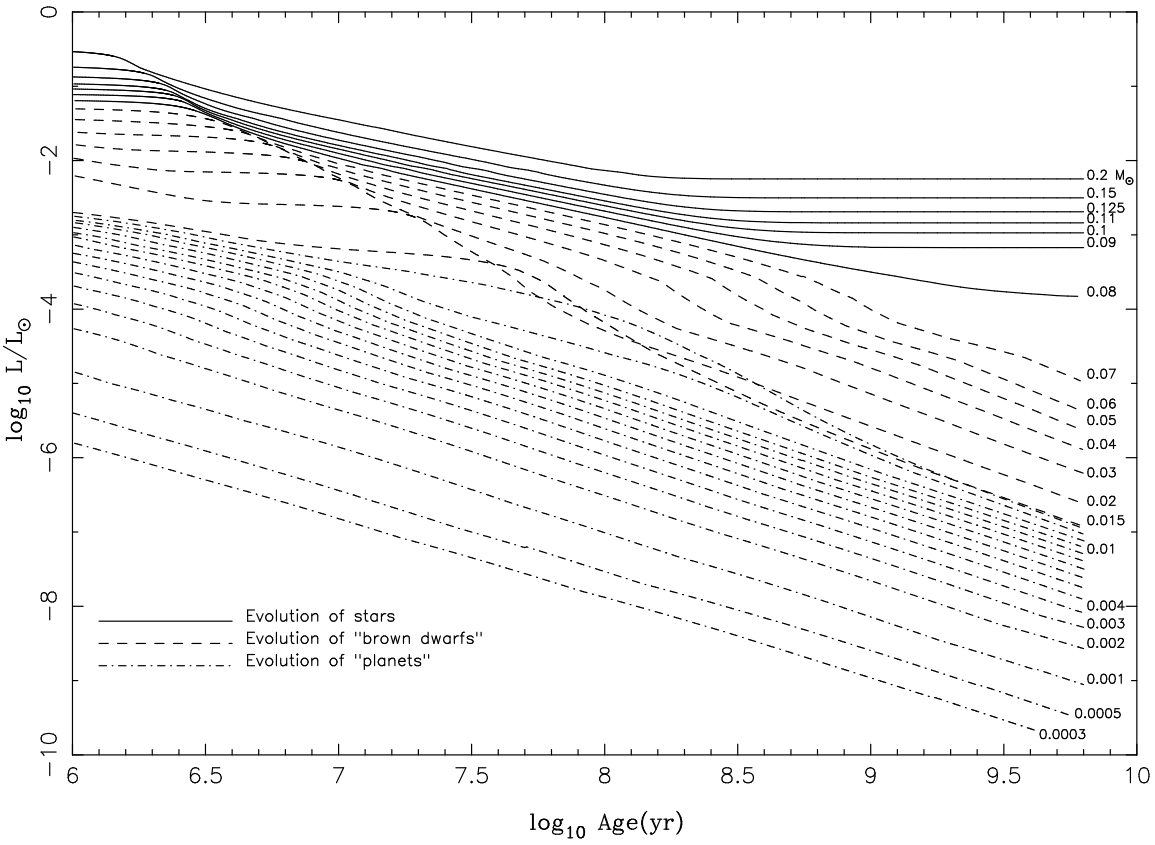

Fig. 10.1. Luminosity as a function of time for very low mass stars (*solid lines*) and brown dwarfs (*dashed lines*). The horizontal plateaus in the tracks at upper left show where the period of deuterium burning halts the pre–main-sequence luminosity decline (for a period of up to a few million years) in very low mass stars, as well as in brown dwarfs. Brown dwarfs models of mass $< 0.015\ M_{\odot}$ (i.e., less than about 15 Jupiter masses) have been designated as "planets" (*dot-dashed lines*) in this figure.

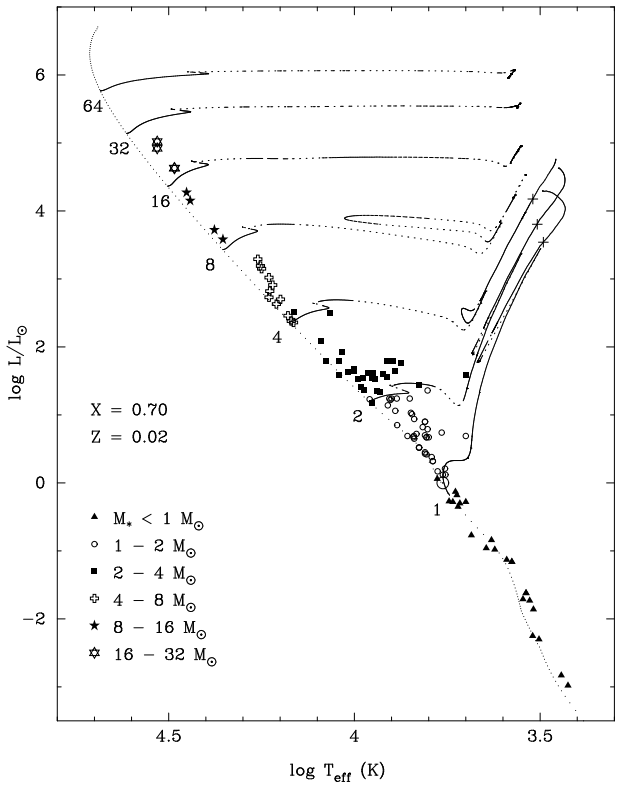

Fig. 10.2. HRD for the ZAMS and several evolutionary tracks, calculated with the Eggleton evolutionary code. The labels are masses in solar units. The symbols indicate components of binaries for which the masses, radii, and luminosities were determined observationally. For the tracks, the solid, dotted, and dashed portions indicate where evolution is on a nuclear, thermal, and intermediate time scale, respectively (evolution is upwards and rightwards from the ZAMS; the brief initial $^{12}C \rightarrow {}^{14}N$ stage is not shown). For masses $\geq 2\ M_\odot$, the end of the main sequence occurs at the first wiggle in the tracks, a bit to the right of the ZAMS. From Pols et al. (1995, MNRAS 274, 964).

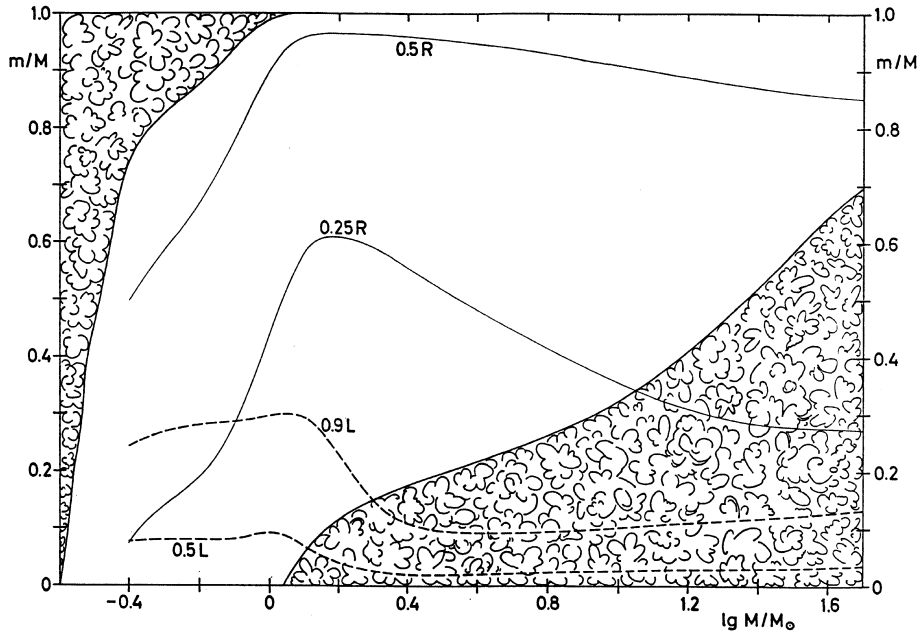

Fig. 10.3. Mass fraction $m/M \equiv M_r/M$ as a function of stellar mass M at the ZAMS. Convective regions are indicated with the curls. The solid lines indicate the fractional masses at which $r/R = 0.25$ and 0.5, and the dashed ones those at which $L_r/L = 0.5$ and 0.9. Taken from KW (their Fig. 22.7).

11. The end of the main sequence

Textbook: §13.1, p. 451ff

Hydrogen exhaustion in the core

For more massive stars, hydrogen exhaustion will happen in a larger region at the same time, while for less massive stars, it will initially just be the centre itself. Since in the core one gets $L_r = 0$, also the temperature gradient $\mathrm{d}T/\mathrm{d}r = 0$, i.e., the core will become isothermal.

From our discussion of polytropes, it was clear that completely isothermal stars cannot exist ($\gamma = 1$ and $n = \infty$), but is it possible to have an isothermal core? In the context of polytropes, one could rephrase this as the requirement that averaged over the whole star one has $\overline{\gamma} > 1.2$ ($\overline{n} < 5$). The result is that for a star in hydrostatic equilibrium, only a relatively small fraction of its mass can be in an isothermal core.

Schönberg-Chandrasekhar limit

For the isothermal core, one can rederive the virial theorem for the case that the pressure external to the object under consideration is not equal to zero. One finds

$$2U_{\rm core} = -\Omega_{\rm core} + 4\pi R_{\rm core}^3 P_{\rm core}, \tag{11.1}$$

where $P_{\rm core}$ is the pressure at the outer boundary of the core.

For an isothermal core (and ideal gas), the internal energy is simply $U_{\rm core} = \frac{3}{2} N_{\rm core} k T_{\rm core}$, with $N_{\rm core} = M_{\rm core}/m_{\rm H}\mu_{\rm core}$ the number of particles in the core. Writing $\Omega_{\rm core} = -q_{\rm core} G M_{\rm core}^2/R_{\rm core}$, and solving for $P_{\rm core}$, one finds,

$$P_{\rm core} = \frac{3}{4\pi}\frac{kT_{\rm core}}{m_{\rm H}\mu_{\rm core}}\frac{M_{\rm core}}{R_{\rm core}^3} - \frac{q_{\rm core}}{4\pi}\frac{GM_{\rm core}^2}{R_{\rm core}^4}. \tag{11.2}$$

Thus, the expression contains two competing terms, the thermal pressure ($\sim \overline{\rho} T_{\rm core}$) and the self-gravity ($\sim R_{\rm core}\overline{\rho g}$). Now consider an isothermal core with fixed mass $M_{\rm core}$. For very low external pressure $P_{\rm env}$, the core can provide a matching $P_{\rm core}$ for relatively large radius where the thermal term dominates. For increasing external pressure, the radius has to decrease, but clearly at some point the self-gravity will become important, and it becomes impossible to provide a matching $P_{\rm core}$. This maximum pressure can be determined by taking the derivative of Eq. 11.2 with respect to radius[2], and setting it equal to zero. One finds,

$$R_{\rm core} = \frac{4}{9} q_{\rm core} G M_{\rm core}\frac{m_{\rm H}\mu_{\rm core}}{kT_{\rm core}} \quad \Rightarrow \quad P_{\rm core,max} = \frac{3}{16\pi}\left(\frac{9}{4}\right)^3\left(\frac{kT_{\rm core}}{m_{\rm H}\mu_{\rm core}}\right)^4\frac{1}{q_{\rm core}^3 G^3 M_{\rm core}^2}. \tag{11.3}$$

Thus, $P_{\rm core,max} \propto T_{\rm core}^4/\mu_{\rm core}^4 M_{\rm core}^2$, i.e., the maximum pressure an isothermal core can withstand *decreases* with increasing core mass.

For the pressure exerted by the envelope, generally $P \approx GM^2/R^4$, $\rho \approx M/R^3$, and, since also $P_{\rm env} = kT_{\rm env}\rho_{\rm env}/m_{\rm H}\mu_{\rm env}$, $T_{\rm env} \approx (m_{\rm H}\mu_{\rm env}/k)(GM/R)$. Combining,

$$P_{\rm env} = C_{\rm env}\frac{1}{G^3M^2}\left(\frac{kT_{\rm env}}{m_{\rm H}\mu_{\rm env}}\right)^4, \tag{11.4}$$

where $C_{\rm env}$ is a constant depending on the precise structure of the envelope.

At the boundary, $T_{\rm env} = T_{\rm core}$ and $P_{\rm env} < P_{\rm core,max}$, i.e.,

$$C_{\rm env}\frac{1}{G^3M^2}\left(\frac{kT_{\rm core}}{m_{\rm H}\mu_{\rm env}}\right)^4 < C_{\rm core}\left(\frac{kT_{\rm core}}{m_{\rm H}\mu_{\rm core}}\right)^4\frac{1}{G^3M_{\rm core}^2}. \tag{11.5}$$

[2] In CO, p. 492, the derivative is taken with respect to mass. This is rather illogical.

Inserting numerical values of $C_{\rm core}$ and $C_{\rm env}$ obtained from more detailed studies, one finds

$$\frac{M_{\rm core}}{M} \lesssim 0.37 \left(\frac{\mu_{\rm env}}{\mu_{\rm core}}\right)^2, \tag{11.6}$$

For a helium core ($\mu_{\rm core} \simeq \frac{4}{3}$) and an envelope with roughly solar abundances[3] ($\mu_{\rm env} \simeq 0.6$), one thus finds a limiting fractional mass $M_{\rm SC} \simeq 0.08M$.

As a function of mass

With the above, we can describe what will happen when hydrogen is exhausted in the core,

- For massive stars ($M \gtrsim 6\,M_\odot$), the convective core at hydrogen exhaustion exceeds 8% of the total mass (see Table 10.1). Thus, an isothermal core cannot form. Instead, the core will contract until helium fusion starts. This happens on a thermal timescale, and causes the star to become a red giant (see next chapter).
- For intermediate-mass stars ($1.4 \lesssim M \lesssim 6\,M_\odot$), an isothermal core will form once hydrogen is exhausted in the centre. Around this core, hydrogen burning will continue, leading to growth of the core. This phase of the evolution is called the *sub-giant* branch. It will continue until the mass of the core exceeds 8% of the total mass, at which time the core has to contract, and the star becomes a red giant on the thermal timescale, as above. For stars more massive than $M \gtrsim 2.4\,M_\odot$, the contraction will be stopped by the ignition of helium burning, while for lower masses degeneracy sets in.
- For low-mass stars ($M \lesssim 1.4\,M_\odot$), the isothermal core becomes degenerate before the critical mass fraction is reached, and no rapid phase of contraction occurs. Thus, the star moves to the red-giant branch on the nuclear time scale of the shell around the core.

For next time

- Ensure you understand why stars of different mass behave differently when Hydrogen is exhausted in their cores.

[3] In general, some processed material will be present in the envelope as well.

12. The various giant branches

Textbook: This supplements (and partly *replaces*) §13.2

General considerations

From observations, we see that stars which have left the main sequence, cluster predominantly near low temperatures, but high luminosity. Thus, their radii are large, i.e., they are giants. From observations of globular clusters, one finds that even low-mass stars can become extremely luminous in this phase (see Fig. 1.2). The two basic questions to be addressed are why stars become so cool, and how they can become so much more luminous than they were on the main sequence. Both properties are reproduced in stellar models, but it is not always simple to point to a specific reason why a star behaves as it does. Indeed, even in the last decade there have been a number of articles with titles like "why stars inflate to and deflate from red giant dimensions" (Renzini et al., 1992, ApJ 400, 280) and, in response, "on why intermediate-mass stars become giants after the exhaustion of hydrogen in their cores" (Iben, 1993, ApJ 415, 767). Out of necessity, therefore, the discussion in this chapter will be somewhat vague. To give a framework, schematic evolutionary tracks for a low-mass ($1\,M_\odot$), an intermediate-mass ($5\,M_\odot$), and a high-mass ($25\,M_\odot$) star are shown in Fig. 12.1. One sees that intermediate-mass stars go through the most contorted track. Therefore, the track for the $5\,M_\odot$ case is shown in more detail as well, with the important physical processes in the various phases indicated; since this track was taken from an early (less accurate) computation, more recent evolutionary tracks are shown in Fig. 12.2, plus a schematic $5\,M_\odot$ case (Fig. 12.3) and $1\,M_\odot$ case (Fig. 12.4) with insets showing schematically the abundance profiles at various stages during the star's evolution.

Regarding the question of the increase in luminosity seen for giants, it is worthwhile to think back to what determines the luminosity on the main sequence. There, in essence, the luminosity is determined by how quickly the envelope can transfer and radiate energy; the star will contract until nuclear fusion generates a matching amount of energy in the core. The principal difference for a giant is that the burning occurs in a shell, whose properties are not just determined by the envelope above, but also by the core below.

As a star's envelope expands and it becomes a red giant (approaching the Hayashi track), the convective envelope eventually comprises most of the tenuous envelope. In other words, the base of the convective envelope moves inwards in mass M_r (though not necessarily in radius), reaching into regions that had been partially processed by nuclear burning on the main sequence (CN-cycle and p-p chain reactions). This processed material is thus mixed throughout the convective envelope to become visible at the star's surface, a process known as **"first dredge-up"** (this stage is indicated in Figs. 12.3 and 12.4). This yields reduced $^{12}\mathrm{C}/^{13}\mathrm{C}$ and C/N ratios at the stellar surface; observations of these ratios in stars during this stage of evolution are in fairly good agreement with what is predicted by computational models.

Low mass giants

For low-mass stars, the contraction of the core after hydrogen exhaustion is stopped by electron degeneracy pressure before the core becomes hot enough for helium ignition. Therefore, the Schönberg-Chandrasekhar limit becomes irrelevant, and the core can grow until something more drastic happens. Since no energy is generated within the core, the temperature in the whole core will equilibrate with that in the surrounding hydrogen-burning shell.

Shell burning around a degenerate core

In the layers near the dense, concentrated core, the pressure structure is dominated by the strong gravitational attraction of the core rather than by the pressure of the overlying envelope. The core

Table 12.1. Dependencies of ρ, T, P, and L in a shell on $M_{\rm core}$ and $R_{\rm core}$.

case	η	ν	α_1	α_2	β_1	β_2	γ_1	γ_2	δ_1	δ_2
CNO, hot	2	13	-3	2.33	1	-1	-2	1.33	7	-5.33
CNO, cool	2	16	-4	3.33	1	-1	-3	2.33	8	-6.33
triple-α	3	22	-4.5	4	1	-1	-3.5	3	8.5	-7

Taken from Refsdal & Weigert (1970, A&A 6, 426). For all cases, it is assumed that electron scattering dominates the opacity (i.e., $a = b = 0$).

becomes more and more dominant as the star evolves, since the core grows in mass and shrinks in size, while the envelope becomes more and more tenuous.

In the limit that the envelope can be considered weightless, and the shell contains a mass much smaller than that of the core (and provided also that the base of the convective envelope does not actually reach *into* the burning shell — see "hot bottom burning" below), the properties of the shell depend only on the mass $M_{\rm core}$ and radius $R_{\rm core}$ of the core. This implies that the length scale in the shell will be set by $R_{\rm core}$, i.e., that if one compares models for different $(M_{\rm core}, R_{\rm core})$, the run of pressure, density, etc., with $r/R_{\rm core}$ will be very similar. For instance, if in a given model, $P/P_{\rm core} = f(r/R_{\rm core})$, where $P_{\rm core}$ is the pressure at the bottom of the shell (i.e., the outer boundary of the core) and $f(r/R_{\rm core})$ a functional dependence on $r/R_{\rm core}$, one then expects that in another model $P'/P'_{\rm core} = f(r'/R'_{\rm core})$. This expectation is confirmed by real models (see Fig. 12.5). Refsdal & Weigert (1970, A&A 6, 426) used such assumptions to derive the dependencies of $\rho(r/R_{\rm core})$, $T(r/R_{\rm core})$, $P(r/R_{\rm core})$, and $L_r(r/R_{\rm core})$ on $M_{\rm core}$ and $R_{\rm core}$ (see also KW, § 32.2). They assumed the ideal gas law, an opacity law $\kappa = \kappa_0 P^a T^b$, and energy production $\epsilon = \epsilon_0 \rho^{\eta-1} T^\nu$ (via reactions with η reactants, where $\eta = 2$ except for the 3α reaction), and found

$$\begin{array}{lllllll}
\rho(r/R_{\rm core}) & \propto & M_{\rm core}^{\alpha_1} R_{\rm core}^{\alpha_2}, & \alpha_1 = -\frac{\nu-4+a+b}{\eta+1+a}, & & \alpha_2 = \frac{\nu-6+a+b}{\eta+1+a}, \\
T(r/R_{\rm core}) & \propto & M_{\rm core}^{\beta_1} R_{\rm core}^{\beta_2}, & \beta_1 = 1, & & \beta_2 = -1, \\
P(r/R_{\rm core}) & \propto & M_{\rm core}^{\gamma_1} R_{\rm core}^{\gamma_2}, & \gamma_1 = 1 - \frac{\nu-4+a+b}{\eta+1+a}, & & \gamma_2 = -1 + \frac{\nu-6+a+b}{\eta+1+a}, \\
L_r(r/R_{\rm core}) & \propto & M_{\rm core}^{\delta_1} R_{\rm core}^{\delta_2}, & \delta_1 = \nu - \eta\,\frac{\nu-4+a+b}{\eta+1+a}, & & \delta_2 = -\nu + 3 + \eta\,\frac{\nu-6+a+b}{\eta+1+a}.
\end{array} \tag{12.1}$$

One sees that the temperature scales with $M_{\rm core}/R_{\rm core}$ independent of details (a, b, n, ν) of the energy generation process and the opacity law (indeed, the scaling follows directly from hydrostatic equilibrium and the ideal gas law). Thus, for a degenerate core with $R_{\rm core} \propto M_{\rm core}^{-1/3}$, one expects $T \propto M_{\rm core}^{4/3}$. The implied strong dependence of the luminosity on the core mass is only partly offset by the fact that the pressure and density actually decrease with increasing $M_{\rm core}$. Indeed, from numerical values (see Table 12.1), one sees that one has stellar luminosity $L \propto M_{\rm core}^{\sim 9}$ for a shell in which hydrogen is burned via the CNO cycle; this is confirmed by detailed models, which find $L \propto M_{\rm core}^{\sim 8}$ on the upper RGB (where the envelope is the most extended).

Thus, we see that the luminosity increases very steeply with increasing core mass. Since the envelope is almost completely convective, and the star is close to the Hayashi line, the effective temperature cannot increase much. In the HR diagram, the star therefore moves almost straight up, along the so-called *ascending* or **red giant branch** (RGB). As the hydrogen shell burns its way outwards in mass M_r, the convective envelope retreats ahead of it: deepest first dredge-up occurs not far above the base of the RGB (see Fig. 12.4).

On the upper RGB of low mass stars (*subsequent to* first dredge-up), there is evidence of some further CNO-cycle processing of envelope material, in spite of the fact that the base of the convective envelope is at temperatures far too low for such nuclear processing. This indicates that a slow "extra" mixing mechanism is at work (probably driven by rotation effects), mixing some material between

the convective envelope and the hydrogen-burning shell. (This is a similar mechanism to that which causes the main-sequence lithium depletion in stars like the Sun.)

Evolution of the degenerate core

While the core grows, it remains approximately isothermal, and at the temperature of the shell surrounding it. In principle, the increase in temperature goes towards lifting the degeneracy, but this is more than compensated for by the increase in core density, $\overline{\rho}_{\rm core} \propto M_{\rm core}/R_{\rm core}^3 \propto M_{\rm core}^2$; see Fig. 3.2.

As one increases the density and temperature, however, the helium ions (which are not degenerate) start approaching each other more and more closely during interactions, and will start to fuse when the core mass increases to $0.45\,M_\odot$ (and $T_{\rm core} \simeq 10^8\,{\rm K}$). [Verify that you understand why this is independent of the total mass of the star.] The fusion will increase the temperature in the core, but will not reduce the density at first, since the pressure exerted by the ions is small compared to the electron degeneracy pressure. With increasing temperature and constant density, energy generation increases exponentially, until finally the thermal pressure becomes high enough to force the core to expand. By this time, the luminosity from the core has become $\sim 10^{11}\,L_\odot$, i.e., roughly equal to that from the entire Galaxy! Unfortunately, it does not seem possible to observe this *helium core flash*: the energy is used to expand the envelope.

From detailed models, it turns out that as the degenerate core grows hotter, in its centre the pressure and temperature are sufficiently high that energy is lost in neutrino creation. As a result, the centre will be slightly cooler, and helium core flash ignition will be in a shell around it. Burning will move inwards as the core is heated (possibly in a succession of mini-core-flashes following the main core flash), until degeneracy is lifted throughout the core.

After the helium core flash

The evolution *during* the helium flash is not very well understood, but it appears to be followed by a phase of quiet helium burning in a non-degenerate core. This core will still have $M_{\rm core} \simeq 0.45\,M_\odot$, but its radius will have increased significantly. Thus, one expects that the luminosity contributed by the hydrogen shell will be much smaller, $\sim 100\,L_\odot$ (down from $\sim 1000\,L_\odot$). During this time, the position of the star in the HR diagram depends on its metallicity, which determines the opacity in the envelope as well as the efficiency of energy generation in the CNO cycle (via $X_{\rm CNO}$). For solar metallicity, stars remains near the Hayashi track, in the so-called *red clump* (see the $2\,M_\odot$ track in Fig. 12.2, and the 1 and $2\,M_\odot$ tracks in Fig. 10.2). For lower metallicities, stars will move to the *horizontal branch* (see Figs 12.1, 12.4, 1.1 and 1.2). The position on the horizontal branch is determined by the envelope mass as well as the metallicity. Mass loss of order $0.2\,M_\odot$ appears to take place between the main sequence and the horizontal branch; possibly there is a mass ejection episode due to the helium core flash (although pure stellar wind mass loss on the RGB has not been ruled out). Some such low mass stars traverse a region of the HR diagram where their outer envelopes are pulsationally unstable, becoming RR Lyrae variables.

After helium is exhausted in the core, the core, now composed of carbon and oxygen, will become degenerate, and burning will continue in a helium shell. This shell will become brighter as the core mass increases, and the star starts to move up the **asymptotic giant branch** (AGB). During the later phases, the burning in the helium shell becomes unstable, leading to so-called *helium shell flashes*, which will be discussed below. During this phase, the envelope mass is reduced by nuclear burning and mass loss. The latter becomes especially important at very high luminosities, when the envelope becomes pulsationally unstable (becoming, e.g., Mira variables, with large pulsation amplitudes). At that time, a so-called "super-wind" starts. Once the hydrogen-rich envelope has dwindled to $\lesssim 1\%$ of the total mass, it deflates, and the star moves towards the blue at essentially constant luminosity, burning what little material remains. (After the star has left the AGB, there is a period when its surface is hot enough to yield UV radiation that ionizes the material lost most

recently, which is then visible as a glowing "planetary nebula" — a misnomer, since it has nothing to do with planets). The star will be left with roughly $10^{-2}\,M_\odot$ of helium and $10^{-4}\,M_\odot$ of hydrogen, around a carbon-oxygen white dwarf. From observations of white dwarfs, one finds masses mostly in the range 0.55–0.60 $M_\odot$. Apparently, the remainder of the envelope mass of low-mass stars is lost in their latest stages.

Intermediate mass giants

For an intermediate-mass star, after hydrogen is exhausted in the core, burning continues in a thick shell around an isothermal core. This can be seen in Fig. 12.6 (following point C), where the changing interior structure of a $5\,M_\odot$ star is shown. This corresponds to the phase between points 4 and 5 in Fig. 12.1. A while after point C, the isothermal core reaches the Schönberg-Chandrasekhar limit, and the star moves rapidly towards the red. During this phase, the surface luminosity drops, but this is mostly because part of the energy generated in the core is used for the expansion of the envelope (see below). The star stabilizes again when helium is ignited in the core, and the envelope has become largely convective (point E in Fig. 12.6, point 7 in Fig. 12.1, point 9 in Fig. 12.3 — *this is the point of deepest first dredge-up in intermediate mass stars*).

At this phase, the core (which initially has mass $\sim 0.75\,M_\odot$ in a $5\,M_\odot$ star) hardly notices that there is another $4\,M_\odot$ of shell and envelope around it, and its structure and luminosity are very similar to what they would have been if the core had been an isolated $0.75\,M_\odot$ helium main-sequence star. This reflects the fact that the envelope has become so dilute that it exerts negligible pressure. Like for the low-mass stars, the conditions in the hydrogen-burning shell depend almost completely on the properties of the helium-burning core.

When the helium core evolves, its "effective temperature" will at first, like that of a hydrogen main-sequence star, become slightly lower, and its radius will become slightly bigger. As a result, the hydrogen shell becomes less luminous. Since the shell produces most of the star's luminosity, the luminosity will drop somewhat (just after point E in Fig. 12.6, between 7 and 8 in Fig. 12.1). The mass of the helium core, however, will increase, and this causes the core to move upward in mass along the helium main-sequence, towards somewhat larger radius and higher temperature. The higher temperature causes an increase in the energy production in the shell, and therewith a rise in the star's luminosity. This corresponds to the increase in luminosity up to point G seen in Fig. 12.6 (between 9 and 10 in Fig. 12.1). During portions of these "blueward loops" in the HR diagram, intermediate mass stars may also lie in regions of the HR diagram where their outer envelopes are pulsationally unstable, becoming Cepheid variables.

When helium is exhausted in the centre, an isothermal carbon-oxygen core forms, and around it helium is burnt in a thick shell (F to G in Fig. 12.6; 10 to 11 in Fig. 12.1). When the core reaches the Schönberg-Chandrasekhar limit, it will collapse (note that the mass of the carbon-oxygen core should be measured relative to the mass of the helium star). As a result, the helium shell will become much more luminous, the layers above it will expand, and the hydrogen shell will be extinguished (H–K, 13–14; note that the extra loop in the HR diagram shown in Fig. 12.1 between points 11 and 14 is probably spurious, as it does not show up in more recent stellar models such as those in Figs. 10.2 and 12.2). This expansion causes the convective envelope to engulf hydrogen-exhausted material that the hydrogen shell had left behind, in a process known as **"second dredge-up"**. (This occurs near point 15 in Fig. 12.3. *Low mass stars*, where the hydrogen-burning shell is not extinguished, *do not experience second dredge-up.*) The core becomes degenerate, and at first there is only a helium shell around it. As the shell eats outwards, it comes close to the position where second dredge-up has left hydrogen-rich material, and the hydrogen shell is re-ignited.

From here on, the evolution becomes similar to the late evolution of low-mass stars. The helium shell becomes unstable, and near the top of the asymptotic giant branch a super wind sets in, which limits the growth of the degenerate core. When the envelope has become too tenuous, it deflates, the star moves to the blue, and a white dwarf is formed.

High mass giants

For even more massive stars, after hydrogen exhaustion the core contracts immediately to helium ignition. This slows down, but does not stop the star from moving across the HR diagram. For the $25\,M_\odot$ star shown in Fig. 12.1, helium is exhausted while the star is only midway over to the red-giant branch. At that point, the core contracts further, and carbon is ignited. After that, things move on very fast, and the star soon explodes as a supernova.

The evolution of these massive stars is complicated greatly by mass loss, even on the main sequence. Due to mass loss, the whole hydrogen-rich envelope may disappear, in which case the star becomes a helium star, and moves to high temperatures in the HR diagram. Indeed, for very massive stars, this is virtually unavoidable, as their luminosity on the way to the red giant branch exceeds the Eddington luminosity, and their envelopes are rapidly blown off. This results in an empty region in the top right of the HR diagram, above and to the right of the *Humphreys-Davidson limit* (see Fig. 1.3). Stars close to this limit indeed are observed to have extremely large and variable mass-loss rates; these are the so-called *luminous blue variables*.

Helium shell flashes (also called "thermal pulses")

Above, it was mentioned that the helium shell could become unstable. To see how this arises, we do a stability analysis for a thin shell and compare this with a similar analysis for a core (which should be stable). For a core, the mass of the burning region goes as $m \sim \rho r^3$, and expansion in reaction to an energy perturbation corresponds to a small increase δr. For a thin shell at radius r_0 and with thickness D, the mass in the burning region goes as $m \sim \rho r_0^2 D$. For a small expansion of the shell, the thickness will increase by δD but r_0 will be approximately constant. The corresponding change in density for the two cases (assuming no change in mass of the burning region) can be written in fractional units as

$$\text{core:}\quad \frac{\delta\rho}{\rho} = -3\frac{\delta r}{r} \qquad \text{shell:}\quad \frac{\delta\rho}{\rho} = -\frac{\delta D}{D} = -\frac{r}{D}\frac{\delta r}{r}. \tag{12.2}$$

In the last equality, we used δr to indicate the change in the outer radius of the shell. Assuming the layers outside the expanding core or shell change homologously with the outer radius, we have for both that $P \propto r^{-4}$, or $\delta P/P \propto -4\delta r/r$. For an ideal gas, the temperature $T \propto P/\rho$, and thus the fractional temperature change is $\delta T/T = \delta P/P - \delta\rho/\rho$. Similarly, given an energy generation rate $\epsilon \propto \rho^\lambda T^\nu$, the fractional change in energy generation rate is $\delta\epsilon/\epsilon = \lambda\delta\rho/\rho + \nu\delta T/T$. For the two cases, these fractional changes can be expressed in terms of the fractional change in radius by

$$\begin{aligned}
\text{core:}\quad \frac{\delta T}{T} &= (-4+3)\frac{\delta r}{r}\,, & \text{shell:}\quad \frac{\delta T}{T} &= \left(-4+\frac{r}{D}\right)\frac{\delta r}{r}\,,\\
\frac{\delta\epsilon}{\epsilon} &= (-3\lambda+\nu(-4+3))\frac{\delta r}{r}\,, & \frac{\delta\epsilon}{\epsilon} &= \left(-\lambda\frac{r}{D}+\nu\left(-4+\frac{r}{D}\right)\right)\frac{\delta r}{r}\,.
\end{aligned} \tag{12.3}$$

For the core, we thus see that a small expansion ($\delta r > 0$), leads to a decrease in temperature and energy generation rate ($\delta T < 0$, $\delta\epsilon < 0$), i.e., the burning is stable. However, for a shell with $D \ll r$ (and $\nu > \lambda$), for a small expansion both T and ϵ actually increase, i.e., *burning in a thin shell is unstable*.

While a shell is eating its way out, it tends to become thinner and thus closer to instability. And indeed the instability also occurs in real and model stars, as can be seen in Fig. 12.7. In the left panel, one sees that at the start of the instability, the density decreases and the temperature increases sharply. As a result, the local luminosity becomes several times the total stellar luminosity. This continues until the shell expands sufficiently (i.e., its thickness is no longer much smaller than the radius). Then it gently settles back, until the instability sets in again.

Note that while the luminosity *in* the shell becomes very high, that *at the top* of the shell does not increase so dramatically. This is because most of the energy is used to expand the shell.

Furthermore, as the helium shell expands, the temperature in the hydrogen shell drops, and hydrogen burning is temporarily extinguished. Therefore, the luminosity of the star actually goes down during a shell flash. As on the RGB, for stars where envelope convection does not reach into the hydrogen-burning shell, the star's (interflash) surface luminosity is determined only by the star's core mass (and metallicity) — after the first few helium shell flashes, a "universal" **core-mass–luminosity relation** is approached, which is almost linear in the core mass.

In the right-hand panels of Fig. 12.7, one sees that a small convection zone appears during the shell flash. This will distribute processed material all through the region between the hydrogen and helium shells. While the shell flash is occurring, the lower boundary of the outer (envelope) convection zone retreats somewhat, in response to the lower hydrogen shell luminosity, and then descends again. Fig. 12.8 shows a case where **"third dredge-up"** occurs, in which the envelope convection descends below the position of the (extinguished) hydrogen shell into the intershell region, and can thus bring up highly processed material to the surface. Observationally, this leads to the formation of S stars (enriched in "s-process" isotopes, that result from slow neutron irradiation) and carbon stars (where the surface C/O ratio exceeds unity).

Surface carbon enrichment (possibly yielding a carbon star) is fairly straightforward, as the 3α reaction during the earlier helium shell flash has enriched the intershell region with ^{12}C. Formation of S stars is less simple. The observed s-process isotopes at the surface of low mass S stars (and carbon stars) would have required slow irradiation of iron nuclei by a fairly large number of neutrons (the iron is present in the original stellar composition, part of the metallicity). The $^{22}\mathrm{Ne}(\alpha,\mathrm{n})$ reaction can produce a few neutrons during the helium shell flash, but not enough — the helium-burning temperature is not high enough for this reaction to be significant. On the other hand, the $^{13}\mathrm{C}(\alpha,\mathrm{n})$ reaction would occur at lower temperatures, but the CNO-cycle burning leaves behind almost no ^{13}C. This problem could be solved if, during the third dredge-up, a relatively small amount of hydrogen was mixed downwards into the carbon-rich intershell region (computational models do not exhibit such behavior, but there are several hard-to-model processes that might yield such a result, e.g., semiconvection, partial convective overshoot, rotation-induced mixing, etc.). As this region heated up again, it would burn up the hydrogen via the $^{12}\mathrm{C}(\mathrm{p},\gamma)$ reaction, yielding a region with a relatively large ^{13}C abundance. Later, this region would grow hot enough for the $^{13}\mathrm{C}(\alpha,\mathrm{n})$ reaction to burn up the ^{13}C and irradiate the local material with neutrons, yielding s-process isotopes. These would be engulfed by the next flash-driven intershell convective region, which would mix them throughout the intershell region; some would then be mixed to the surface in the following dredge-up episode (see Fig. 12.8).

Hot bottom burning

In stars of mass $\gtrsim 4\ M_\odot$, the base of the convective envelope eventually reaches into the hydrogen-burning shell during the interflash period ("hot bottom burning"). This can result in CNO-cycle processing of the envelope, affecting the envelope CNO isotope ratios. When hot bottom burning occurs, the shell's properties no longer depend only on the core mass: it is also linked to the surface via the the envelope convection. The star's luminosity increases significantly above the value that would have been expected from the core-mass–luminosity relation mentioned above.

The envelope

In the above discussion, we have mostly ignored the envelope. This is not unreasonable if it is as tenuous as it has to be when the star has swollen to giant dimensions, but we have not yet addressed why this swelling actually happens. It is clear that real stars do it, and their behavior can be reproduced by models, but it is not so clear what physical mechanism dominates this process. Indeed, as was clear from the beginning of this chapter, this question is still debated (see the references quoted there for more detail).

Partly, it seems it is related to the way the opacity varies with density and opacity. Quite generally, as a star becomes more luminous, its radius increases and effective temperature decreases a little. This in itself is not enough to bring the star over to the red giant regime. As the temperature in the outer layers decreases, however, the opacity there increases quite strongly, since it is dominated by bound-free processes (the lower temperature leads to lower ionization states of the metals, which therefore can absorb photons more easily). Therefore, the luminosity cannot easily be transported anymore, and part of it is trapped, leading to further expansion. At some point, this apparently can become a runaway process, in which the envelope cools more and more, becomes more and more opaque, traps more and more of the luminosity, and expands to larger and larger radii. It only stops when the star reaches the Hayashi line, where the envelope has become almost completely convective, and energy can be transported more easily.

This runaway expansion may be responsible for intermediate-mass stars crossing the HR diagram very fast. Observationally, this results in a lack of stars between the main sequence and the giant branches, in the so-called *Hertzsprung gap*. When the luminosity decreases, it appears the inverse instability can happen, where the envelope heats a little, becomes less opaque, therefore shrinks a little, releasing energy which increases the temperature, etc. This deflation instability might be responsible for the blue loops seen in the evolutionary tracks of intermediate-mass stars.

For next time

– Read textbook §15.1 on the fate of high mass stars, and §15.3 on core collapse (up to p. 534).

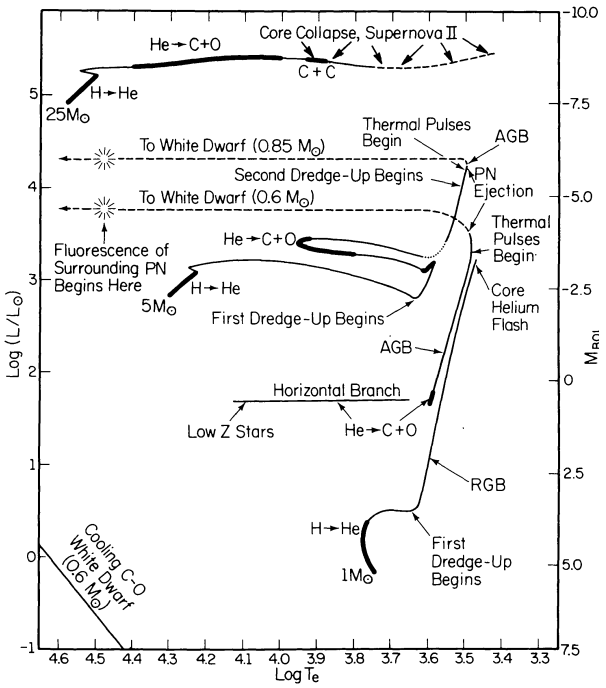

Fig. 12.1. *(Left)* Schematic evolutionary tracks in the HR diagram for stars of low, intermediate, and high mass. Heavy portions indicates phases where the evolution proceeds on a slow, nuclear timescale. Indicated are the first and second "dredge up," phases in which the outer convection zone reaches down to layers with processed material. A third dredge-up occurs during the thermal-pulse phase, which is also indicated. Note that the luminosity at which a star leaves the AGB is a conjecture based on observed white-dwarf masses. *(Bottom)* Evolutionary track of a $5\,M_\odot$ star in detail, with important physical processes for the different phases indicated (note that the loop from point 11 to point 14 is probably spurious — this track was taken from a less accurate computation, performed several decades earlier). Both figures taken from the review of Iben (1991, ApJS 76, 55).

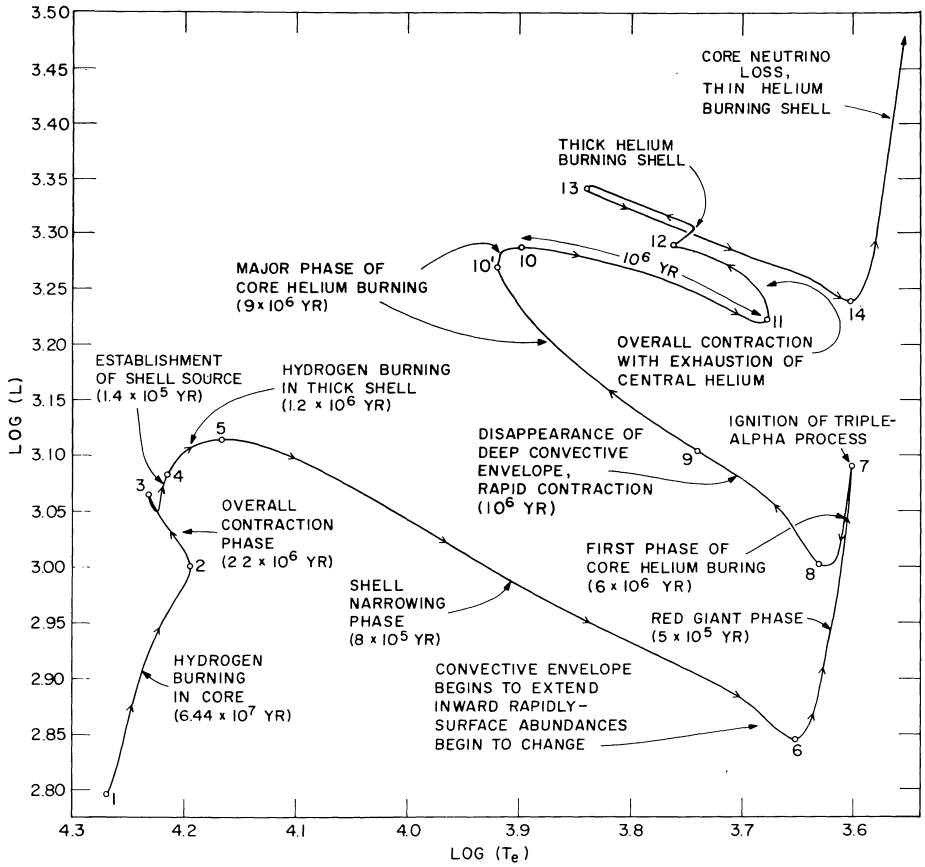

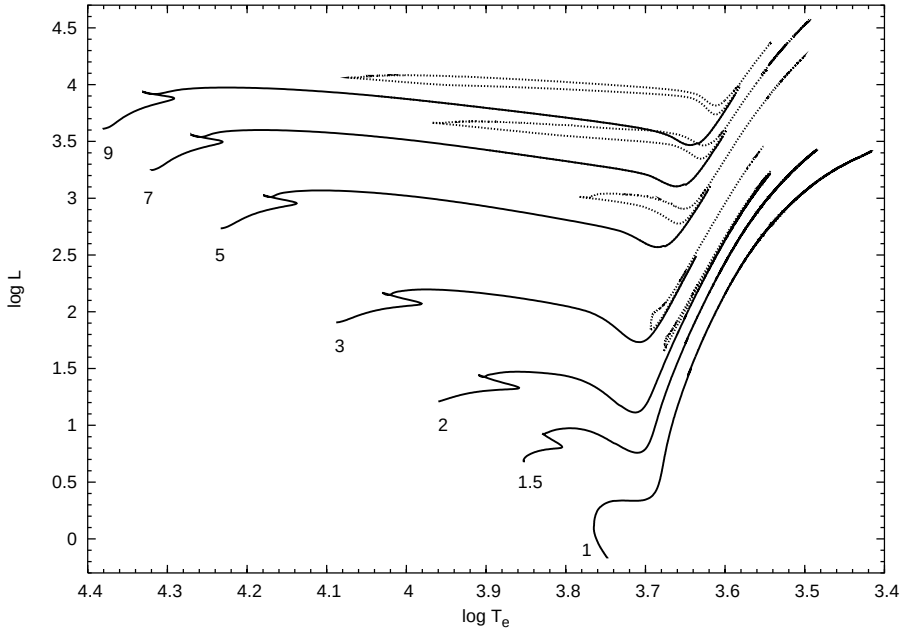

Fig. 12.2. Evolution of solar-metallicity stars of low and intermediate masses. *Solid lines:* evolution from the ZAMS to core helium ignition; *dotted lines:* subsequent evolution. For the 1 and 1.5 $M_\odot$ cases, evolution is shown only up to the beginning of the helium core flash (at the tip of the RGB). For $2-7$ $M_\odot$ cases, evolution is shown up to the first helium shell flash (on the AGB, but *not* its tip) — the 2 $M_\odot$ track *includes* the helium core flash. For the 9 $M_\odot$ case, evolution is shown up to core carbon ignition.

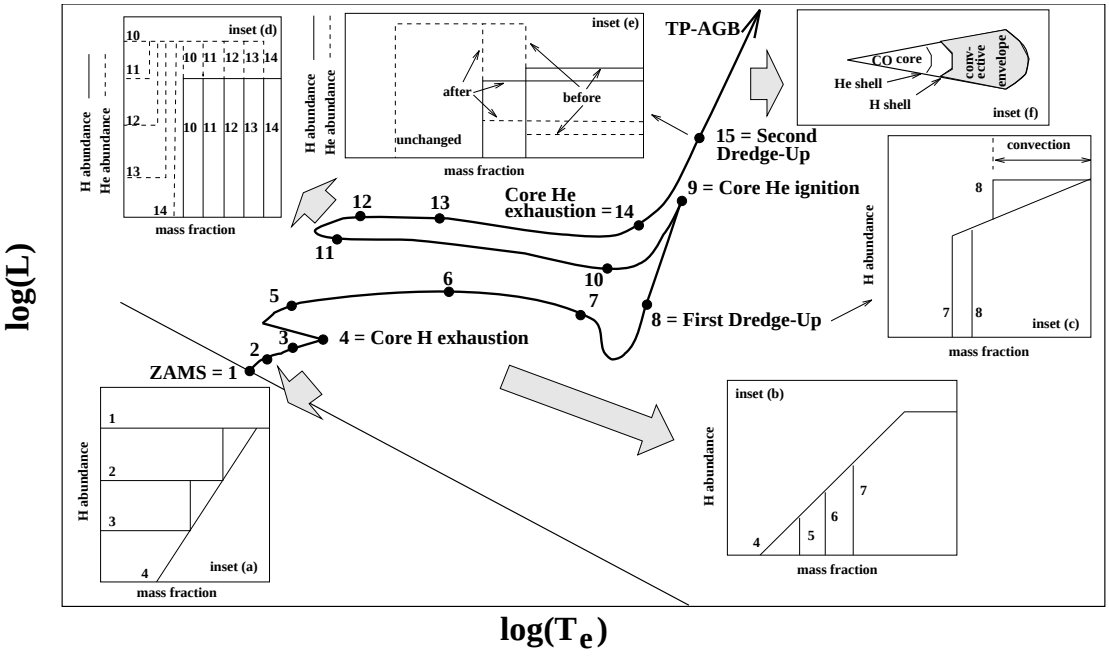

Fig. 12.3. Schematic evolution of a 5 $M_\odot$ star (from Lattanzio & Boothroyd 1995).

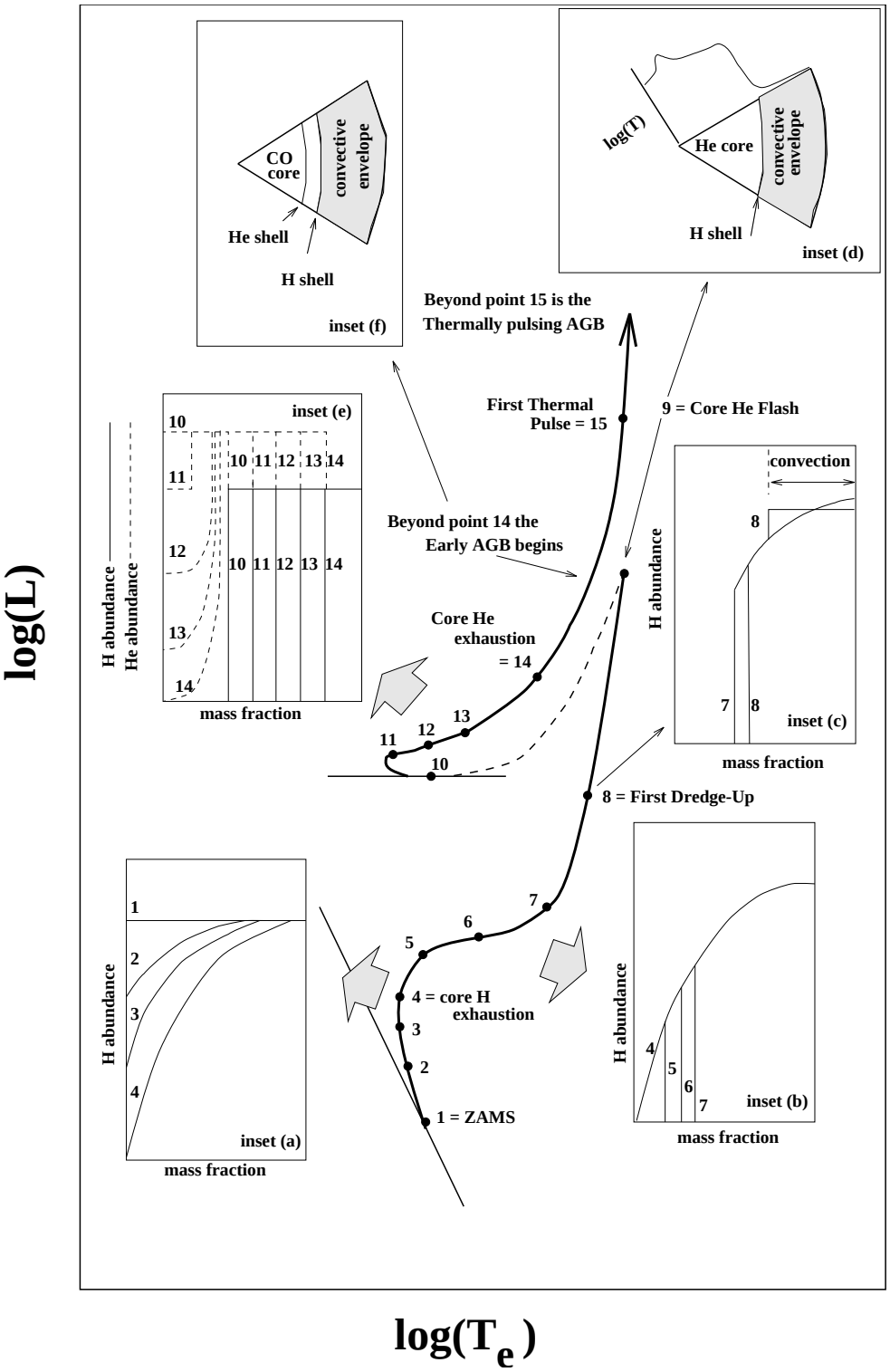

Fig. 12.4. Schematic evolution of a 1 $M_\odot$ star (from Lattanzio & Boothroyd 1995).

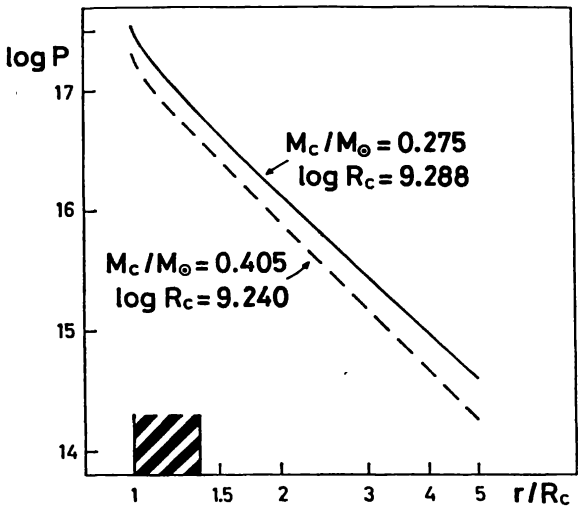

Fig. 12.5. Run of pressure as a function of radius in units of the core radius for two RGB models with $M = 1.4\,M_\odot$ but different core masses and radii. Note how similar the two curves are, apart from a constant offset (which is a function of the core properties only). The striped area indicates the extension of the burning region within the shell ($0 < L_r < 0.99L$). Taken from Refsdal & Weigert (1970, A&A 6, 426).

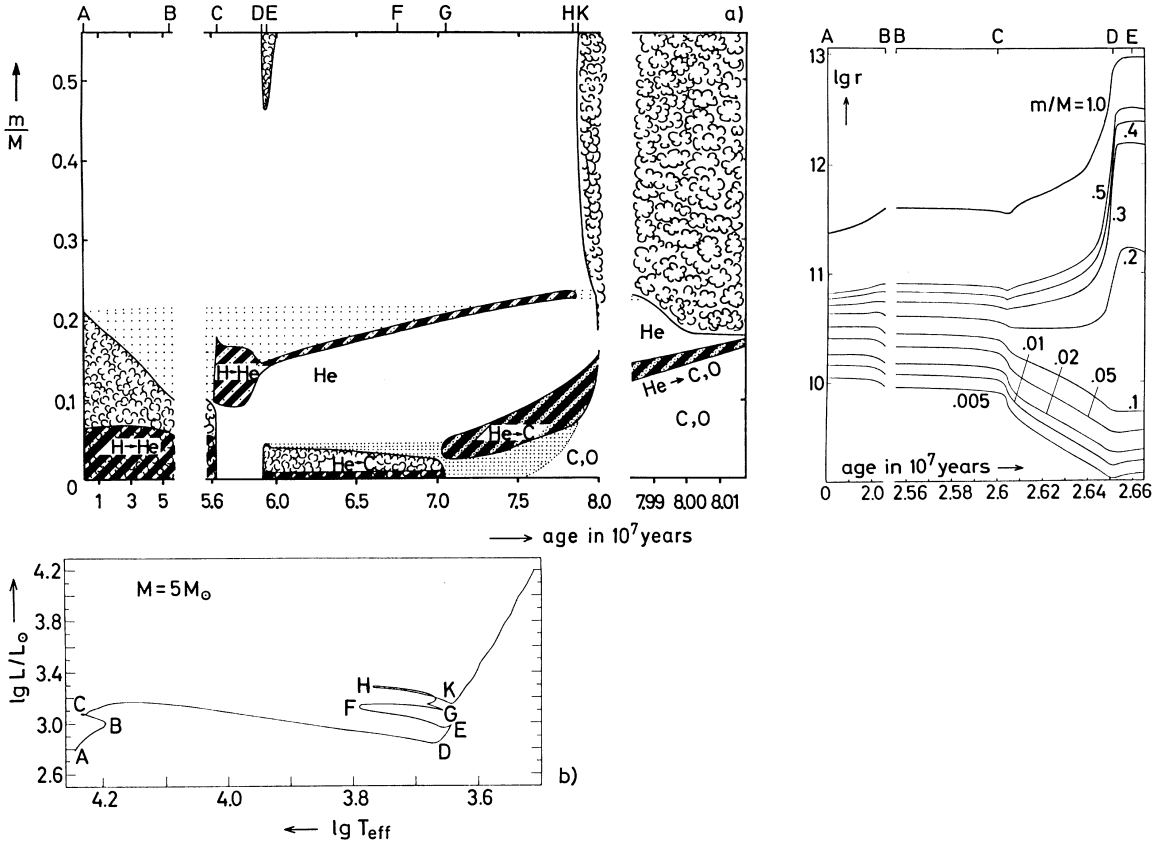

Fig. 12.6. *(Upper left)* Interior structure of a $5\,M_\odot$ star during its evolution. "Clouds" indicate convective regions, heavy shading energy generation at rates $\epsilon > 10^3$ erg g^{-1} s^{-1}, and stippling variable chemical composition. *(Lower left)* Evolutionary track in the HRD for the same model. *(Right)* Radial variation of different mass shells during the evolution of a $7\,M_\odot$ star. The letters A,...,E correspond to the same evolutionary phases labeled for a $5\,M_\odot$ star in the left-hand panels. Taken from KW, their Figs 31.2, 3.

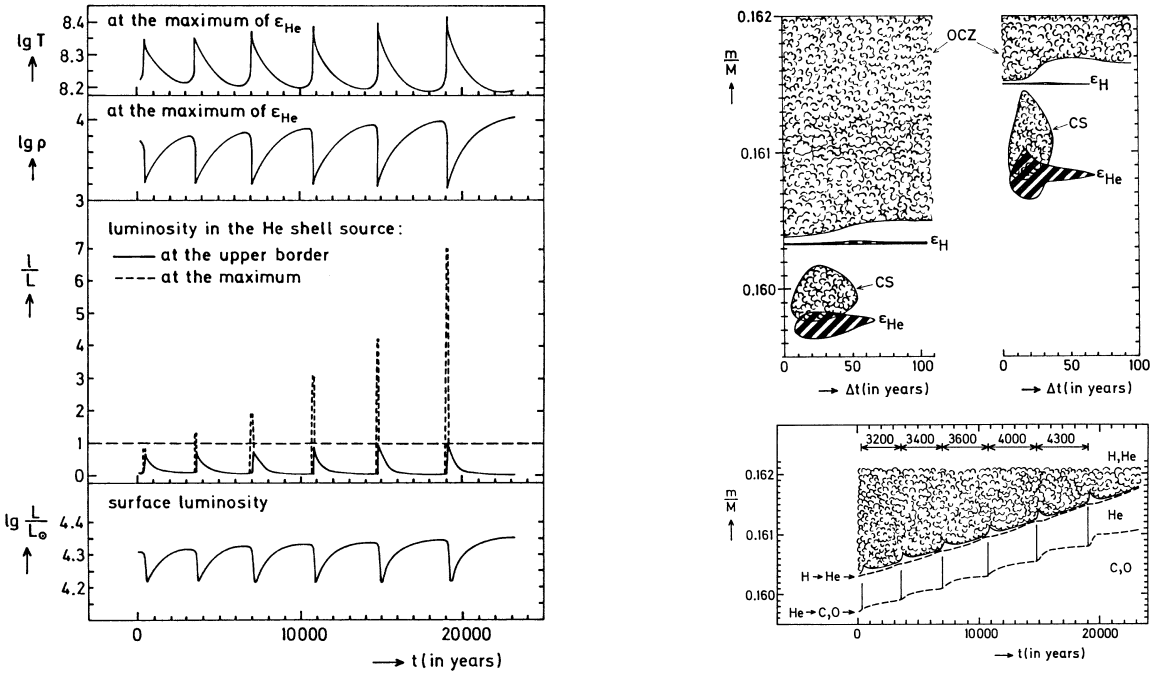

Fig. 12.7. Shell flashes. *(Left)* The four panels give the evolution of the temperature and density in the shell at the position of maximum energy generation, luminosity at that position and of the shell as a whole, and surface luminosity. *(Top right)* Details of the star's structure near the shell during two shell flashes. *(Bottom right)* Evolution of the star's structure during a series of shell flashes. Taken from KW, their Figs 33.3, 4, 5.

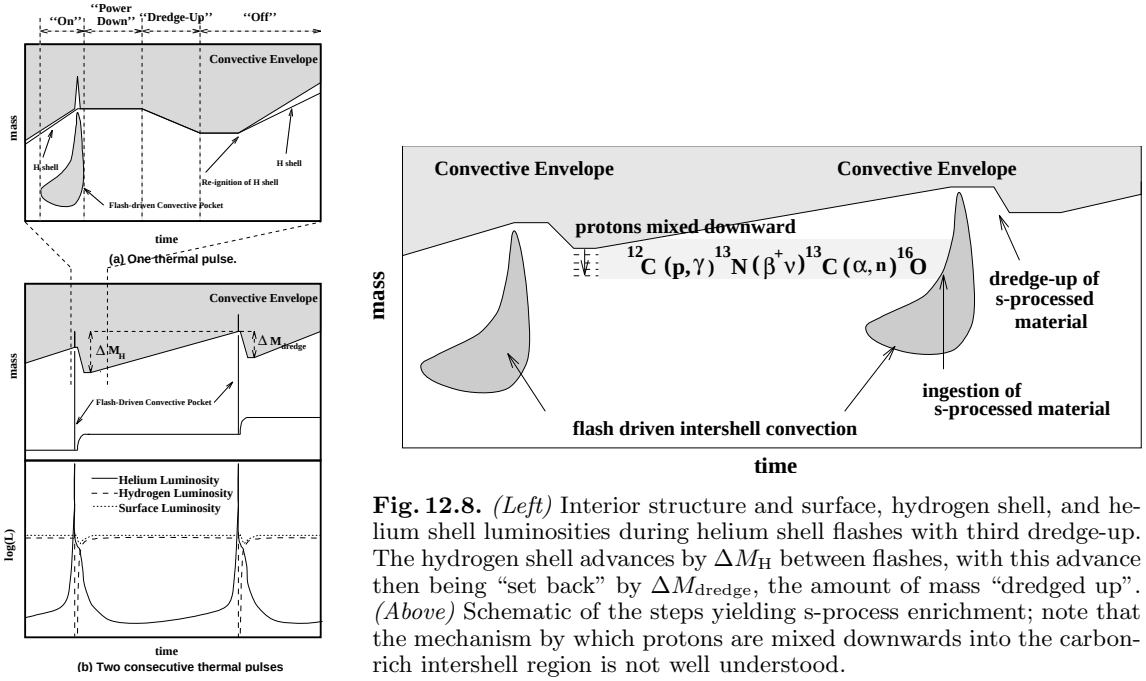

Fig. 12.8. *(Left)* Interior structure and surface, hydrogen shell, and helium shell luminosities during helium shell flashes with third dredge-up. The hydrogen shell advances by $\Delta M_{\rm H}$ between flashes, with this advance then being "set back" by $\Delta M_{\rm dredge}$, the amount of mass "dredged up". *(Above)* Schematic of the steps yielding s-process enrichment; note that the mechanism by which protons are mixed downwards into the carbon-rich intershell region is not well understood.

13. The end of a star's life

Textbook: §15.1, 15.3 (up to p. 534; different emphasis)

Dwindling into oblivion ...

A very simple picture of the evolution of a star can be obtained from looking just at the changes in central density and temperature, as is done in Fig. 13.1. While a star contracts more or less homologously, and the core is not degenerate, one has $\rho \propto R^{-3}$ and $T \propto R^{-1}$, from which it follows that $T \propto \rho^{1/3}$. This behaviour can indeed be seen in the lower left corner of the figure.

The demarcation between the regions in ρ, T space where the ideal gas law holds and where degeneracy is important, is described by a line $T \propto \rho^{2/3}$. Therefore, during contraction, the core of a star comes closer and closer to being degenerate. Before doing so, however, it may reach conditions sufficient to start nuclear processing, indicated by the various ignition lines in the figure. If it does not even reach hydrogen ignition, it becomes a brown dwarf.

When hydrogen is ignited, the properties can remain similar, while the star is on the main sequence. When hydrogen is exhausted, however, the core starts to contract again. For low-mass stars, we saw that the core becomes degenerate before helium is ignited. If the star does not have sufficient mass, the core cannot grow up to $0.45\,M_\odot$, and helium will not be ignited; the star will dwindle, and become a helium white dwarf.[4]

For both low and intermediate-mass stars, the carbon-oxygen cores become degenerate after helium burning. In principle, if the star were massive enough, the core might grow sufficiently due to shell burning to ignite carbon burning. If so, the star would likely explode, leaving no remnant. In practice, however, it seems the super wind intervenes, and no carbon-oxygen cores above $\sim 1.2\,M_\odot$ are formed.

... or going out with a bang

For high-mass stars, the carbon-oxygen cores do not become degenerate, igniting core carbon burning instead, and these stars can continue to further burning stages as described in §8. The stages follow each other more and more rapidly, as neutrino losses become more and more important, while the energy gain from the fusion dwindles (Fig. 8.1). Some typical numbers are listed in Table 13.1. (It is *possible* that stars in a narrow mass range near $8\,M_\odot$ may proceed no farther than carbon burning, and end up as oxygen-neon-magnesium white dwarfs.)

While the next stage starts in the core, the burning of lighter elements will still continue in shells. As a result, the structure of a high-mass star near the end of its life becomes somewhat akin to that of an onion, in which regions with different chemical compositions are separated by burning shells (see Fig. 13.2).

When an iron core is formed, no further energy can be gained by fusion, since iron has the largest binding energy of all elements. In order to match the neutrino losses, therefore, the core has to shrink. This will cause the temperature to rise, and at $T > 5\,10^9\,\mathrm{K}$ the photons become energetic enough to break up the iron nuclei, into α particles, protons and neutrons. These reactions are endothermic and thus cool the core. As a result, the pressure drops, the core shrinks further, more iron becomes disintegrated, etc. At the same time, neutrinos keep on removing energy. Furthermore, as the density increases, electrons are being captured by remaining heavy nuclei (leading to neutronisation, i.e., converting a proton into a neutron, with the emission of a neutrino), thus reducing the pressure further. All these processes quicken the collapse.

[4] Such low mass stars have not yet had time to finish their main-sequence lives even if they were formed very early on — the universe has not lived long enough. In binaries, however, somewhat more massive stars can be "stripped" of their envelopes by mass transfer onto a binary companion while they are on the red giant branch, and these can indeed leave helium white dwarfs.

Table 13.1. Neutrino luminosities and timescales of late burning phases

Burning stage	..... $15\,M_\odot$ ..... L_ν/L ($L \simeq 10^4\,L_\odot$)	τ (yr)	..... $25\,M_\odot$ ..... L_ν/L ($L \simeq 3\,10^5\,L_\odot$)	τ (yr)
C	1.0	$6.3\,10^3$	8.3	$1.7\,10^2$
Ne	$1.8\,10^3$	7	$6.5\,10^3$	1.2
O	$2.1\,10^4$	1.7	$1.9\,10^4$	0.51
Si	$9.2\,10^5$	0.017	$3.2\,10^6$	0.004

Taken from KW, their Table 33.1

At first, the core collapses roughly homologously (i.e., velocity proportional to radius), but soon this would require speeds in excess of the free-fall speed in the outer region. Thus, one has an inner collapsing core, with the outer core following on the free-fall time. The latter is of order one second. The collapse of the inner core will stop only when the neutrons become degenerate, at $\rho \gtrsim \rho_{\rm nuc} \simeq 10^{14}\,{\rm g\,cm^{-3}}$. The outer layers are still falling in, however, which leads to the development of a strong shock wave, which will start to move outward. At the same time, the inner core will become more massive and, since it is degenerate, smaller.

We now estimate a few quantities for the core, taking $M \simeq 1.4\,M_\odot$ and $\overline{\rho} \simeq 10^{14}\,{\rm g\,cm^{-3}}$, and, therefore, $R \simeq 2 \times 10^6\,{\rm cm}$. For these numbers, the potential energy is roughly

$$E_{\rm pot} \simeq \frac{GM^2}{R} \simeq 3 \times 10^{53}\ {\rm erg}. \tag{13.1}$$

Since the core was much larger before the collapse, we see that a couple $10^{53}\,{\rm erg}$ has to be liberated. We can compare this with the energy required to dissociate the iron in the core. For every nucleon, $\epsilon_{\rm diss} \simeq 9\,{\rm MeV} \simeq 1.4\,10^{-5}\,{\rm erg}$ is required (see Fig. 8.1). Thus,

$$E_{\rm diss} = \epsilon_{\rm diss}\frac{M}{m_{\rm H}} \simeq 2 \times 10^{52}\ {\rm erg} \tag{13.2}$$

which is substantially less than the total energy available. Next, compare the potential energy with the kinetic energy given to the envelope in a supernova explosion. With an envelope mass of $10\,M_\odot$ and a typical (observed) velocity of $\sim 10^4\,{\rm km\,s^{-1}}$, the total kinetic energy is,

$$E_{\rm kin} = \frac{1}{2}M_{\rm env}v_{\rm env}^2 \simeq 10^{52}\ {\rm erg}. \tag{13.3}$$

Thus, there is ample energy available to expel the envelope. The energy emitted in optical light is $\sim 10^{49}\,{\rm erg}$, negligible in comparison, but leads to a luminosity similar to that of an entire galaxy during the roughly one month it lasts. By far most of the energy is lost in neutrinos.

While there is enough energy to expel the envelope, it has proven very difficult to reproduce the expulsion in models. There are three effects which can help.

1. The shock. There is enough energy in the shock for expulsion, but a lot of the energy is lost as the shock goes through the relatively dense inner part of the envelope (which is still falling in). This is because material is shock-heated to such an extend that neutrino losses and dissociation become important. From simulations, it seems only a very strong shock could cross through these layers and lead to a *prompt hydrodynamic explosion*.
2. Neutrino radiation pressure. The core is so dense that it is optically thick to neutrinos. As a result, the neutrinos have to diffuse out, and for a few seconds the core is a strong neutrino source (with $L_\nu \simeq 10^{53}\,{\rm erg\,s^{-1}}$). Above the "neutrinosphere", a fraction of the neutrinos will still be scattered, causing a radiation pressure term just like that due to photons. By equating the force due to neutrino scattering, $f_\nu = \kappa_\nu(L_\nu/4\pi R^2 c)$, with that due to gravity, $f_{\rm g} = GM\rho/R^2$,

one can define a neutrino equivalent of the Eddington luminosity, $L_{\mathrm{edd},\nu} = 4\pi GMc/\kappa_\nu$. From calculations, it appears that the pressure due to the neutrinos in itself is insufficient to expel the outer layers, but that an explosion can be produced in combination with the shock, via strong heating and convective motion, in the so-called *delayed explosion mechanism*.

3. Thermonuclear reactions. When the shock arrives outside the original iron core, the shock heating will increase the speed of the fusion reactions in those regions dramatically. At the increased temperature, Si-burning results mostly in $^{56}_{28}$Ni. This is an unstable isotope, which decays to $^{56}_{27}$Co through β-decay, with a half-life time of 6.1 d. $^{56}_{27}$Co is unstable as well, and decays to $^{56}_{26}$Fe (half-life 77.7 d). These and other decay processes keep the supernova bright for a longer time.

Note that the above description of the explosion of a massive star applies to a **Type II** supernova (classified as such by virtue of possessing hydrogen lines in its spectrum). Type I supernovae show no hydrogen lines in their spectra. **Type Ia** supernovae (with a strong Si II line at 6150 Å) result from a different mechanism: the explosion of a carbon-oxygen white dwarf, which has ignited due to accretion from a binary companion. **Type Ib** supernovae (with helium lines) and **Type Ic** supernovae (with no helium lines) appear to be the explosions of massive stars, similar to those described above, but which have lost their hydrogen envelope, or even their helium envelope, by the time of their explosion.

Enrichment of the interstellar medium

Supernovae are a major source of heavy elements in the interstellar medium, contributing some helium, carbon, nitrogen, oxygen, iron, and many other elements. Intermediate mass stars (and even low mass stars) contribute some heavy elements due to the mass loss that removes their envelopes, yielding mainly helium, carbon, nitrogen, and s-process elements. There are other sources as well, including novae (recurrent thermonuclear explosions on the surfaces of accreting white dwarfs in binary systems) and cosmic rays (which produce beryllium, boron, and lithium by spallation as they hit heavier nuclei such as carbon in the interstellar medium).

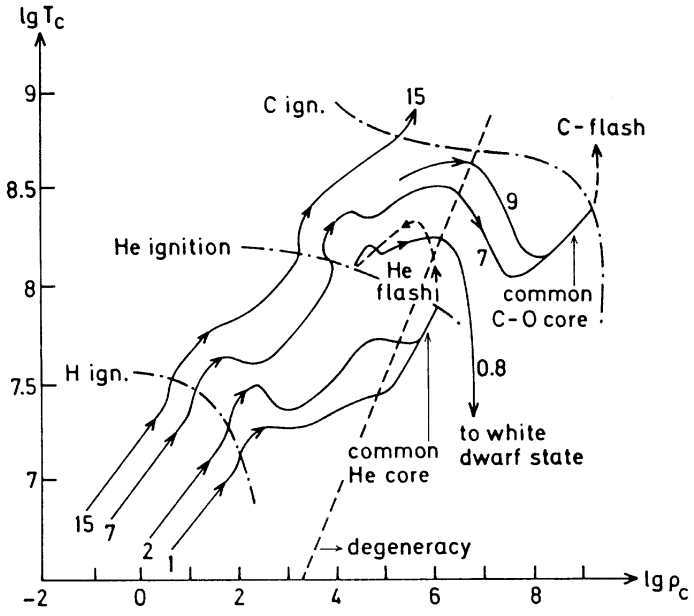

Fig. 13.1. Variation of central density and temperature during the course of the evolution of stars of various masses. The long-dashed line indicates the approximate limit to the right of which the core becomes degenerate. Dash-dotted lines indicate regimes where hydrogen, helium, and carbon are ignited. (Note that these earlier models showed a $9\,M_\odot$ star's core becoming degenerate, rather than igniting carbon burning non-degenerately. Mass loss appears to terminate AGB evolution before the C-O core reaches the "C-flash" ignition line in this diagram.) Taken from KW, their Fig. 33.6.

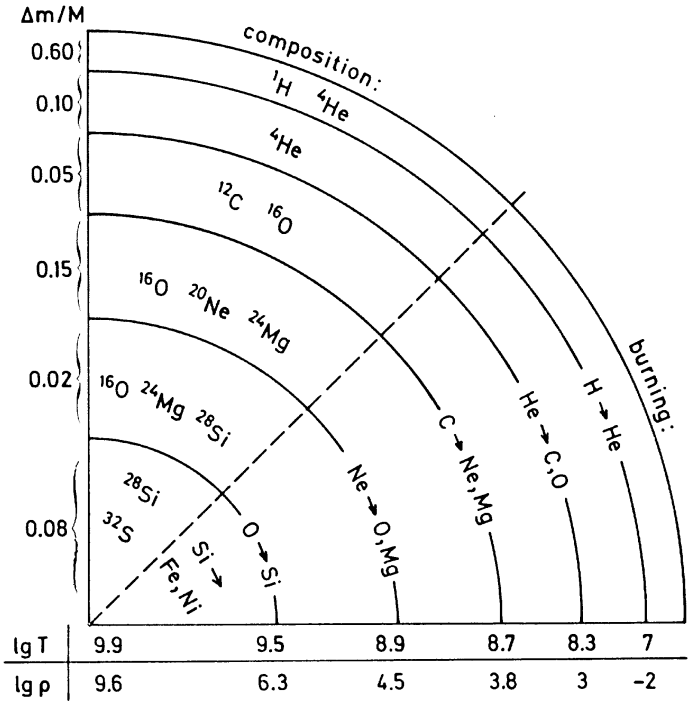

Fig. 13.2. "Onion-skin" structure of a massive star in the very last stages of its life (not to scale). Typical fractional masses, temperatures (K), and densities ($\mathrm{g\,cm^{-3}}$) are indicated along the axes. Taken from KW, their Fig. 33.1.